DEVELOPMENT OF ULTRASOUND IMAGE CONTRAST ENHANCEMENT AND SPECKLE NOISE REDUCTION FOR KNEE OSTEOARTHRITIS EARLY DETECTION

MD BELAYET HOSSAIN

DISSERTATION SUBMITTED IN PARTIAL FULFILLMENT OF THE REQUIREMENTS FOR THE DEGREE OF MASTER OF ENGINEERING

DEPARTMENT OF BIOMEDICAL ENGINEERING
FACULTY OF ENGINEERING
UNIVERSITY MALAYA
KUALA LUMPUR

2014

UNIVERSITY MALAYA
ORIGINAL LITERARY WORK DECLARATION

Name of Candidate: Md Belayet Hossain Passport No:

Registration/Matric No: **KGA120044**

Name of Degree: Master of Engineering Science

Title of Project Paper/ Research Report/ Dissertation/ Thesis ("This Work"):
Development of Ultrasound Image Contrast Enhancement and Speckle Noise Reduction for Knee Osteoarthritis Early Detection.

Field of Study: Biomedical Imaging

I do solemnly and sincerely declare that:

(1) I am the sole author/writer of this Work;
(2) This work is original;
(3) Any use of any work in which copyright exists was done by way of fair dealing and for permitted purpose and any excerpt from, or reference to or reproduction of any copyright work has been disclose expressly and sufficiently and the title of the Work and its authorship have been acknowledge in this Work;
(4) I do not have any actual knowledge nor do I ought reasonably to know that the making of this work constitutes an infringement of any copyright work;
(5) I hereby assign all and every rights in the copyright to this work to the University of Malaya (UM), who henceforth shall be owner of the copyright in this work and that any written consent of UM having been first had and obtained;
(6) I am fully aware that if in the course of making this work I have infringed any copyright whether intentionally or otherwise, I am be subject to legal action or any other action as may be determined by UM.

Candidate's Signature Date:

Subscribed and solemnly declared before,

Witness's Signature Date:

Name:

Designation:

ABSTRAK

Lutut Osteoartritis (OA) adalah salah satu penyakit yang paling biasa di kalangan warga tua. Biasanya, rawatan perubatan tidak diutamakan sehingga penyakit itu telah berkembang ke titik di mana ia tidak mungkin didiagnosis secara berkesan. Hal ini sering disebabkan oleh kebimbangan terhadap kos pengesanan semasa peringkat awal. Ultrasound (US) pengimejan mempunyai beberapa kelebihan sebagai teknik pengimejan. Ia merupakan satu kaedah diagnostik yang kos rendah, tidak invasif, tidak mengionkan dan dapat menyediakan visualisasi yang intuitif. Terdapat perubahan yang ketara dalam bentuk rawan kerana perkembangan OA yang berkiat dengan degenerasi tulang rawan. Dengan menggunakan pengimejan US, ia dapat mengesan penyempitan ruang lutut. Namun, nisbah kontras yang rendah dan bunyi belu yang menghadkan penggunaan produk ini. Objektif tesis ini adalah untuk mencadangkan cara baru yang dapat menambahkan kostras dan mengurangkan beru yang akan mengatasi had-had tersebut. Dalam kaedah yang dicadangkan itu, peningkatan nilai-nilai optimum kontras, kecerahan dan pemeliharaan terperinci akan diambil kira. Kebanyakan kaedah peningkatan konvensional hanya menekankan satu watak manakala kaedah yang dicadangkan melibatkan penubuhan titik pemisah di segmen histogram untuk kontras optimum, kecerahan dan pemeliharaan terperinci dalam masa yang sama. Tiga metrik akan digunakan dalam pengoptimuman ini, iaitu Pemeliharaan Fungsi Skor Kecerahan (PBS), Fungsi Kontras Skor Optimum (OCS), dan Pemeliharaan Fungsi Skor Terperinci (PDS) ditakrifkan. Untuk mengurangkan bunyi belu dan mengekalkan ciri-ciri kelebihannya, fungsi kemeresapan baru dan kecerunan empat ambang digunakan dan bukan satu. Untuk menganalisis prestasi, analisis kuantitatif dan kualitatif telah dijalankan dengan menggunakan kedua-dua imej ultrasound sintetik dan nyata. Keputusan membuktikan bahawa kaedah yang dicadangkan melebihi kaedah yang sedia ada.

ABSTRACT

Knee Osteoarthritis (OA) is one of the most common diseases among the elderly. Typically, medical attention is not sought until the disease has progressed to a point at which it is not possible to diagnose effectively, often due to concerns over the cost of detection at an earlier stage. Ultrasound (US) imaging has a number of advantages as an imaging technique; it is a low cost diagnostic method, non-invasive, non-ionizing and able to provide intuitive visualization. There is a significant change in the shape of cartilage due to the progression of knee OA and its associated cartilage degeneration. By using US imaging, it is possible to detect knee joint space narrowing. Nevertheless, the low contrast ratio and presence of speckle noise limit this application of US. The objective of this thesis is to propose a new contrast enhancing and speckle reducing method which will overcome the existing limitations. In the proposed method, contrast enhancement for optimum values of contrast, brightness and detail preservation will be taken into consideration. Most of the conventional contrast enhancing methods emphasize only one character; in contrast, the proposed method involves establishing a separating point to segment histogram for optimal contrast, brightness and detail preservation simultaneously. Three metrics will be used in this optimization, namely Preservation of Brightness Score function (PBS), Optimum Contrast Score function (OCS), and Preservation of Detail Score function (PDS), each of which will be defined. To both reduce speckle noise and preserve edge features, a new diffusivity function and four gradient thresholds instead of one are used. For performance analysis, quantitative and qualitative analysis has been performed using both synthetic and real ultrasound images. Results prove that the proposed method out-performs existing methods.

ACKNOWLEDGEMENT

With the deepest gratitude I wish to thank my beloved supervisor, Dr. Lai Khin Wee for providing a define guidance and intellectual support. Dr. Belinda Murphy is willing to spend her time to teach and explain to me whenever I encountered problems. Without them, I would not be able to excel my projects successfully.

Secondly, I would like to acknowledge and express my gratitude to the Dr. Dipankar Choudhury who has provided his idea for the project. Never forgetting to thank Mr. Heamn and Prof. Dr. John George, who helped me a lot for collecting the US images of knee joint.

Last but not least, I wish to express my appreciation to everyone who has come into my life and inspired, touched, and illuminated me through their presence. I have learned something from all of you to make my project a valuable as well as an enjoyable one.

Thank you.

TABLE OF CONTENTS

LIST OF FIGURES

LIST OF TABLES

LIST OF SYMBOLS

$*$	Convolution
C	Constant for Stabilizing Equation
Λ	Diffusion Control Rate
G	Diffusivity Function
Δ	Difference of pixels by using mask
S	Estimated Gradient Threshold
D	Euclidian distance
$G(\sigma)$	Gaussian kernel function
ϕ	Generated Brightness Flow
∇	Gradient Operator
μ_x	Mean Brightness of Input Image
μ_y	Mean Brightness Output Image
σ_x	Normalized Root Mean Square contrast of the input image
σ_y	Normalized Root Mean Square contrast of the output image
R	Number of Recursion of HE methods
I_0	Original Image
I_t	Output image after t iterations
η_s	Spatial pixel neighborhood
Σ	Standard Deviation
α, β, ϕ	Shape parameters

LIST OF ABBREVIATIONS

AD	Anisotropic Diffusion
ASD	Average Structural Difference
AMBE	Absolute Mean Brightness Error
ASSF	Adaptive Speckle Suppression Filter
AWMF	Adaptive Weighted Median Filter
BBHE	Brightness Preserving Bi-Histogram Equalization
CS	Contrast Score
CT	Computed Tomography
CEDU	Contrast Enhancement Diagnostic Ultrasound
DSIHE	Dualistic sub-image histogram equalization
E	East
Ent	Entropy
EPS	Edge Preservation Score Function
FSE	Fast-Spin Echo
FP	False Positive
FN	False Negative
FOM	Figure of Merits
HE	Histogram Equalization
JSN	Joint Space Narrowing
MAE	Mean Absolute Error
MRI	Magnetic Resonance Imaging
MSE	Mean Square Error
MMBEBHE	Minimum Mean Brightness Error bio-Histogram Equalization
MMSE	Minimum Mean Square Error
MBORBHE	Multipurpose Beta Optimized Recursive Bi-Histogram Equalization

N	North
NB	Normalized Brightness
NC	Normalized Contrast
ND	Normalized Detail
NCS	Normalized Contrast Score
NPDS	Normalized Preservation of Detail Score
NPBS	Normalized Preservation of Brightness Score
NCD	Nonlinear Complex Diffusion
ND	Normalized Detail
NE	North-East
NLM	Non Local Mean
NPV	Negative Predictive Values
NOCS	Normalized Optimum Contrast Score Function
NRMS	Normalized Root Mean Square
OA	Osteoarthritis
OCS	Optimum Contrast Score function
PBS	Preservation of Brightness Score function
PDF	Probability Density Function
PD	Proton density
PDS	Preservation of Detail Score function
PES	Preservation of Edge Score
PM	Perona-Malik
PPV	Positive Predictive Values
PSNR	Peak Signal to Noise Ratio
RF	Radio Frequency
RMSHE	Recursive Mean Separate Histogram Equalization

RSIHE	Recursive sub-image histogram equalization
RLBHE	Range Limited Bi-Histogram Equalization
RSWHE	Recursive Separated and Weighted Histogram Equalization
S	South
SE	South-East
SNR	Signal to Noise Ratio
SRAD	Speckle Reducing Anisotropic Diffusion
SRHE	Sub Region Histogram Equalization
SSIM	Structure Similarity Index Measurement
TP	True Positive
TN	True Negative
US	Ultrasound
USG	Ultrasonography System
W	West
WN	West-North
WS	West-South
WTHE	Weighted Threshold HE
WCHE	Wight Clustering Histogram Equalization

CHAPTER 1
INTRODUCTION

1.1 Background

Osteoarthritis (OA) is the most common form of arthritis. The initial symptoms are characterized by joint pain, developing later as joint effusion. More than 80% of people worldwide are thought to have radiographically demonstrable OA by the age of 65 (Buckwalter & Martin, 2006). When the water content of cartilage increases due to natural aging processes, the protein level of cartilage also degrades. As a result, the cartilage covering the articular surfaces of synovial joints begins to degenerate by flaking or forming tiny crevasses. Eventually, cartilage and synovial fluid cease to function as cushioning and lubrication in the joints.

Because of the high incidence and high impact on quality of life, early diagnosis and consequently early treatment is highly attractive. MRI currently represents the "gold standard" for radiographic evidence of early OA (Farshad-Amacker, Lurie, Herzog, & Farshad, 2013). As its resolution is very high compare with other medical imaging system. However, MRI is expensive and not suitable for patients with implants. X-ray imaging emits harmful ionizing radiation, and Computed Tomography (CT) also emits ionizing radiation and is costly. Given these difficulties, ultrasound (US) is potentially beneficial in terms of cost and availability. However, it has some limitations, including the inability to detect sub-chondral bone changes. Its resolution is also poor compared to MRI imaging and its efficiency dependent on operator skill. However, US has potentiality to be a very precise tool for diagnosing early OA, if the images can be improved by image processing.

Therefore, the aim of this thesis is to improve US image processing so that US can be utilized for the early diagnosis of knee OA. In this thesis, US images of knee joint cartilage and meniscus, mainly collected from a male population, have been used as test data. The outcome of the thesis will be a novel technique for obtaining information on early OA by using Ultrasound Imaging.

1.2 Significance of the study

Presently, OA is a burden to one-third of adults worldwide, and the prevalence of this disease is higher among the elderly people (Felson DT, 1987). Oliveria et al (Oliveria SA) conducted a study to find the prevalence of OA among the people of a health maintenance organization in Massachusetts, which has revealed that OA of the knee is more prevalent than OA of other joints, and shown in the Table 1.1 Furthermore, as Table 1.1 also shows clearly, OA disease is more common in women than men. The prevalence of knee OA in different countries is also given in Table 1.2. Indeed, OA is considered as a major burden to any health care system. The yearly financial cost of knee OA and other arthritis is much higher than other chronic diseases. For example, for the treatment of arthritis, around 95 billion USD per year is spent in the United States ("CDC. Public health and aging: Projected prevalence of self reported arthritis or chronic joint symptoms among persons aged 65 years in United States, 2005-2030.," 2003). The amount excludes the cost of lost employment opportunities of patients. However, by using demographic prediction it is estimated that more than 20% of the population having an age over 60 will be affected by knee osteoarthritis by 2040 (HamermanD, 1995).

Table 1.1: Incidence of osteoarthritis in different joints(Oliveria, Felson, Reed, Cirillo, & Walker, 1995)

Women(Age)	Synovial Joint					
	Knee	Hip	Hand	Finger	Thumb	Total
20-29	0	0	0	0	0	0
30-39	5	1	0	0	0	6
40-49	22	0	11	2	8	43
50-59	30	6	21	15	8	80
60-69	74	27	40	30	23	194
70-79	106	58	53	39	30	286
80-89	33	14	10	8	5	70
All	679					

Men(Age)	Synovial Joint					
	Knee	Hip	Hand	Finger	Thumb	Total
20-29	1	0	0	0	0	1
30-39	10	2	2	2	0	16
40-49	23	4	2	1	0	30
50-59	27	3	3	3	1	37
60-69	49	16	21	16	9	111
70-79	67	36	26	17	12	158
80-89	14	6	6	5	2	33
All	386					

Table 1.2: Rate of prevalence of knee OA in different countries

Country	Years	Diagnostic Criteria	Prevalence (Ages, per 100,000)
South Africa (Davis MA, 1988)	1971-1975	Grading based on Kellgren & Lawrence criteria	Male: 20,238 (Age: 35+) Female: 30,208 (Age: 35+)
US civilian, non-institutionalized Population (I)	1971-1975	Radiographs graded according to Kellgren & Lawrence criteria; grades 3-4	Male: 3,800 (Age: 25-74) Female: 7,600 (Age: 25-74)
Lawrence Tavern, Jamaica (Lawrence JS Bremner JM, Miall WE)	1956 & 1964	Radiographs graded according to Kellgren & Lawrence criteria; grades 2-4	Male: 20,000 (Age: 35-64) Female: 28,500 (Age: 35-64)
Spanish population (L)	1998-1999	Clinical and ACR criteria	Male: 5,720 (Age: 20+) Female: 14,007 (Age: 20+)
Zoetermeer, Holland (HA, 1980)	April 1975-April1978	Radiological degenerative changes.	Male: 14,100 Female: 22,800
Sofia, Bulgaria (VT)	-	Radiographic	Male: 8,791 Female: 10,244
Karachi, Pakistan. Survey (Gibson T)	-	Clinical assessment	Male: 2,369 Female: 6,211
Japan (Tamaki M)	1979 &1986	Radiographic, joint space narrowing	Male: 12,000 (Age: 47-72) Female: 26,100 (Age: 47-72)

Table 1.2 represents the prevalence of knee joint OA among the people from different countries. From the table above, it is clear that the prevalence of knee OA

among the women is higher than men. Most patients with early knee OA are reluctant to seek a physician to obtain a diagnosis. This reluctance arises from the limited availability of diagnostic facilities and high costs involved in many clinics. For example, an MRI image costs about USD 280 in Malaysian public hospitals. Conventional X-rays are more economic but not radiation free. CTs are expensive and also use ionized radiation. However, US can overcome these limitations since it is portable, radiation free, capable of generating a real time image, and also cost effective. If the exponential increase of knee OA is to be reduced, it is necessary to detect early knee OA. If this is possible, then the increased consequence of knee OA on world health and economy may be partly averted.

1.3 Problem Statement

Although US imaging has a lot of advantages, including real time imaging, low cost, intuitive visualization, and being non-invasive, it suffers from two drawbacks, namely low contrast ratio and speckle noise which challenge the interpretation of image. For that reason, an experienced radiologist is required to inspect US images to detect early knee OA. To detect early OA using US is a big challenge for any radiologist or sonographer. However, if US images can be processed so that their contrast ratio is increased and speckle noise is reduced, then it will be more convenient for the early detection of OA (Keen, Wakefield, & Conaghan, 2009). The reluctance to obtain diagnosis of early knee OA could also be minimized since US images have a lot of benefits over other medical imaging systems, including being radiation free, suitable for a general clinical environment, painless, readily clinically accessible, low cost, non-invasive, portable (A.B A.Achim, 2001; B.Sahiner, 2008; J.S. H.D.Cheng, W.Ju,Y.Guo,L.Zhang, 2010) and bringing continuing improvement in the image quality. Real time visualization is also possible by using ultrasound. Its low contrast

ratio can be ameliorated by using Histogram Equalization (HE) (Chen et al., 2005). Likewise, speckle noise can be reduced by using anisotropic diffusion (AD)(Sun, Hossack, Tang, & Acton, 2004).

For that reason assistance has been sought improve the conventional HE method and anisotropic diffusion method to overcome their existing limitations. In the case of the conventional HE method, selecting the appropriate separating point for segmenting the histogram is the main challenge. By using the proposed HE method the optimum separating point for segmenting the histogram will be selected, so that brightness and detail preservation occur at the same time as contrast enhancement of the US image. For obtaining the optimum separating point three objective functions will be considered, namely Preservation of Brightness Score function (PBS), Optimum Contrast Score function (OCS) and Preservation of Detail Score function (PDS). Different types of artifact also make US images harder to interpret and to use in obtaining quantitative information. Noise in US images can be divided into two main components; first, thermal or electronic noise (additive noise), and second, multiplicative noise called 'speckle' (Achim, Bezerianos, & Tsakalides, 2001). Speckle is a random deterministic interference pattern in an image which is formed with coherent radiation of a medium, comprising of many sub-resolution scatterers. The superposition of acoustic echo generates an intricate interference pattern as the US pulse randomly interferes with objects of comparable size to the sound wavelength. Constructive and destructive coherent summation of ultrasound echoes produces speckle (Burckhardt, 1978). The undesirable consequence of the US image formation process in coherent US image is the speckle noise. This formation of speckle has a great impact on the US image, and leads to diagnostically important features of the US image being greatly deteriorated, and a subsequent lack of accuracy in the diagnosis of disease. For accurate diagnosis, it

is very important that the speckle noise from the US image can be reduced without compromising the important details of the image, particularly in terms of differentiating between the gradient of the edge and the gradient of the noise.

Although speckle noise is almost unavoidable in image preprocessing (since it is associated not only with transducer characteristics but also with the interrogation of a medium), it can be reduced by using an appropriate filter without compromising any of the important features of the US images. The diffusivity function, the gradient threshold and the stopping criterion control the anisotropic diffusion process. For the proposed AD method four gradient thresholds will be used instead of one, and a new diffusivity function will be proposed. It is hoped this will overcome the current limitations of the AD method. By using the proposed method for Histogram Equalization (HE) and Anisotropic Diffusion it is possible to reduce the limitations of low contrast and speckle noise of the US image. This will increase the popularity of US medical imaging as well as reduce the percentage of patients who are disabled and suffer a low quality of life due to knee OA.

1.4 Objectives

The prime objective of the thesis is to overcome the limitations (Low contrast & Speckle noise) of US imaging. To accomplish this, the following tasks will be undertaken:

i. To implement a new contrast enhancing method in US images to overcome the limitations of conventional HE methods.
ii. To find an improved AD method to overcome the limitations of conventional AD method for reducing speckle and preserving edge of US image.

1.5 Methodology

Flow chart of research Activities:

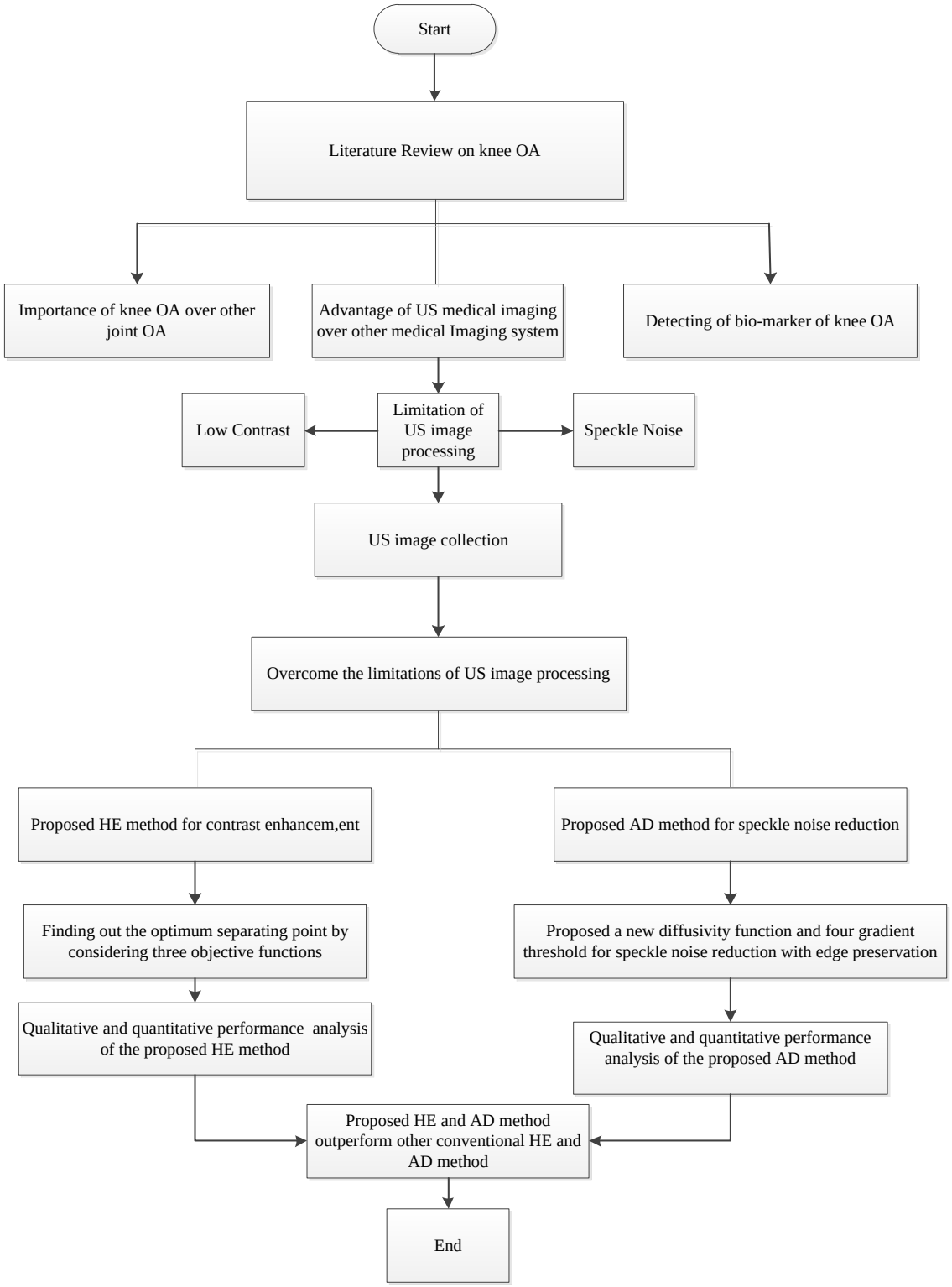

Figure 1.1: Flowchart of research Activities

Fig. 1.1 shows the flow chart of the overall research activities. Research started from literature studies and focused on both technical and clinical information related to knee

OA detection. From the literature review, it became clear that knee OA is more common than other human joint OA. Ultrasound imaging modality has been selected to encounter the problem statement mentioned at section 1.3. Nevertheless, it has two limitations include; low contrast ratio and speckle noise. For that reason, a novel contrast enhanced and speckle noise reduction method has been proposed in this thesis. A series of qualitative and quantitative analyses has been performed and we managed to conclude that our proposed methods outperform other conventional HE and AD methods.

1.6 Overview of each chapter

1.6.1 Chapter 1

Chapter 1 is the introduction of the thesis. This chapter discusses the necessity of knee OA detection. Why is knee OA is more important than other joint OA? This chapter explains the prevalence of knee OA in different countries. The problem statement of US image for detecting knee OA also has been discussed in this chapter.

1.6.2 Chapter 2

Different medical imaging modalities including their advantages and disadvantages are discussed in this chapter. The mechanism of US medical imaging has also been described; which includes the limitations of US medical imaging, relations between cartilage thickness and formation of knee OA, and biomarkers of knee OA. Technical review of different conventional HE and AD system has been mentioned in this chapter. Three controlling parameters of the AD method, namely the diffusivity function, gradient threshold and stopping criterion and their importance are explained thoroughly.

1.6.3 Chapter 3

This chapter starts with the data acquisition for the research. The difference between meniscus and cartilage in knee joints is clearly described in chapter 3. Construction of three objective functions and obtaining a final equation from these three objective

functions for HE method has been proposed. Lastly, selected performance metrics for the proposed HE and AD method are defined in this chapter.

1.6.4 Chapter 4

The qualitative analysis of the output image of cartilage and meniscus from different HE and AD methods including our proposed method has been analyzed. In addition, quantitative analysis by using numerical values of different performance metrics has been explained. Last but not least, we have concluded the chapter with the precision of the method using Fisher's Least Significant Difference Test and Duncan Test.

1.6.5 Chapter 5

Conclusion and future work has been discussed in this chapter. The limitation of the proposed HE and AD method has also been described in chapter 5.

CHAPTER 2
LITERATURE REVIEW

2.1 Background

A literature review has been carried on non-technical parts as well as technical parts. A lot of research has already been conducted on image processing for improving the quality of US images. Generally, US images suffer from two drawbacks; namely low contrast ratio and speckle noise. For increasing the contrast of the US image different Histogram Equalization (HE) methods have been used. A new HE method will be proposed that will overcome the limitations of conventional HE methods. AD filtering can also successfully remove the speckle noise, preserve the edge, small structure and region boundary if its crucial parameters are scaled accurately. The behavior of the AD filter is controlled by three parameters known as gradient thresholds, conductance function and stooping criterion. By considering the first two of these three parameters an improved AD method will also be proposed that will overcome the limitations of the conventional AD method.

2.2 Different medical imaging systems

There are different types of imaging in medical imaging systems. Among them are X-rays, Computed Tomography (CT), Magnetic Resonance Imaging (MRI) and Ultrasound (US), which are the key diagnostic imaging tools used in modern health care systems for studying illnesses.

2.2.1 Radiograph: X-Ray

Hillary et al (Hillary J. Braun a, 2012) mentioned that despite the vast development of modern imaging modalities, radiography is still the most popular medical imaging system in the evaluation of knee osteoarthritis. Generally, the

evaluation of knee joint is performed by using the extended-knee radiograph, which is a bilateral anterior posterior image, It is acquired with weight-bearing patients having both knee in full extension, Wilson et al (Wilson, 2009) has shown that X-ray imaging has traditionally used film to capture the images. The formation of the images is dependent on absorption of X-rays by structures of the body. The X-rays that are not absorbed pass through the body and strike a film behind the area of the body. The light and radiation sensitive film is sandwiched between two intensifying screens enclosed in a light proof cassette. The screens convert the X-ray radiation into light, which acts in the film. The film is then developed using chemicals, in the same way as for a photograph. The film can then be placed on a light box to be viewed, and a diagnosis made. Currently, flexed-knee radiographs having various degree of X-ray bean angle and flexion have been used for improving intra articular visualization. For evaluating joint space narrowing (JSN) and the formation of osteophyte radiographs are useful. The grading schemes, namely the Kellgren-Lawrence grading scheme and the established guidelines of Osteoarthritis Research Society International Classification Score are popular for the diagnosis of knee osteoarthritis progression. A.J. Teichtahl, et al. (A.J. Teichtahl, 2008) determined that JSN, a continuous measure, has been employed as the outcome in studies of disease progression in knee osteoarthritis.

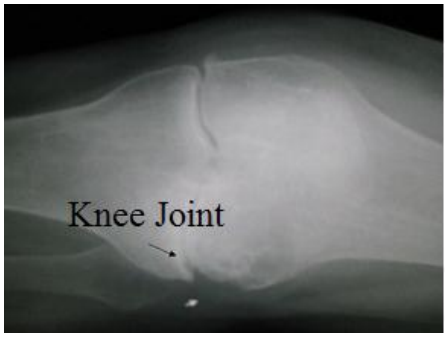

Figure 2.1 X-ray image of right knee

Fig 2.1(Source: http://en.wikipedia.org/wiki/Osteoarthritis') shows the x-ray image of right knee joint.

2.2.2 Computed Tomography (CT)

Computed Tomography (CT) uses cross-sectional images created multiple scans in order to produce images of articular cartilage almost in real time. The endoscope is placed at the cartilage at the time of endoscopy. It provides quantitative information on the progression of disease, including information on structural changes in collagen as a result of acute trauma or degenerative osteoarthritis. A computer assembles data from the images to produce a resultant high resolution image in three dimensions. Here *tomos* means "slice", and *graphein* means "write" (Evans, Godber, & Robinson, 1994). As it combines slices of images together to obtain the resultant image.

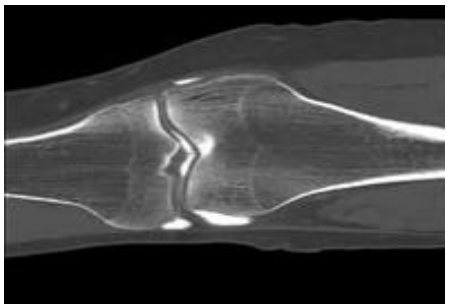

Figure 2.2 C.T. image of right knee

Fig2.2.(Source:https://www.radiology.wisc.edu/sections/msk/interventional/Knee_CT_arthrogram/index.php) shows the C.T. image of right knee joint. The knee OA detection of C.T. imaging has the same potentiality as the X-ray imaging as it generated from several finely focused X-ray together.

2.2.3 Magnetic Resonance Imaging (MRI)

MRI is an imaging modality that produce images of structures and organ inside the body by using pulse echo radio wave energy and a magnetic field. For imaging,

firstly the magnet of MRI scanner will create a magnetic field. The patients are then passed through this magnetic field. The human body consists of 70% water. The hydrogen atoms of water make up their individual magnetic field, this field is affected by the stronger magnetic field created by the magnet of MRI scanner. This causes the change of direction of the spin or magnetic moment of the atoms. This is then accompanied by a radio frequency pulse which makes the spins align and spin at Larmour Frequency. These data are collected by a computer and processed to create an MRI image. Magnetic Resonance Imaging (MRI) imaging is very popular as it gives a very high resolution image. According to (Hillary J. Braun a, 2012) image contrast is manipulated by MRI to highlight different types of tissue. Common contrast methods include proton density (PD), 2D or multi-slice T1-weighted and T2-weighted imaging. For evaluation of focal cartilage defects, spin echoes and fast-spin echo (FSE) imaging techniques are very useful. More recently, the use of turbo-spin or fast-echo imaging, water excitation and fat saturation has seen enhanced contrast.

Scoring takes place through one of a number of existing systems, mostly employing semi-quantitative and morphological measures. The modified outer bridge scale is used for cartilage defect geometry, and whole-organ assessment is used to assess cartilage articulation as a whole. This latter method has proved to be specific, reliable, and able to monitor lesion progression. Amongst these, the Knee Osteoarthritis Scoring System, the Boston Leeds Osteoarthritis Knee Score and Whole-organ Magnetic Resonance Imaging (MRI) Score, are commonly used (Hunter et al., 2008).

Besides, L. Menasheyz et al (L. Menashe yz, 2012) has examined the performance of MRI for diagnosis of knee OA. By using different parameters such as positive and negative predictive values (PPV, NPV), specificity, positive and negative likelihood value, sensitivity and accuracy MRI is able to differentiate between subjects having

knee OA or not. All the results gathered by using true negative (TN), true positive (TP), false negative (FN) and false positive (FP) is termed as 'overall sensitivity' used for OA detection. MRI is considered as the gold standard for knee OA detection. (Source: http://www.physiopedia.com/Diagnostic_Imaging_of_the_Knee_for_Physical_Therapists)

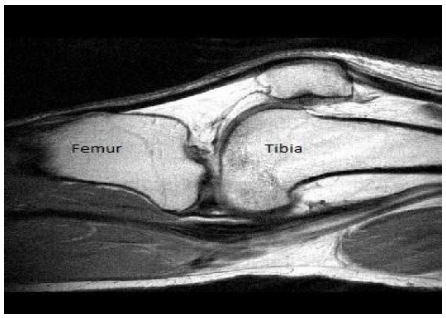

Figure 2.3 MRI image of right knee

Fig.2.3.(Source:http://blog.remakehealth.com/blog_Healthcare_Consumers0/bid/8031/What-does-an-MRI-Scan-of-the-Knee-show) shows the MRI image of right knee joint. The contrast ratio is high, not affected by speckle noise. The edge of tibia and femur are easily detectable and the cartilage layers are very clear.

2.2.4 Ultrasound

A.J. Teichtahl et al (A.J. Teichtahl, 2008) stated that ultrasound is widely employed to provide imaging guidance for procedures such as intra-articular injection and biopsy for both the investigation and treatment of joint arthropathies. Thus, US is helpful for detection of early osteoarthritis even without other clinical. Łukasz Paczesny et al (Łukasz Paczesny, 2011) states "a reliable knee ultrasound examination requires devices with modern software and high-frequency probes". The probe frequency will depend on the structure, but in general it will be between 7 and 10MHz, with the upper end providing finer detail. Even higher frequencies, that is, approximately 13 MHz will help to produce a "soft image" with high level of detail. This is because almost all

tissues around the knee that are examined by ultrasound are located superficially; the need to use lower frequencies is limited to visualization of popliteal fossa and cruciate ligaments. Besides, linear probe is a standard for musculoskeletal sonography and this does not change in the knee. However, there are some specific situations, such as visualization of the deeply located cysts in the popliteal region or posterior cruciate ligament assessment, when convex, lower frequency probe (approximately 5 MHz) fits better. Color Doppler and Power Doppler technique can be useful in complete knee ultrasound diagnostics. It allows for the assessment of the vascularization of soft tissues thus enhancing diagnostic possibilities in arthritis, tendinitis, tumors, and in the monitoring of the healing processes. Henning Bliddal et al. (Hillary J. Braun a, 2012) determined that the transducer frequencies of ultrasound systems higher than 12 MHz produce sectional imaging with axial and lateral resolution which is less that 200 mm. This allows ultrasound a perfect imaging modality to evaluate soft tissues surrounding different joints. By using Doppler technique it is also possible to detect inflammatory hyperemia as well as to quantify. Ultrasound is able to produce sound waves. These sound waves are passed through the body, producing return echoes, these echoes are collected by the transducer to produce visualize structure of body beneath the skin. The ability of transducer to measure difference among the echoes reflected from various tissues of the body allows an US image to be captured. The ultrasound technology is especially suitable for observing accurate interference between fluid filled and solid spaces. Unfortunately, the performance of ultrasound is not same for all joints. It differ from one joint to another as well as one part of joint to another part. This causes as, changes of depth of penetration will change the speed of ultrasound echo. For example, the femoral articular cartilage of any kind can be investigated with ultrasound, whereas it is almost impossible in case of tibial cartilage (Bliddal, Boesen, Christensen, Kubassova, & Torp-Pedersen, 2008).

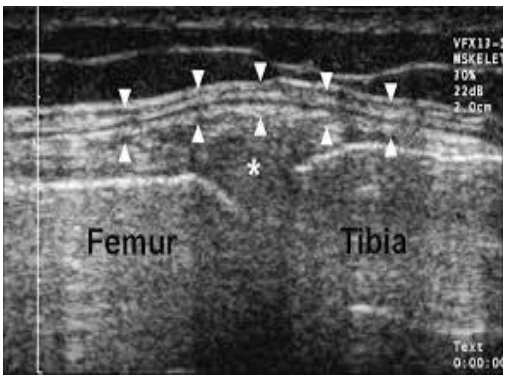

Figure 2.4 US image of right knee

Fig. 2.4 (Source: http://imaging.birjournals.org/content/14/3/188/F12.large.jpg) shows the US image of right knee joint. It is highly affected by speckle noise. The edges are fully undetectable.

Table 2.1 Comparison of different medical imaging for OA assessment

MRI	X-RAY	C.T.	ULTRASOUND
High resolution image.	Ionizing radiation	Painless and non invasive.	Non-ionizing radiation
Non ionizing radiation.	Available.	Higher level of radiation	Cost effective.
Expensive.	High risk of getting cancer.	Complication undetectable	Portable
Non-implanted patients.	Wavelength: (0.01 ~ 10) nanometre	Not suitable for detecting inflammation or infection.	No need for special environment
Claustrophobia.			Applicable to any patients
			Real time imaging. Painless.

2.3 Procedure of US scanning protocol

The process of imaging with ultrasound is based on the reflection of sound waves. The sound wave which passes through the body, reflects back to the ultrasound machine in various ways depending on the characteristics of the sounds and the medium. The reflected waves register as a function of time, and the duration between releasing a pulse and receiving an echo exposes the depth of the tissue interference of the reflected objects. The information on the acoustic properties of the objects is obtained from the

intensity of the echo objects. By using the received echo signal the US images are constructed.(Source;http://www.physics.utoronto.ca/~jharlow/teaching/phy138_0708/lec04/ultrasoundx.htm). To enhance the diagnostic utility of ultrasound images, contrast agents have been developed. These contrast agents are injectable suspensions of gas bodies that provide strong echoes from poorly echo genetic blood–filled regions as they circulate in the blood. Contrast enhancement diagnostic ultrasound (CEDU) is described in Douglas et al. (Douglas L. Miller, 2011) and has been used for the examination of, kidney, Liver and other organs. The experiments by Scott et al. (Scott B. Raymond, 2008) showed the enhancement of ultrasound in case of the delivery of small fluorescent agents and large biological immunotherapeutic for transgenic mouse models carrying Alzheimer's disease. It was also described by William et al. (William J. Tyler, 2008) that US has the ability to modulate neuronal activity . For accomplishing this firstly it is needed the temporary suppression of spontaneous activity then US transmission through the crayfish ventral nerve cords (Gavrilov LR, 1996). The ultrasound guided method by Amanda et al. (Amanda Shanks Huynh, 2011) has concluded that US is more suitable for examining the influence of immunotherapy on tumor growth compare to the subcutaneous model. As US is a rapid imaging technique, so by using ultrasound-guided HIFU it may possible to monitor real time tissue responses (Tinghe Yu, 2011), as a result it decreases untoward lesions (G, 2007; JE, 2005). CT and MRI biopsies do not offer a real time image update but, based on fundamental B-scan ultrasound image guided biopsies, it is possible to perform real time image guided biopsies (Ernst Michael Jung, 2012).

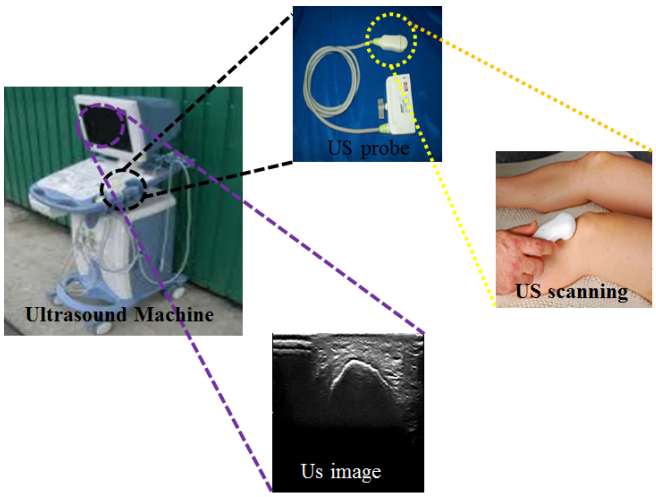

Figure 2.5 Procedure of Image scanning by US machine

The steps of US image scanning are shown in Fig. 2.5. US images were taken from different positions of the probe. The lateral side of the knee joint has been imaged because by using this side, it was possible to better observation of the cartilage of the knee joint. A 8MHz probe was used, as a high frequency probe can give a better resolution of US image. With a high frequency, the wavelength will be smaller; smaller imaging particles become detectable by using a higher frequency US probe. For the US imaging of knee joint, notch was very important because the probe would be placed beside the patella by using notch.

2.4 Problems with US medical imaging system

Though US imaging has a lot of advantages it suffers from two drawbacks, namely speckle noise and low contrast ratio (O.Michailovich, 2006; P.M.Shankar, 2006). Low contrast is a major problem of US imaging. For enhancing contrast of the US image, contrast enhancing gel is used. But still the contrast of the US image is very poor. The low contrast of the US image is due to the mechanism of US imaging. It depends upon the properties of the echo signal. Contrast of the US image can be enhanced by using post processing in US images. Histogram Equalization (HE) is very

popular for contrast enhancement of the US images as it is very simple and effective. However, the conventional HE method has some limitations. In this thesis a novel contrast enhancement method will be used that will overcome the limitations of the conventional contrast enhancing method.

Speckles occur in US images when a non-coherent detector and a coherent source are used to interrogate a medium having a rough surface on the scale of the typical ultrasound wavelength. US speckle noise generally occurs in soft organs such as the liver or kidney, as the underlying structure of these organs is very small compared to the large wavelength (L.C.Gupta, 1998) of ultrasound. Speckle noise generally consists of a high gray level of intensity which qualitatively ranges from hyperechoic (bright) to hypoechoic (dark) domains. They are more granular at low frequency than at a high frequency. There are many factors associated with speckle noise, including the phase sensitivity of a transducer, the number of scattered beams, and their coalition, the distance between objects and the transducer, and the transducer frequency (D. Adam, 2006). The consequence of speckle noise (A.K.Jain, 1989) is a poor image quality, including ruined spatial and contrast resolution. It also reduces the signal to noise ratio (SNR), the peak signal to noise ratio (PSNR), the structure similarity index measurement (SSIM), the edge preservation index, and increases the mean square error (MSE). However, speckle sometimes holds some useful information in US images, which is obscured due to the low resolution and contrast. Therefore it is highly desirable to reduce speckle noise without compromising any of the important features of the US images (C.B.Burckhardt, 1987; F.Zhang, 2007b).

There are two basic techniques for reducing speckle noise (Navalgund Rao, 2002) from ultrasound images: a) compounding approach, and b) post-processing approach (Adam, 2006). The compounding approach involves modifying data acquisition by generating a

single image from a number of images focused in the same region (Behar, 2003; Jespersen, 1998; Stetson, 1997; Trahey, 1986). On the other hand, the post-processing approaches include a variety of filtering techniques for image processing to reduce speckle from US images. The compounding approach is much more expensive compared to the post-processing approaches. Filtering techniques are post-processing approaches which will be mainly discussed in our thesis. Filtering techniques have proven to be useful for reducing unwanted speckle and enhancing image quality. There are two basic types of filtering techniques available in the literature, namely linear filtering and nonlinear filtering.

Linear filtering approaches (A. Lopes, 1990; D.T. Kuan, 1987; J. S. Lee, 1986; X. Hao, 1999) applied in early speckle suppression systems. However, linear methods had some limitations such as suppression being accomplished at the cost of significant smoothing of structural details, and a lack of balance between edge preservation and noise reduction. Non-linear filtering methods were found to be more successful as they were able to overcome the limitations of linear filters. A number of research studies have investigated the improvement of the nonlinear filtering approach. The improvement of the US image filtering method for speckle reduction is a continuous process. Different techniques (multi look method, spatial averaging, and homomorphic filtering) are being used for suppressing the speckle of US images. Among them, the AD method is the most popular method for suppressing the speckle of the US image (Ovireddy & Muthusamy, 2014). However, it suffers from some drawbacks such as having to make a compromise between speckle noise reduction and edge preservation during noise suppression. In this thesis, a new anisotropic diffusion (AD) method will be proposed by considering its three parameters known as the diffusivity function, gradient threshold

and stopping criterion, which together control the efficiency of the AD method. The proposed method will overcome the limitations of the conventional AD method.

2.5 Relationship between cartilage thickness and formation of OA

Cartilage loss is the main feature of the knee OA. By using MRI it is possible to directly visualize the articular hyaline cartilage. Assessments of cartilage morphology from knee MRI are emerging as promising measures for monitoring OA disease progression (Eckstein F, 2006). Knee alignment is also associated with the progression of knee OA. By using joint space narrowing it is also possible to determine the stage of knee OA. But this is not possible due to cartilage quantification being as yet imprecise through medical imaging. By using medical imaging systems, it is however possible to detect a small change of the cartilage of the knee joint, if image processing is accomplished on the captured US images. A few investigators have reported that 4-8% of cartilage loss occur due to OA progression in each year(Eckstein F, 2006).

2.6 Biomarkers of knee OA

To diagnosis knee OA radiographs are very helpful. The OA affected knee joints are characterized as follows. (1) With the progression of knee OA, cartilage will be wear away, as a result joint space between knee bones will be narrower. (2) Since cartilage will be destructed, the body will attempt to repair the knee joint, therefore fluid-filled cavities or cysts will be formed. (3) Due to knee OA progression, cartilage will be reduced, therefore knee bone will rub against each other, consequently creating friction and uneven joints. (L.J. Bremner JM, Miall WE, 1968).

2.7 Benefits of US medical imaging over other medical imaging system

X-ray and CT are involved with ionized radiation and MRI is contra-indicated for patients with metallic implants and patients having claustrophobia. C.T. exposes the

patient to higher levels of radiation and is limited to the detection of complications such as fracture. Though MRI gives high resolution images it is costly and time consuming.

On the other hand, US is free from these limitations. US is a very popular diagnostic tool capable of accessing patients without any restrictions, being painless, low cost, non-invasive, and portable (A.Bezerianos A.Achim, 2001; B.Sahiner, 2007; J.Shan H.D.Cheng, W.Ju,Y.Guo,L.Zhang, 2010). Most importantly, it provides real time imaging which is not possible by using most other medical imaging systems. V.P. Subramanyam Rallabandi et al (Rallabandi, 2008) mentioned that in the case of CT and MRI, it is required to inject a blood pool contrast agent, which gives less spatial image resolution and it has a low volumetric imaging speed for laymen visualization of large vessels, a limitation on the utility of CT and MRI. US is easy to operate. Its potentiality is high, for example, its resolution is as high as MRI for soft tissue (T. Marshburn, 2004; V. Noble, 2003). High frequency sound ranges from 20 kHz up to the several GHz used in US imaging (K., 2002). In case of remote areas MRI, CT and X-ray facilities are almost impossible. In these areas only US medical imaging system can be easily provided for diagnosis, because US probes are portable and easy to carry.

For the above mentioned reasons the use of US is growing at least at a rate of 8% per year. On 2009-10, 34.4% of the total diagnostic imaging methods used were ultrasound-based. In the financial year of 2005-06 the total service by the ultrasound images was 4,716,304, and in 2009-2010 it was 6,251,413. (Source: Date of processing Medicare data, Australia) ("Medical Benefits Reviews Task Group Diagnostic Imaging Review Team Department of Health and Ageing February 2012 Review, Australia,"). In Malaysia, ultrasound machines have been widely used in hospitals. They are used for imaging of the uterus, ovaries, pelvic organs, and for the presence of a foetus via the

abdomen. Recently, ultrasound machines are becoming popular for the imaging of joints such as knees or hips. From National Medical Device Statistics of 2009, US machines are widely available in the country, with the higher numbers in the public (62.7%) rather than in the private sector (37.3%). Overall, Selangor and Putrajaya reported the highest number of ultrasonography systems (USG) (130), followed by Johor (74) and Kedah (60), in contrast to Perlis, Melaka and Terengganu which recorded 7, 9 and 18 devices respectively. From these statistics, it appears that the application of US procedures has been positively received by Malaysia. New developments and research into US applications will possibly increase these statistics further.

2.8 Technical Review of HE and AD method

In case of contrast enhancement, (HE) is very popular as it is very simple and effective. But conventional HE has some limitations, such as there being a mean shift of the output image. The brightness preservation and detail preservation does not occur at the same time during the contrast enhancement. Either brightness or detail preservation occur during contrast enhancement. So the aim of our proposed method will be to preserve brightness and details during the contrast enhancement of the US image.

On the other hand, in case of a conventional AD method, its effectiveness depends on the ability of the diffusivity function that will differentiate between the gradient of edge and gradient of noise, the gradient threshold parameters and diffusion stopping criterion. So for improving the efficiency of the proposed AD method a new diffusivity function as well as four gradient thresholds instead of one will be considered for effective edge preservation and successful noise reduction.

2.8.1 Review of existing contrast enhancement system

The conventional HE (Lau, 1994) method is described as follows:

If the input image is $X(i,j)$, total number of pixels are n in the gray scale level ranges from $[x_0 - x_{N-1}]$. Then the probability density function Pr_l for level of r_l is defined as

$$Pr_l = \frac{n_l}{n} \quad (2.1)$$

Here, n represents the total number of pixels in the image and n_l is the frequency of the occurrence of the level r_l in the input image and $l = 0,1, \ldots \ldots, N-1$. The histogram of the image is defined as plot of n_l against r_l. The cumulative density function is given by

$$C(r_l) = \sum_{i=0}^{l} Pr_i \quad (2.2)$$

Histogram Equalization is then used to map the image into the entire dynamic range $[X_0 - X_{N-1}]$. It is done by using the cumulative density function, shown as the following equation

$$f(X) = X_0 + (X_{N-1} - X_0) * C(r_l) \quad (2.3)$$

which flattens the histogram of an image and causes a significant change in the brightness.

The equation of the output image of the HE is $Y = \{Y(i,j)\}$, which can be expressed as

$$Y = f(x) = \{fX(i,j) \mid \forall X(i,j) \in X\} \quad (2.4)$$

A new brightness preservation method based on HE, named Brightness Preserving Bi-Histogram Equalization (BBHE), was proposed by Kim (Kim:, 1997). Based on the threshold of separation of the input histogram, different types of bi-histogram equalization methods can be proposed. The input image X can be decomposed into two sub-images, $X_L$and X_U, based on the threshold of separation. If X_T is the threshold of separation then $X_T \in \{X_0 X_1 \ldots \ldots X_{N-1}\}$. From this, the following can be obtained:

$$X = X_L \cup X_U \quad (2.5)$$

where

$$X_L = \{X(i,j) | X(i,j) \leq X_T, \forall X(i,j) \in X\}$$

and

$$X_U = \{X(i,j) | X(i,j) > X_T, \forall X(i,j) \in X\}$$

Thus the PDF of the sub-image X_L and X_U can be written as

$$P_L(X_K) = \frac{n_k}{n_L}, \qquad k = 0,1, \dots \dots \dots T \tag{2.6}$$

and

$$P_U(X_K) = \frac{n_k}{n_U}, \qquad k = T+1, T+2, \dots \dots L-1 \tag{2.7}$$

where the number of X_K in X_L and X_U is represented by n_k. n_L is the total number of sample in X_L, and n_U is the total number of sample in X_U. Thus, the cumulative density functions of X_L and X_U are defined as

$$C_L(X_K) = \sum_{k=0}^{T} p_L(X_K) \tag{2.8}$$

and

$$C_U(X_K) = \sum_{k=T+1}^{L-1} p_U(X_K) \tag{2.9}$$

In HE, the cumulative density function acts as a transform function. Like HE, the cumulative density function of each sub-images is

$$f_L(X_k) = X_0 + (X_T - X_0) C_L(X_K), \quad k = 0,1, \dots \dots \dots, T \tag{2.10}$$

and

$$f_U(X_k) = X_{T+1} + (X_{L-1} - X_{T+1}) C_U(X_K), \quad k = T+1, \dots \dots \dots \dots \dots, L-1 \tag{2.11}$$

In BBHE, the threshold of the separating point (X_T) is the mean brightness of the input image. By using this process, it is possible to preserve the image original brightness which is not possible if using conventional HE.

DSIHE (Dualistic sub-image histogram equalization) has been proposed by Wan et al.(Yu W, 1999), which is the extension of BBHE. It functions by selecting the threshold separating point at the median of the histogram. DSIHE has been proven able to outperform BBHE in terms of brightness preservation and entropy. However, both BBHE and DSIHE may fail to enhance and preserve their original brightness under certain conditions. MMBEBHE (Minimum mean brightness error bio-histogram

equalization) was proposed by Chen and Ramli (Soong-Der C, 2003b), which is the extension of BBHE, in which the yield minimum difference between input and output mean is known as Absolute Mean Brightness Error (AMBE). However, this method is also not free from undesirable effects. After that, Chen and Ramli proposed RMSHE (Recursive Mean Separate Histogram Equalization) (Soong-Der C, 2003a). It functions by recursively making partitions of the given image histogram. Each segment is equalized independently and the contrast enhanced output image is achieved by the union of all the segments. A similar method, named Recursive sub-image histogram equalization (RSIHE), was proposed by Sim et al. (Sim KS, 2007). The difference between RMSHE and RSIHE is that, in the case of RMSHE, the mean is used as the separating point, whereas median is used as the separating point in case of RSIHE. Next, Weighted Thresholded HE (WTHE) (Wang Q, 2007) was also proposed. It can control the enhancement process by using an adaptive mechanism. It has two merits; viz. ease of control and ability to adapt to different images. There are also two more weighing techniques; are Recursive Separated and Weighted Histogram Equalization (RSWHE) (Kim M, 2008) and Weight Clustering Histogram Equalization (WCHE) (HK., 2008). SRHE (NSP, 2009) (Sub Region Histogram Equalization) was proposed by Ibrahim and Kong. In this method, a Gaussian filter is used for partitioning the input image. Recently, Zuo et al proposed RLBHE (Range Limited Bi-Histogram Equalization) (Zuo Chao, 2012). A threshold which can minimize the intra class variance is used as the separating point for RLBHE. However, the above mentioned methods only consider one of the characteristics of the image while neglecting the others. For example, BBHE, MMBEBHE, RMSHE and RSIHE only consider on brightness preservation and pay less attention on detail preservation. On the other hand, the clipping methods of ‘Kim et al.’ and ‘Seungjoon et al.’ (Kim T, 2008; Seungjoon Y,

2003) only focus on detail preservation while neglecting the importance of brightness preservation.

The aim of the thesis is to propose a HE method which can preserve the brightness and detail while enhancing the contrast of the image, which can be done by using the Multipurpose Beta Optimized Recursive Bi-Histogram Equalization (MBORBHE) method. For this reason three objective functions named Preservation of Brightness Score function (PBS), Optimum Contrast Score function (OCS) and Preservation of Detail Score function (PDS) will be considered. By using these three objective functions we will find the optimum separating point for segmenting the histogram of the input image. This method improves the traditional method used in HE, where histogram equalization emphasizes only one criterion but ignores the others. The motivation of this work is to produce a more comprehensive and natural output image by taking all properties into account.

2.8.2 Review on existing speckle reduction methods

A suitable method of speckle reduction is one which enhances the value of signal to noise ratio while preserving the lines and edges of the image. Gaussian noise is an additive noise, whereas speckle noise is in multiplicative form (Tur, Chin, & Goodman, 1982).

$$v = u.n \qquad (2.12)$$

Where *u* denote the image to be recovered. *v* is the corrupted image and *n* is the speckle noise. The recovery of speckle noise is much harder than the recovery of conventional Gaussian additive noise. The reason of this is that speckle noise is signal correlated as well as its distribution being much more complicated compared with additive Gaussian noise.

Temporal averaging (Fuk-kwok, 1983) is the first widely used speckle reduction method for US images. This method is based on averaging multiple uncorrelated frames of the same scene to prevent the speckle effect. Though this method was very simple and fast, it produced blurry images and detail was lost. To overcome this, Loupas et al (Loupas, McDicken, & Allan, 1989) proposed a speckle reduction filter which was named the adaptive weighted median filter (AWMF). In this method weight median is used for suppressing the speckle noise. By using local statistics for each pixel smoothing characteristic and weight coefficient is adjusted. After that, the adaptive speckle suppression filter (ASSF) was proposed by Karaman et al(Karaman, Kutay, & Bozdagi, 1995). It was also based on the local statistics of the pixel. By using appropriate size and shape of the local filtering kernels filter adaptation was achieved. After that Czerwinski et al.(Czerwinski, Jones, & O'Brien, 1999) proposed a 'stick' method which will detect the tissue boundaries and suppress speckle noise. On the other hand another group of researcher has proposed some other speckle reduction filters such as Box filter (F.-K. Li, Croft, & Held, 1983), Median filter, Lee filter (J.-S. Lee, 1980), Frost filter(Frost, Stiles, Shanmugan, & Holtzman, 1982) and Kuan filter (Kuan, Sawchuk, Strand, & Chavel, 1987).

A box filter is a conventional Low pass filter. It can smooth the details (such as edge and point) and remove the noise of high frequency spectrum. It is a simple average filter. A median filter is effective for speckle reduction. The use of median intensity of a properly shaped and sized filtering window which surrounds the central pixel acts as the output of the target pixel. It can successfully reduce noises whose size is less than half of the filtering window. As filtering window size determines the rate of smoothing in case of median filter, it sometimes removes some high frequency signals which lead to

blurring the edge of the image. This filter also undermines the effectiveness of despeckling as it does not consider the statistical characteristic of speckle.

In the case of Lee filter, for filtering multiplicative noise, additive noise and the mix of the two, it uses minimum mean square error (MMSE) for designing. By a weighted average based on the variance and mean of sub-region, its output is estimated. In the case of the frost filtering method it is designed by using an exponentially damped convolution kernel adapted to image fine details. Based on the local statistics its output is calculated. Lee and frost filter are also called statistical adaptive filters as they take into account the statistical characteristics of speckle. The Kuan filter is similar to the Lee filter but its weighting function is different from the Lee filter. The performance of these filters is better but they have to compromise between smoothing in homogeneous regions and preserving edges or sharp features of the original image.

The Non Local Mean (NLM) filter (Buades, Coll, & Morel, 2005) uses a high degree of redundancy in the original image for denoising. It is a weighted Gaussian filter. As it uses region comparison, it performs better in sharp edge preservation and Gaussian noise suppression. But it does not show good result in the case of US imaging as speckle in US imaging is subject to Rayleigh distribution.

Perona-Malik proposed a new definition of scale-space through Anisotropic Diffusion (AD) (P. Perona, 1990) which is based on a non-linear partial differential equation based diffusion process. It has recovered the demerits of linear smoothing, for example, blurring the edge and eliminating important detail during speckle noise reducing process. After that Yu and Acton (Y. Yu, Acton, S.T., 2002) used statistical method to analyze speckle suppression and proposed Speckle Reducing Anisotropic Diffusion

(SRAD). It is space-variant and nonlinear filter. This method reduces speckle by applying isotropic diffusion in homogeneous region and preserves edges by stopping diffusion across the edges. This obtains a balance between speckle reducing and edge preserving. Though this method is better, sometimes the SRAD based method generates visually disappointing output when they are applied to filter primary noise contained in US images, which is assumed to be Gaussian distribution. After that Zhang et al (Zhang, 2007) proposed LPND (Laplacian pyramid nonlinear diffusion). This method is able to control the diffusion process more precisely and give the better result compare to SRAD method. In this method to decompose the image into different sub-band Laplacian pyramid has been utilized as a multi-scale analysis tool. After that, for suppressing noise from each sub-band, anisotropic diffusion with different diffusion flux has been used. But this method has also some limitations such as it is sensitive to several key parameters. Due to the adopted model of the speckle, this approach was not very robust. For the speckle reduction of optical coherence tomography image, Gilboa et al. (G.Gilboa, 2004) proposed nonlinear complex diffusion (NCD) method. It combines the property of both forward and reverse diffusion and removes the limitations of conventional Peroma-Malik model. The Perona-Malik model has a lot of practical and theoretical demerits. Catte et al.(F.Catte´ 1992) has proved that the diffusivity functions of Perona-Malik are ill posed. In the case of noisy images the gradient generated by the image features is comparable to the gradient generated by the noise. As a result in this case, the conditional smoothing does not reduce the noise effectively rather than in case of some images it enhances the noise. It has also no contribution in preserving the edge as gradient of image are comparable to the gradient of noise. AD filtering can successfully smooth the noise and preserve the edge along with small structures and region boundaries if its crucial parameters are scaled accurately. The behavior of the AD filter is controlled by three parameters known as gradient threshold perimeters,

diffusivity function and stooping criterion. If the gradient threshold is overestimated then the resultant image will be over smoothed. On the other hand, its noise reduction ability will degrade due to underestimation of the gradient threshold. Therefore, selecting suitable gradient thresholds is very important for getting better resultant images. In AD several conductance functions can be used, and different conductance functions will differentiate the filtering results, which is shown in Black et al. (Black, Sapiro, Marimont, & Heeger, 1998). For improving the performance of the AD method it is important to choose an appropriate conductance function and scale it in such a way so that it preserves the edge efficiently. It is also necessary for the gradient threshold parameter will be decreasing function of time, which is depicted in (X. Li & Chen, 1994). In this way, it can preserve edge above a certain decreasing threshold. Our method has been proposed by considering the gradient threshold parameters and the diffusivity function.

There are wide range of applications of anisotropic diffusion (Gerig, Kubler, Kikinis, & Jolesz, 1992; K.Z.Abd-Elmoniem, 2002; Krissian & Aja-Fernández, 2009; Krissian, Westin, Kikinis, & Vosburgh, 2007; Mittal, Kumar, Saxena, Khandelwal, & Kalra, 2010) in the field of biomedical imaging. The goal of our thesis is to make the optimum choice and scale of the diffusivity function of the AD method to get a better quality of output image. Estimating the gradient threshold parameters is also considered for effective noise reduction and edge preservation of the US image.

2.8.3 Anisotropic diffusion (AD) model

Perona and Malik (P.Perona, 1990) first proposed the following non-linear diffusion model for speckle reduction or smoothing image in the continuous domain.

$$\begin{cases} \frac{\partial I}{\partial t} = div[g(|\nabla I|).\nabla I] \\ I(t=0) = I_0 \end{cases} \quad (2.13)$$

Here *div* is the divergence operator. **∇** is the gradient operator. ‖ indicate the magnitude, $g(|\nabla I|)$ is the diffusion coefficient or edge stopping function. I_0 is the original image. Anisotropic diffusion method will reduce the noise of the original image and make the image smoother. Diffusion is encouraged in the homogeneous region and discouraged across boundaries with step gradients. Perona and Malik suggested two diffusivity function.

$$g(|\nabla I|) = \frac{1}{1+(|\nabla I|/k)^2} \quad (2.14)$$

and

$$g(|\nabla I|) = \exp[-(|\nabla I|/k)^2] \quad (2.15)$$

Where the edge magnitude parameter is denoted by *k*. It has a vital role to differentiate the gradients generated by edges and those by noise.

In the case of the anisotropic diffusion method, the gradient magnitude $|\nabla I|$ is used as the edge detector. It is used to detect an image boundary or edge as a step discontinuity. When $|\nabla I|$ >>k, than $g(|\nabla I|) \rightarrow 0$ it will be all pass filter and diffusion flux is suppressed and when $|\nabla I|$ <<k, then $g(|\nabla I|) \rightarrow 1$, it will be Gaussian filtering and the diffusion flux will be encouraged. In fact *k* serve as a threshold for the diffusion process if the value of *k* is larger, smoother homogenous region will be produced and vice versa. The discretization form of Perona and Malik model is as follow

$$I_{t+1}(s) = I_t(s) + \frac{\lambda}{|\eta_s|}\sum_{p\epsilon\eta_s} g_k(\left|\nabla I_{s,p}\right|)\nabla I_{s,p} \quad (2.16)$$

Here, discretely sampled image is denoted by I_t, pixel position in the discrete 2-D grid is indicated by *s*, the iteration steps are *t*. *k* is the gradient threshold parameter and *g* is the conductance function. $\lambda\epsilon(0,1)$ controls the rate of diffusion, η_s represent the spatial 4-pixel neighbourhood of pixel *s*. Here $\eta_s = \{N, S, E, W\}$ where *N*,*S*,*E* and *W* are North,

South, East and West neighborhood of pixel *s*, respectively. As a result $|\eta_s|$ is equal to 4. The symbol ∇ denotes the gradient operator of continuous form. It also represent a scalar defined as the difference between the center and neighboring pixel of each direction.

$$\nabla I_{s,p} = I_t(p) - I_t(s), \qquad p \epsilon \eta_s = \{N, S, E, W\} \tag{2.17}$$

Though Perona and Malik's model is very popular, it suffers from two practical and theoretical drawbacks. The first one is very obvious and every researcher will raise questions about it. If the signal is noisy with white noise then it will introduce very large, unbounded oscillation of gradient ∇I. In this case the conditional smoothing proposed by the model will not work as these noise edges will be untouched. However, Perona and Malik's model also proposed to include some low pass filters for smoothing the image before applying the diffusion equation. The drawback of this is introducing a new parameter in the method (low pass filter). On the other hand it seems to adopt again what it tried to avoid, introducing a non-adaptive filter which causes the loss of the edge preservation(Black et al., 1998).

The second drawback arises from the diffusivity functions type of $g(p) = e^{-p}$ or $g(p) = (1 + p^2)^{-1}$. For these functions, no correct theory of (2.13) is available. For obtaining both uniqueness and existence of the conductance function *g*, it has to be verified so that *pg(p)* is non-decreasing. If it is not non-decreasing then the process will become unstable. Now the reason that the Perona-Malik model is unsuitable if *pg(p)* is non-increasing will be explored. Firstly it will be considered in case of one-dimensional signal. In that case the Perona Malik equation will be

$$\frac{dI}{dt} - (g(I')I')' = 0 \tag{2.18}$$

Which can be written as $$\frac{dI}{dt} - \big(g'(I')I' + g(I')\big)I'' = 0 \tag{2.19}$$

If at some point *p, pg(p)* is decreasing with a negative derivative *–a* at *p,* that will cause *I'(x) =p,* at some point *x*. Then the equation near *x* will look like $\frac{dI}{dt} + aI'' = 0$. Which is known as the inverse heat equation. It is an ill-posed equation for image processing as the inverting of this equation is a perfect de-blurring algorithm (Osher & Rudin, 1990).

To overcome these two drawbacks Catte et al. (F.Catte´ 1992) has proposed the following diffusion equation. Which is the modification of Perona-Malik model and known as *Catte_PM* diffusion model (J. Yu, Tan, & Wang, 2010).

$$\begin{cases} \frac{\partial I}{\partial t} = div[g(|\nabla(G(\sigma) * I)|)] \\ I(t=0) = I_0 \end{cases} \quad (2.20)$$

where

G(σ)= Gaussian kernel function and σ is the standard deviation. * denotes the convolution and *G(σ)*I* denotes a convolution of the image at time t with Gaussian kernel. By using this equation *Catte_PM* model became noise insensitive to the noises whose scale smaller than σ. By this way the probability of noise misinterpreted near the edge is vastly reduced. The diffusivity of the *Catte_PM* is computed as follows

$$g(|\nabla I|) = \frac{1}{1+\left(\frac{|\nabla(G(\sigma)*I)|}{k}\right)^2} \quad (2.21)$$

$$g(|\nabla I|) = \exp[-(|\nabla(G(\sigma) * I)|/k)^2] \quad (2.22)$$

For our proposed method *Catte_PM* model of (2.20) will be used as it will efficiently denoise the image having high level of noise and overcome the above mentioned demerits. In this case to automatically determine the value of σ relating to the Gaussian noise of the image, a window size from *20×20* and *65×65* pixel is considered. It is done for the satisfactory statistical calculation. By using this window size the most uniform block of pixel in the image is determined. The pixels standard deviation of each block is calculated. Finally the standard deviation of the most uniform block will be used as the

σ of the Gaussian filter. The smoothing Gaussian filter size is determined by using the value of σ as described in (Petrou & Petrou, 2010).

The effectiveness of the AD method depends upon three factors; viz the ability to differentiate between the gradient of edge and the gradient of the noise, the preciseness of edge stooping function from preventing edge being smoothed, and the determination of termination time of diffusion process automatically (J. Yu, Wang, & Shen, 2008). It is known that noise in US images is multiplicative in nature, which means that the variance caused by noise may be equal or larger than the variance caused by the edge. For that reason to design an edge detection method that will separate noises from the edge during conducting the diffusion process is not an easy task. Because of this the conventional AD method proposed by Perona-Malik is ineffective in case of US image despeckling. Therefore, the aim of this thesis is to propose an AD method that will give emphasis on effective edge detection during speckle reduction. For that reason it will be required firstly to obtain knowledge about diffusivity/conductance functions, Gradient thresholds, and stopping criteria of the AD method. Then these parameters for the proposed method will be defined.

2.8.3.1 Diffusivity function

In the AD method several diffusivity functions can be used, although different diffusivity functions will differentiate the filtering results, which is shown in Black et al. (Black et al., 1998). So, for improving the performance of the AD method it, is important to choose an appropriate diffusivity function and scale it in such a way so that it preserves the edge efficiently. In the case of the Perona Malik model, the first diffusivity function (2.14) gives an emphasis on a wide region over a smaller one. On the other hand, the second diffusivity function (2.15) puts emphasis on high contrast

edge over low contrast edge. Another diffusivity function has been proposed by Black et al. (Black et al., 1998) which generates a sharper edge, showing better experimental results of noise reduction, as the diffusion process converges fast. The diffusivity function proposed by Black et al is as follows:

$$g_3(x) = \begin{cases} \frac{1}{2}\left[1 - \left(\frac{x}{s}\right)^2\right]^2, & x \le s \\ 0 & otherwise \end{cases} \quad (2.23)$$

Where, $S = k\sqrt{2}$ and $x = \nabla I$

The flow function is defined as follows

$$\varphi(x) = g(x)x \quad (2.24)$$

Where $\varphi(x)$ represents the total generated brightness flow. At a location where $x=k$, maximum flow will occur. For understanding the behavior of different diffusivity functions, we will give emphasis on the scaling as well as comparison done by Black et al.(Black et al., 1998) For comparing the efficiency, Black et al. has scaled the diffusivity functions g1, g2 and g3 in such a way, so that their flow functions reach the same maximum value, and that means an equal amount of brightness at the same point x=0.2 shown in Fig.2.1 Which makes the modified version of following g1, g2 and g3.

$$g1(x) = \exp\left[-\left(\frac{x}{k\sqrt{2}}\right)^2\right] \quad (2.25)$$

$$g2(x) = \frac{1}{1+\left(\frac{x}{k}\right)^2} \quad (2.26)$$

$$g3(x) = \begin{cases} 0.67\left[1 - \left(\frac{x}{k\sqrt{5}}\right)^2\right]^2 & x \le k\sqrt{5} \\ 0 & otherwise \end{cases} \quad (2.27)$$

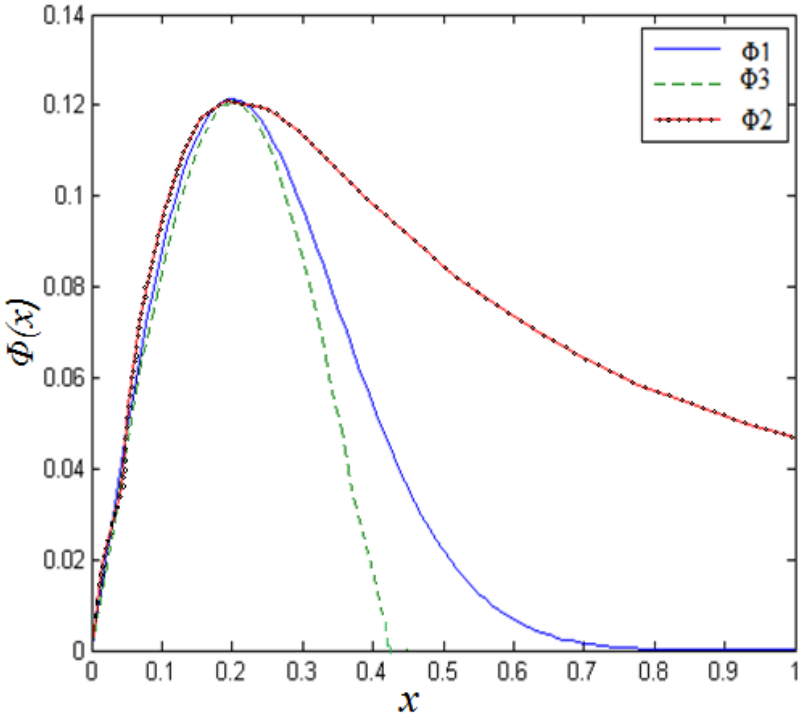

Figure 2.6 Three flow functions are scaled so that maximum flow occur at the same point at x=0.2

By observing Fig.2.1, it can be said that the flow functions ϕ1 and ϕ2 reduce slowly and smooth the image. On the other hand, in case of flow function ϕ3, the flow reduces dramatically and stops the diffusion, which prevents the edge of the image from over smoothing and becoming blurred. Suppose an image is characterized as having an edge above a certain threshold at x=0.4. In that case the turkey bewight function (ϕ3) will stop diffusion after x=0.4, and above this point, it will consider it to be an edge. But the other two functions will also continue smoothing above the point x=0.4 and it will over smooth and blur the edge (as shown in Fig.2.1). Function scaling and comparison support g3 function as it stop smoothing by descending faster after a certain threshold and prevent the edge from over smoothing. The point at x=0.4 is treated as the boundary between the noise and edge, which means the gradient value less than x=0.4 will smooth the noise where gradient value above x=0.4 will be considered as the outlier(Black et al., 1998), and preserve this by stooping diffusion. For comparing the behavior of the diffusivity functions, it is required to scale the diffusivity function as

well as flow function to become zero at the same point. As the g2 function decreases very slowly, it smooths the noise efficiently. As it becomes zero at infinity so its edge preservation ability is very weak. So if it is possible to scale the function g2, so that its value will become very low at the point where g3 is zero, then its edge preservation ability will increase. In the proposed method, function g2 will be scaled so that its value becomes very low at the point where g3 is zero and generates the same maximum value as g3. The flow function $\phi 2$ is very efficient for smoothing speckle noise as it decreases very slowly but is very weak for preserving edges. In this thesis the diffusivity function g2 will be scaled, as the flow function $\phi 2$ descends faster to stop diffusion after a certain threshold. G2 can preserve the edge and smooth the speckle noise simultaneously.

2.8.3.2 Gradient Threshold

The value of gradient threshold plays a vital role in effective edge detection. If the gradient threshold is overestimated then the resultant image will be over smoothed. On the other hand its noise reduction ability will be weakened due to underestimation of the gradient threshold. So, selecting suitable gradient thresholds is very important for getting a better resultant image. The gradient threshold parameters should be a decreasing function of time, which is shown in X Li et al. (X. Li & Chen, 1994). In this way, it can preserve the edge above a certain decreasing threshold. Gradient threshold plays a paramount role on the performance of the diffusion process. So, selection of a wise value of gradient threshold is required for effective noise suppression as well as efficient edge preservation. In the case of the AD method, only one gradient threshold is used. In the case of the proposed method, four gradient thresholds instead of one will be used for better edge preservation and effective noise reduction.

2.8.3.3 Stopping criterion of AD method

The performance of the AD method also depends on the criterion to terminate the diffusion process. It is common to terminate the diffusion process after a certain number of iterations. As the anisotropic diffusion (AD) method is very sensitive to the number of iterations, it is crucial to choose the exact stopping time (t). In the case of overestimating the number of iterations, resultant images will be blurred while an underestimating of the number of iterations will result unsatisfactory noise suppression. For overcoming these limitations, researchers have proposed different solutions. A de-correlation based method has been proposed by Mrazek and Navara et al. (Mrázek & Navara, 2003). In this case, stopping time has been chosen based on when the correlation between the noise and the signal in the output image is a minimum. In the case of an ultrasound image this de-correlation based method is not suitable, as, in case of US images, speckle originates from the signal. Gilboa et al. (Gilboa, Sochen, & Zeevi, 2006) proposed a method for obtaining maximum signal to noise ratio for the output image I_t. He used different equations for finding out the number of iterations for which the SNR of the output image will be at a maximum. By using this stopping criterion, it is possible to effectively reduce the noise of the output image but the preservation quality of edges is not up to a standard level. Mean Absolute Error (MAE) has been proposed by Zhang et al. (Zhang, 2007). In this case, the MAE value is used to stop diffusion automatically between two consecutive diffusion iterations. As the MAE criterion uses the Mean Absolute Error value between two consecutive diffusion iteration, it is suitable for US images. Therefore, the proposed method has used this stopping criterion.

Our AD method has been proposed by considering the gradient threshold parameters and the diffusivity function. The goal of our method is to make a right choice and scale

of the diffusivity function for the AD method to obtain a better quality output image. Proper estimation of the gradient threshold parameters has also been considered for effective noise reduction and edge preservation.

CHAPTER 3
METHODOLOGY

3.1 Introduction

The main purpose of the research is to propose improvement on the quality of US medical images by using US medical imaging to detect early knee OA. The US medical imaging is processed by two steps (proposed HE and AD). It is known that US medical imaging suffers from two drawbacks which are low contrast ratio and speckle noise. The purpose of this research is to enhance the contrast of the US image, as well as to reduce the speckle noise of the US image. This will be helpful for US imaging for detecting early knee OA. To enhance the contrast of the US imaging Multipurpose Beta Optimized Recursive Bi-Histogram Equalization (MBORBHE) method is used to overcome the limitations of conventional HE method. To reduce the speckle in US imaging, an improved AD method is used by considering two of the following three factors which are diffusivity functions, gradient thresholds and stopping criteria which control the effectiveness of the AD method.

3.2 Data acquisition

For data acquisition, the US images of the cartilage and the meniscus of the knee joint. For collecting US images of knee joint cartilage, we visited University Technology Malaysia, Johor Bahru, Malaysia. The name of the ultrasound (US) machine was ‘aplio MX’ of TOSHIBA brand. We used a 2D, 8MHz (PLT-805AT) linear probe for obtaining the US images. The DICOM image sizes were 528×285. We chose linear probe to take the image of knee joint as it contained higher frequency (8MHz) probe. An experienced and registered sonographer took the US images of the knee joint. 20 volunteer subjects willing to give the images of their knee joint. We took US images from different positions of the probe. The lateral side of the knee joint had

been given priority for imaging, as from this side, it would be possible for better observation of the cartilage of the knee joint. We used a high frequency 8MHz probe, as high frequency probe can give better resolution of US images. With high frequency, the wavelength would be smaller, thus smaller imaging particles would be possible to detect by using high frequency US probe. For the US imaging of knee joint, notch was very important because the probe would be placed beside the patella by using notch. A radiologist, Mr Heamn had given a lot of help in collecting the data.. The US images of knee joint cartilage collected from UTM are shown in Fig. 3.1. The cartilage images were taken from different positions of the knee joints.

Meanwhile, the US image of Meniscus of knee joint, were obtained from the University of Malaya Medical Collage (UMMC). Prof. Dr. John George, a professor at the department of Biomedical Imaging in UMMC, had helped us a lot in collecting the US images of knee joint meniscus. Meniscus images of knee joint collected from UMMC are shown in Fig.3.2. These images were taken from different positions of the US probe. For this experiment we used a 6.5 MHz linear probe. Prof. Dr. John George himself had taken the US images of knee meniscus from different position of US probe.

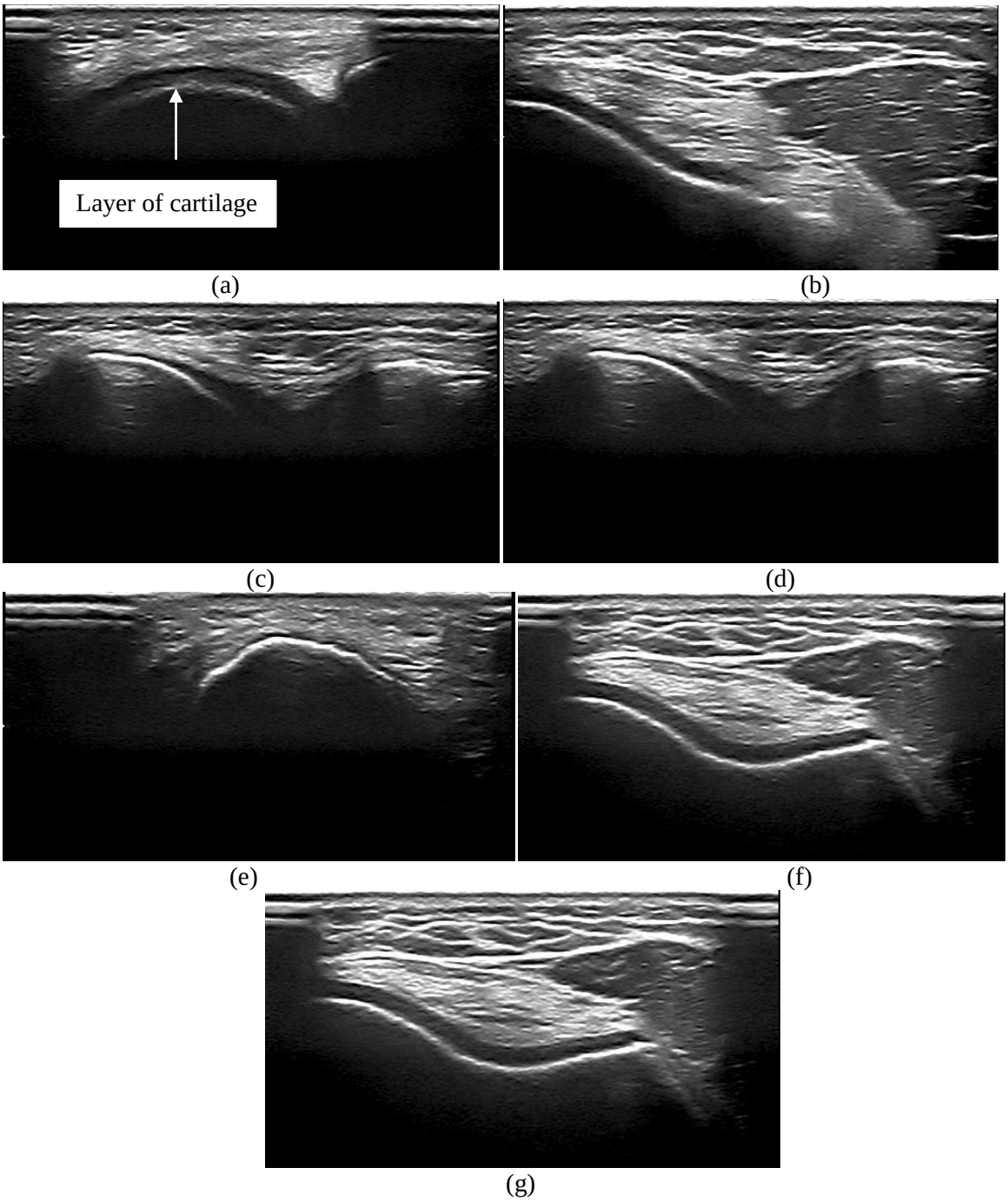

Figure 3.1: (a-g) is ultrasound images of knee joint Cartilage collected from UTM (Healthy subjects)

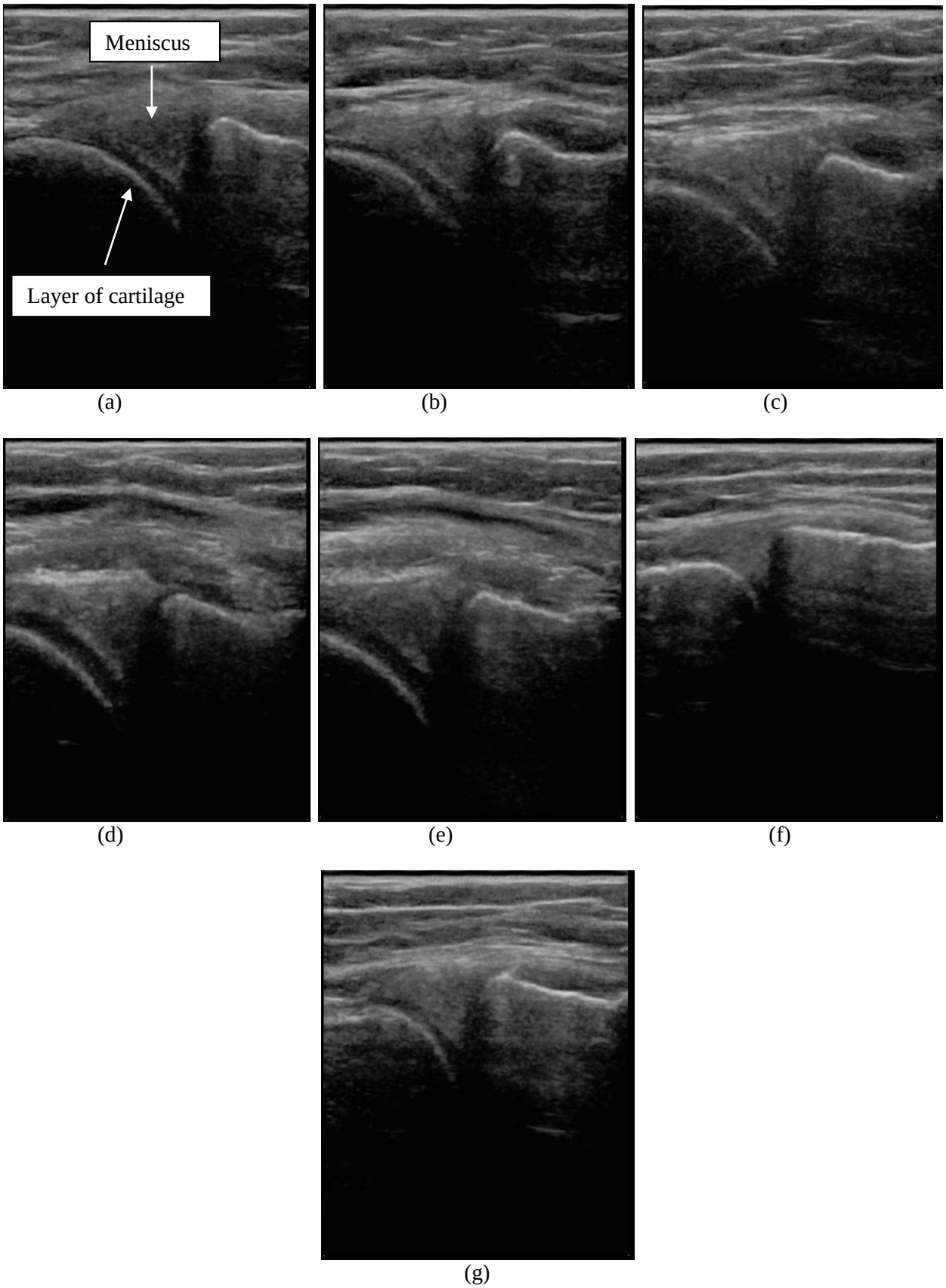

Figure 3.2: (a-g) is ultrasound image of knee joint Meniscus collected from UMMC (Healthy subjects)

3.3 US image of meniscus and cartilage of the knee joint

From Fig.3.3 shows the location of cartilage and meniscus, referred from data which collected from the Lucile Packard Children's Hospital, Source: http://www.daviddarling.info/encyclopedia/K/knee.html), The location of meniscus is between the layers of cartilage. The ultrasound images may be denoted as meniscus image or cartilage image. Though both images were taken at the knee joint, one is named as meniscus image as a large portion of the image is covered by meniscus, as shown in Fig.3.2. On the other hand, the other US image is named as cartilage image, as large part of the image is covered by cartilage, as shown in Fig. 3.1.

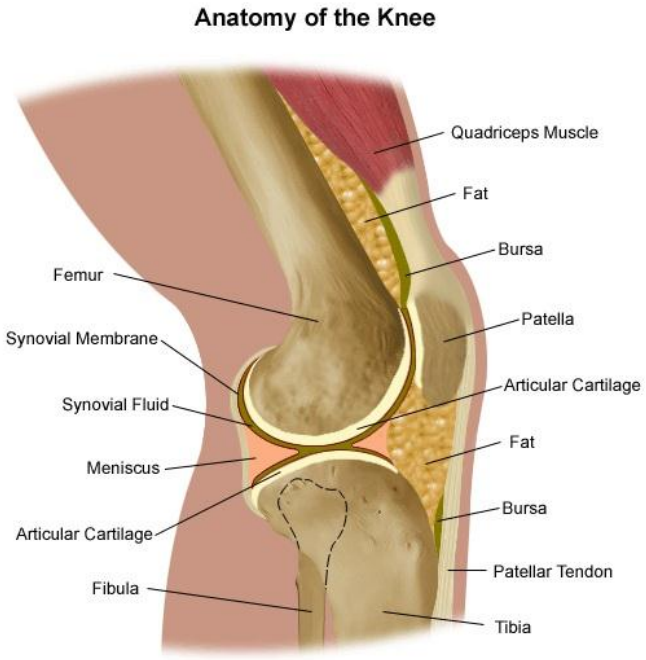

Figure 3.3 Knee joint of a normal knee

3.4 Proposed contrast enhancement method

3.4.1 Multipurpose beta optimizes recursive bi-histogram equalization

In this study, Multipurpose Beta Optimized Recursive Bi-Histogram Equalization (MBORBHE) method had been used for contrast enhancement of the cartilage and meniscus US images of the knee joint. The main idea of the method was to find out the optimum separating point for which brightness and detail preservation could

be achieved while enhancing the contrast of the US image. For that reason, each possible separating point was used for decomposing the input image into two sub-images. For converging output image mean brightness to the input image mean brightness, recursive separation was performed. After that, conventional HE was performed in each sub-image independently. For measuring the contrast enhancement, detail retention and brightness preservation of the output image, three metrics were defined. Weighted sum approach was used for constructing the final objective function which combined the three defined metrics. The functional output was computed by iterating each possible decomposition point for bi-histogram equalization, and resulting image was obtained for each maximum objective function.

3.4.2 Different objective functions

In case of ideal HE, the mean brightness difference of input and output image should be as close as possible. At the same time, it should also be able to enhance the contrast as well as to retain the detail and preserve the brightness of the image. To achieve this goal it had designed the objective functions to regularize different metrics. Three metrics for the proposed method were considered, which were Preservation of Brightness Score function (PBS), Optimum Contrast Score function (OCS), and Preservation of Detail Score function (PDS). Beta distribution is a very well-known distribution function. It is a versatile way to represent outcomes like probabilities or proportions. To specify various relationships between model expert opinions and random variables by having various functions over a certain desirable range, beta function is very useful. Beta distribution is defined in the interval of 0 to 1. For realizing the proposed algorithm, the beta distribution had been used. For complete model of the final objective function, the three metrics had been combined. By using final objective function, iteration had been performed in all possible gray levels to find the possible

separating gray level to maximize the objective function. Step by step construction of different objective function is described below.

3.4.2.1 Preservation of Brightness Score function (PBS)

The first metric is regarded as Preservation of Brightness Score (PBS). This function serves to gauge the brightness deviation of resultant image relative to input image. This brightness deviation is modelled as the difference between the mean illumination of input image, μ_x and the mean illumination of output image μ_y,

$$\mu_x = \frac{1}{M\,N}\sum_{I=0}^{M}\sum_{j=0}^{N} I_{X^{(i,j)}} \qquad (3.1)$$

$$\mu_y = \frac{1}{M\,N}\sum_{I=0}^{M}\sum_{j=0}^{N} I_{y^{(i,j)}} \qquad (3.2)$$

where *M* represents the height of the image in term of pixels number, and *N* represents the width of the image in term of pixels number. The pixel intensity in spatial location of (*i*,*j*) in input image and output image are represented by $I_{X^{(i,j)}}$ and $I_{y^{(i,j)}}$ respectively.

Therefore, the mean illumination difference can be intuitively described as $\mu_y - \mu_x$. However, this difference is not yet suitable to be used due to two problems: firstly, there is no standard bounding value which is important to compare later with the detail retention and enhanced contrast; secondly, it lacks of flexibility in manipulating its expected behavior.

Hence, to resolve the first issue, it is crucial to map illumination difference score onto the unit interval [0,1] so that the value will represent the degree of illumination deviation instead of the absolute value of illumination difference. This mapping is performed by using the normalization formula for relative brightness deviation as follow. The definition of normalized brightness (*NB*) is

$$NB(\mu_y, \mu_x) = \frac{|\mu_y - \mu_x|}{\mu_x + \mu_y + C} \quad (3.3)$$

where c is any arbitrary small constant used to assure computation stability in extreme cases. The range of (3.3) is described by $Norm(\mu_y, \mu_x) \in [0,1]$. As the output value of NB function approaches unity, it implies that the degree of deviation in brightness or illumination between the input image and output image is high, and vice versa.

To solve the second problem of manipulating the expected behaviour, it is needed to insert the output of (3.3) as input of another function. This function's purpose is to model the expected behaviour. For the sake of generality, this function is required to exhibit different behaviours or function output's shape by controlling only a few parameters in order to model the expert's opinion and knowledge conveniently. In this case, It opted for beta distribution function with parameter $\alpha_1$and β_1, and this function was termed as Preservation of Brightness Score *PBS*:

$$PBS = \frac{\Gamma(\alpha_1 + \beta_1)}{\Gamma(\alpha_1) + \Gamma(\beta_1)} (1 - NB)^{\beta_1 - 1} NB^{(\alpha_1 - 1)} \quad (3.4)$$

$$\Gamma(x) = \int_0^1 e^{-t}\, NB^{(X-1)} d(NB) \quad (3.5)$$

where *Γ(.)* is the Gamma function.

Again, to assure the output of PBS is of unit interval, it is normalized by using the maximum value of the function as the ratio of PBS to the maximum value of PBS over the range of NB. This normalized value of PBS is termed as the normalized Preservation of Brightness Score, NPBS.

$$NPBS = \frac{PBS}{argmax(PBS)} \quad (3.6)$$

The aim of *NPBS* is to model the perception of human visual system. An expert in visual application can use it to adjust the optimum value of desired range of brightness difference. The output value of *NPBS* can be viewed as the membership function of brightness deviation value. As *NPBS* approaches unity, it implies that the resultant

image is more preferable. The parameters of *NPBS,* determine the location of high values and low values of *NPBS* and hence determine the preference of brightness deviation by the user.

Using PBS makes it possible to measure the difference between mean brightness of input and output image. However, the very small brightness difference that was found in previous researches was not able to be found by using *NB.* Thus, human visual perception was not favorable in case of *NB.* For that reason, *PBS* or *NPBS* had been used in this study. *NPBS* is a normalized function, defined as the ratio of *PBS* and maximum value of *PBS.* In the experiment, *NB* was mapped by using *NPBS* to a new set of value ranging from 0 to 1. Beta distribution had been used for mapping by using parameters α_1 and β_1. *NPBS* provided us some values that were used to measure the brightness preservation quantitatively. However, in case of traditional method, even the smallest brightness difference would indicates the superiority of the resultant image. Good or bad brightness preserving ability can be defined by using *NPBS* function with the help of *NB.*

3.4.2.2 Optimum Contrast Score (OCS) function

The second metric is defined as Contrast Score (CS). This score quantifies the degree of contrast enhancement. It is modelled by using the difference of standard deviation of both the histogram equalized and input image. Similar to the previous metric, the bound values of CS range are denoted as of unit interval by using parameter α_2 and β_2.

In this thesis, the Standard deviation of input image and resultant image of M by N size are defined as (3.7) and (3.8) respectively. The relative difference of standard deviation is defined as in (3.9).

$$\sigma_x = \sqrt{\frac{1}{MN}\sum_{i=0}^{M-1}\sum_{j=0}^{N-1}\left(I_x(i,j) - \mu_x\right)^2} \quad (3.7)$$

$$\sigma_y = \sqrt{\frac{1}{MN}\sum_{i=0}^{M-1}\sum_{j=0}^{N-1}\left(I_y(i,j) - \mu_y\right)^2} \quad (3.8)$$

The Normalized Contrast (NC) was defined as follows

$$NC = 1 - \frac{\sigma_y - \sigma_x}{\sigma_y + \sigma_x + C} \quad (3.9)$$

Here, *c* is a constant to assure computational stability. The values of NC range from 0 to 1. It is used to gauge the difference between the contrast of the input and output image. The definition of OCS and NOCS are analogous to PBS and NPBS. The definition of OCS and NOCS are as given below.

$$OCS = \frac{\Gamma(\alpha_2+\beta_2)}{\Gamma(\alpha_2)+\Gamma(\beta_2)}(1-NC)^{\beta_2-1}NC^{(\alpha_2-1)} \quad (3.10)$$

where

$\Gamma(.)$ is the Gamma function.

$$NOCS = \frac{OCS}{argmax(OCS)} \quad (3.11)$$

In case of MBORBHE, relatively low or high contrast is not good, where only a certain optimum contrast value is good for human visual perception. As pertinent features of cartilage are obscured by low contrast and high contrast, they produce over-enhance contrast artifacts in the cartilage. Therefore, only the optimum contrast is suitable for the image to reveal the pertinent features of the US image of cartilage.

3.4.2.3 Preservation of Detail Score function (PDS)

The third metric is the detail retention metric or normalized detail (ND). This metric gauges the extent of how the information is altered. This degree of altered

information is modelled by first computing the difference in each pixel's intensity, with the mean brightness in input image and resultant image, and then multiplying both results as shown in (3.12). If the output of (3.12) is a negative value, it indicates that this particular pixel relationship with the mean image is different between the input image and resultant image, and hence implies an occurrence of alteration of information. This negative value is given a score of '1' and if it returns positive, it is given a score of '0'. This computation process is repeated to all the pixels, and then the score are summed up, as explained in equation (3.13).

$$d(x_{i,j}\, y_{i,j}) = \left(y_{i,j} - \mu_y\right)\left(x_{i,j} - \mu_x\right) \tag{3.12}$$

$$ND(X,Y) = \frac{1}{MN}\sum_{i=0}^{N} s\left(x_{i,j}, y_{i,j}\right) \tag{3.13}$$

Where,

$$s(x_{i,j}, y_{i,j}) \begin{cases} 1 \; if \; d(x_{i,j}, y_{i,j}) < 0 \\ 0 \; if \; d(x_{i,j}, y_{i,j}) \geq 0 \end{cases}$$

The range of ND's values is of unit interval. As ND approaches unity, it implies greater degree of structural alteration (detail loss), or lower degree of detail retention. Similar to the above two metrics, this ND score is further modelled by using Beta distribution function using α_3 and β_3 as function parameters as explained in equation (3.14). This function is termed as Preservation of Detail Score (PDS), and the normalized PDS as NPDS.

$$PDS = \frac{\Gamma(\alpha_3+\beta_3)}{\Gamma(\alpha_3)\Gamma(\beta_3)}(1-ND)^{\beta_3-1}ND^{(\alpha_3-1)} \tag{3.14}$$

where

$\Gamma(.)$ is the Gamma function.

$$NPDS = \frac{PDS}{argmax(PDS)} \tag{3.15}$$

The high score of NPDS indicates high detail loss which implies indirectly the chance that important information that might have been obscured is higher. This obscured

information is crucial to provide clues in identifying knee osteoarthritis. However, if the NPDS is overly low, it might signal inadequate contrast enhancement has been performed to emphasize potential relevant features. Therefore, there is a need to seek for an optimum value of NPDS.

3.4.3 Beta distribution

Beta distribution is a very well-known distribution function. It is a versatile way to represent the outcomes like probabilities or proportions. To specify various relationships between model expert opinions and random variables by having various functions over a certain desirable range, beta function is very useful. Beta distribution is defined in the interval of 0 to 1. In realizing the proposed algorithm in this study, beta distribution had been used.

3.4.4 Construction of final score function

To form the final objective function, the correct relation among NB, NC and ND to the corresponding score in NPBS, NOCS and NPDS respectively, is required. It is also required to determine suitable tune parameters for this relationship. The parameter setting of MBORBHE generally varies according to various images. For complete regularization function, the relationship of each function to the ideally expected one should be verified. This will help in finding out the value of mean brightness of the input and output image, as well as the peak value of NPBS. These two values should be as close as possible. The contrast enhancement should also be as close as possible to the peak value of NOCS. Lastly, it must also be considered that the feature of the HE image should not be distorted, diminished or over enhanced. The value of NPDS should be close to 1. Each characteristic functions as constraint to impede other characteristics. By considering all the optimum values of the three metrics, a

mathematical solution has to be established. One way was to find the optimum values of the three metrics is by finding the separating point. Nevertheless, in most cases, this is impossible. For that reason, the best solution is to find the separating point that could best satisfy the above mentioned criteria. The final objective function considering all three metrics is given below

$$NObj(NBPS, NOCS, NDPS) = \frac{\alpha(NBPS)+\beta(NOCS)+\Phi(NDPS)}{(\alpha+\beta+\Phi)} \quad (3.16)$$

For all recursive HE method, the value of r=4 is usually used. In this study, different US images of knee cartilage and meniscus were used for the performance evaluation of the proposed method. The qualitative analysis was performed by comparing the visual effects of different methods such as conventional HE, BBHE, DSIHE, MMBEBHE and RSIHE with the proposed method.

3.5 Proposed AD Method

In this study, for the evaluation of the proposed AD method, the parameters of AD method had been considered. There are three parameters that affect the efficiency of AD method. The main effort to overcome the limitations of these three parameters to reduce the speckle noise as well as efficiently preserve the edge of the US image. The three parameters of the proposed AD method are described below.

3.5.1 Diffusivity function for the proposed AD method

For studying our proposed method, *Catte_PM* diffusion model of equation (2.20) had been used. In this case, to automatically determine the value of σ relating to the Gaussian noise of the image, a window size of 20×20 and 65×65 pixels was considered. This was done to satisfy statistical calculation. By using this window size, the most uniform block of pixels in the image could be determined. The pixel standard deviation of each block was calculated. Finally, the standard deviation of the most

uniform block was used as the σ of the Gaussian filter. The size of the smoothing Gaussian filter as determined by using the value of σ as described in (Petrou & Petrou, 2010).

In our proposed method, the diffusivity function g2 is scaled so that its flow function $\phi 2$ become very small or near zero at x=0.4 or after a certain threshold level, above which it will stop diffusion and consider it as the edge.

Brightness is quantized into 256 levels in case of digital image processing. In that case, it can be implied that digital 0 is equal to 0.5/256=0.0020. The enhancement of image means subjective improvement of the image, so the grey tone difference that human can perceive should be considered. Human cannot distinguish less than *2~3* levels difference in grey scale image of 256 levels. Thus, it can be considered that *g2(x)=0* when it takes the value of *(0.0020)*3=0.0060~1/(1+(12.17)^2)*. By considering this the conductance functions, Equations (2.26) and (2.27) become

$$g2(x) = \frac{1}{1+\left(\frac{12.17x}{k}\right)^2} \qquad (3.17)$$

$$g3(x) = \begin{cases} \frac{1}{5} \times 0.67\left[1-\left(\frac{x}{k\sqrt{5}}\right)^2\right]^2, x \le k\sqrt{5}, \\ 0 \qquad otherwise \end{cases} \qquad (3.18)$$

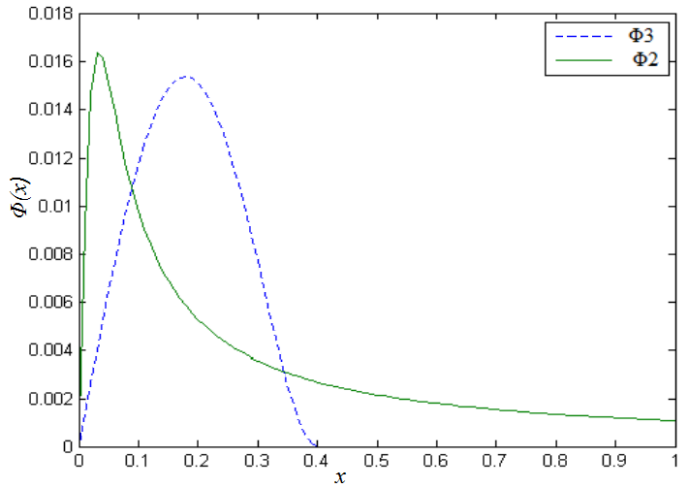

Figure 3.4: The flow function ϕ2 and ϕ3 are scaled so that the value of ϕ2 is near zero at x=0.4 where it is zero for ϕ3

As seen in Fig.3.4 it was obvious that the flow of *g2* descended faster, which resulted into expected sharp discontinuities. At *x=0.4* where the value of $\phi 3=0$, the value of $\phi 2$ became less than *0.006*. Thus, this value of $\phi 2$ can be considered as zero at *x=0.4* (in case of Fig.3.4).

3.5.2 Estimation of gradient threshold for the proposed AD method

In Equation (2.17), diffusion of the output image is not fully accomplished. It only consider the 4 neighboring pixels of four directions *(N, S, E, W)*, but it does not consider the neighboring pixels of other four directions such as *(NE, WN, WS, SE)*. As a result, its diffusivity and edge direction are only considered for four directions, where other four directions are not brought into concern. In our proposed method, all the 8-directions of the neighborhood pixels, as shown in Fig 3.5 are considered. For that reason, in case of our proposed method $\eta_s = \{N, S, E, W, NE, WN, WS, SE\}$, where *NE,WN,WS* and *SE* are North-East, West-North, West-South and South-East neighborhood of pixel *s*, respectively

and $\nabla I_{s,p} = I_t(p) - I_t(s), \qquad p \epsilon \eta_s = \{N, S, E, W, NE, WN, WS, SE\}$ (3.19)

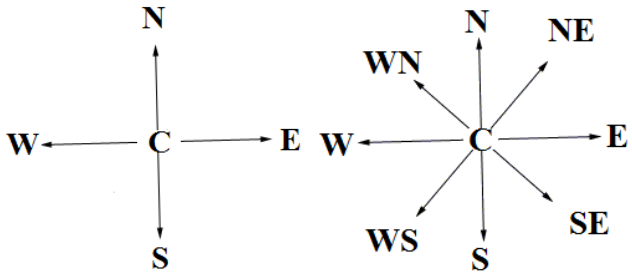

(a) AD method (b) Proposed AD method

Figure 3.5 C is the central pixel of [3×3] mask and (a)Four pixels of four directions has been considered (b) Eight pixels of eight directions has been considered

It is $\nabla I_{s,p}$,the brightness difference of the pixel *s*, and each one of its eight neighbors in the 8-pixel neighborhood η_s as shown in (3.19). This occurs as the operator ∇ indicates a scalar which defines the difference among the neighboring pixels, rather than a single gradient vector as in the continuous form. From this, comes an idea that eight different gradient threshold parameters should be used, where every threshold parameter is estimated by using respective differences along the eight directions. If the entire region of an image is given, then from the statistical sense, it can be said that the absolute values of north and south difference are almost equivalent, so for north and south directions one instead of two gradient thresholds can be considered. The same should also be applied in case of east and west, west-north and south-east, north-east and west-south. For this reason, the estimation of four gradient threshold parameters is proposed, which are S_{NS} S_{EW} S_{WNSE} S_{NEWS}. Here, S_{NS} refers the estimated threshold in North-south direction, S_{EW} denotes the estimated threshold in east-west direction, S_{WNSE} indicates the estimated threshold in west-north and south-east direction, and lastly S_{NEWS} refers to the estimated threshold in north-east and west-south direction. This will change Equation 2.16 into the following equation.

$$I_{T+1}(s) = I_t(s) + \frac{\lambda}{|\eta_s|}\left[\sum_{p\epsilon N,S} g\left(\nabla I_{S,P}\right)\nabla I_{S,P} + \sum_{p\epsilon E,W} g(\nabla I_{s,p})\nabla I_{s,p} + \right.$$

$$\left.\sum_{P\epsilon NE,WS} g\left(\nabla I_{s,p}\right)\nabla I_{s,p} + \sum_{p\epsilon WN,SE} g(\nabla I_{s,p})\nabla I_{s,p}\right] \quad (3.20)$$

In Equation 3.20 for the first $g\left(\nabla I_{S,P}\right)$, the estimated gradient threshold is S_{NS}, while for the second $g\left(\nabla I_{S,P}\right)$ the estimated gradient threshold is S_{EW}. For the third $g\left(\nabla I_{S,P}\right)$, the estimated gradient threshold is S_{NEWS} and for the last $g\left(\nabla I_{S,P}\right)$, the estimated gradient threshold is S_{WNSE}.

Estimating four gradient thresholds will give much more precise result in terms of noise reduction and edge preservation, compared to the result of using only a single gradient threshold vector as in continuous form. The experimental result will also be better in term of smoothing, as smoothing that takes place for each direction is not the same. It will vary according to the strength of difference of each direction. The gradient threshold parameter will also vary, as larger difference will obtain higher value of *S* parameter compared to other directions.

Corresponding histogram of the absolute value of the gradient component in each direction will be used for estimating the four gradient threshold parameters. The knee algorithm is used for finding out the threshold between two populations of histogram having a long tail and one peak that fit with straight lines, by the sense of least square error. After one iterative process, each population will lead to the estimation of the threshold. Elaboration on the knee algorithm can be found in a research paper by Petrou et al.(Petrou & Petrou, 2010).

In our method, the population has roughly flat distribution, creating long tail, which defines the difference attribute to the true edge. On the other hand, population having

steeper distribution is the difference attributed to the noise. Between the two parameters, the estimated threshold is *S*.

3.5.3 Stopping Criterion for the proposed AD method

In our proposed method, MAE stopping criterion is used. This process is based on the surveillance of exponential reduction of the MAE value with the number of iteration. When the value of MAE between two iterations is sufficiently small, the diffusion process is terminated automatically. The MAE criterion is suitable for US image. For this reason, this stopping criterion is used in our proposed method. For better performance, according to the fitness of small structure of the image, different MAE threshold should be used. In the proposed method, the MAE of the diffused image is utilized to stop the diffusion, which is written as follows:

$$MAE(I_t) = \frac{1}{m \times n} \times \sum_{(i,j)=1}^{m,n} \sqrt{(I_t^{i,j} - I_{t-1}^{i,j})^2} \qquad (3.21)$$

where $I_t^{i,j}$ and $I_{t-1}^{i,j}$ are the filtered value of pixel *(i,j)* in the diffused images at time t and t-1, respectively. The number of row and column of the diffused image are denoted by m and n. The tissue structure and edge information are filled by the region of the diffused image. If the values of MAE become small and stable, the diffusion terminates and protects the diffused image from over smoothing.

3.6 Summary of the proposed AD method

Firstly, it is necessary to find out the standard deviation (σ) of the pixel within most uniform blocks of the noisy image. The size of smoothing Gaussian filter (G_σ) is constructed from the value of σ. Here, I_0 is the original image. The number of iteration is denoted by t. Then, I_t is convolved with G_σ and the values of δ_{N*}, δ_{S*}, δ_{E*}, δ_{w*}, δ_{NE*}, δ_{SE*}, δ_{SW*} and δ_{NW*}, the differences of each pixel, are computed. After that, the method

is used to find out the values of δ_N, δ_S, δ_E, δ_w, δ_{NE}, δ_{SE}, δ_{SW} and δ_{NW}, which are also the differences of each pixel by using different 2D convolution mask. Then, by using knee algorithm, the S_{NS} from δ_N and δ_S, S_{EW} from δ_E and δ_w, S_{WNSE} from δ_{WN} and δ_{SE}, S_{NEWS} from δ_{NE} and δ_{WS} can be estimated. By using the above values, the final diffused image is calculated with the help of the following equation

$$I_t = I_{t-1} + \frac{\lambda}{\eta_s}[g(\delta_{N*}.S_{NS})\delta_N + g(\delta_{S*}.S_{NS})\delta_S + g(\delta_{E*}.S_{EW})\delta_E + g(\delta_{W*}.S_{EW})\delta_W + g(\delta_{WN*}.S_{WNSE})\delta_{WN} + g(\delta_{SE*}.S_{WNSE})\delta_{SE} + g(\delta_{WS*}.S_{NEWS})\delta_{WS} + g(\delta_{NE*}.S_{NEWS})\delta_{NE} \quad (3.22)$$

Finally, the *MAE* value is measured for each iteration and the diffusion is terminated when the *MAE* value becomes sufficiently small..

3.7 Measurement tools to assess US image quality

For quantitative analysis of the real US image, different performance metrics can be used. The performance metrics are usually chosen based on the determination of effectiveness of the contrast enhancement and speckle reduction methods.

3.7.1 In case of the proposed HE method

Our main objective in the proposed HE method is to preserve the brightness and detail when enhancing the contrast of the US image. In this study, for quantitative analysis, Signal to Noise Ratio (SNR), Structural Similarity Index Measurement (SSIM) and Entropy had been used. SNR and Entropy had been also used for assessing the brightness preservation and the degree of contrast enhancement, respectively. For the measurement of the detail preservation, SSIM had been used. A bar chart of mean shift of the original image, histogram equalized image and image of proposed method had been also drawn for determining the ability of brightness preservation of the proposed method.

Next, MSE was used to measure the effectiveness of noise reduction, by measuring the square of difference between two images. The lower the value of MSE, the higher the effectiveness of noise reduction will be. *MSE* is defined as follows:

$$MSE = \frac{1}{M.N}\sum_{m=0}^{M-1}\sum_{n=0}^{N-1}[I(m,n) - I'(m,n)]^2 \quad (3.23)$$

Here, I is the original image, while I' is the filtered image of different contrast enhancement or speckle reduction method, which need to be compared for finding out the best one. *M* and *N* are the number of rows and columns of the pixel in the images. Here, *I (m,n)* indicates the input image pixel intensity at spatial location of *(m,n)* and $I'(m,n)$ indicates the output image pixel intensity at the spatial location of *(m,n).*

The definitions of SNR, SSIM and Entropy are given as follows:

$$SNR = 10\log_{10}\frac{\sum_{m=0}^{M-1}\sum_{n=0}^{N-1}[I(m,n)]^2}{MSE} \quad (3.24)$$

SNR is used to evaluate the standard of the output image quality. It is measured in decibels (dB). Hence, the higher the SNR value, the better the resultant image is.

Structural Similarity Index Measurement (SSIM) is calculated on different windows of an image. The equation for SSIM between two windows *x* and *y* of similar size is given below:

$$SSIM(x,y) = \frac{(2\mu_x\mu_y + C_1)(2\sigma_{XY} + C_2)}{(\mu_x^2 + \mu_y^2 + C_1)(\sigma_x^2 + \sigma_y^2 + C_2)} \quad (3.25)$$

where μ_x and μ_y are the average of *x* and *y* respectively. σ_x^2 and σ_y^2 are variance of *x* and *y* respectively. σ_{XY} is the co-variance of *x* and *y*. C_1 and C_2 are the two constants for stabilizing the division with weak denominator, where $C_1 = (k_1 L)^2$ and $C_2 = (k_2 L)^2$. L is the dynamic range of the pixel value, k_1=0.01 and k_2=0.03. The resultant of SSIM is in decimal value and it ranges from -1 to 1. If two data sets are identical, then the result of SSIM will be 1.

Entropy is used for measuring the robustness of contrast enhancement. The mathematical equation of entropy is given below.

$$Ent[p] = -\sum_{k=0}^{L-1} p(k) \log_2 p(k) \quad (3.26)$$

Here in Eq. 3.26, $Ent[p]$ is the entropy. The probability density function (PDF) is p. L is the number of gray level.

3.7.2 In case of Speckle noise reduction

For evaluating the performance of the proposed AD method over other AD methods, the following performance metrics had been used: Peak signal to noise ratio (PSNR)(Tsiotsios & Petrou, 2013), Mean Square Error (MSE)(F.Zhang, 2007a), Structural Similarity Index Measurement (SSIM) (Wang, Bovik, Sheikh, & Simoncelli, 2004) and Pratt's Figure of Merit (FOM)(Y. Yu, Acton, S.T., 2002). The proposed method was then compared with conventional Perona-Malik, SRAD, LPND and NCD method.

PSNR is used for measuring how much noise has been reduced from the noisy image. The commonly used unity of PSNR is (dB). The Higher the value of PSNR, the larger amount of the noise reduced from the noisy image.

$$PSNR = 10 \log_{10} \frac{max(I(m,n))^2}{MSE} \quad (3.27)$$

SSIM is used for measuring adaptation of human visual system about the information of structure of the scene. In this measurement method, three different important measurements such as contrast, luminance and structure, are considered. The definition of SSIM is given in Equation 3.25

For comparing the performance of edge preservation among different methods *FOM* is used. *FOM* is defined as follows:

$$FOM = \frac{1}{\max\{N_{real}, N_{ideal}\}} \sum_{i=1}^{N_{real}} \frac{1}{1+d_i^2 e} \quad (3.28)$$

Here, N_{ideal} and N_{real} are the number of ideal and detected edge pixels. The Euclidian distance between the nearest ideal edge pixel and *i*th detected edge pixel is denoted by d_i. e is a constant whose value generally is 1/9. The value of FOM ranges from 0 to 1. The higher the value of FOM, the better edge detection can be obtained.

CHAPTER 4
RESULT AND DISCUSSION

4.1 Introduction

In this thesis, the performance of the MBORBHE method and proposed AD method had been evaluated qualitatively and quantitatively. In case of MBORBHE, for qualitative and quantitative analysis, the US images of meniscus and cartilage of knee joint had been enhanced by using contemporary contrast enhancement techniques, such as conventional HE, BBHE, DSIHE, RSIHE, MMBEBHE and the proposed MBORBHE method. For the evaluation of brightness preservation, the shift of mean of conventional HE methods and proposed method from the original image had also been evaluated. In the proposed AD method for qualitative and quantitative analysis, the real US image of meniscus and cartilage of knee joint has also been used. The proposed AD method had been compared with Perona-Malik, NCD, SRAD and LPND for performance evaluation. Qualitative analysis had been performed in term of human visual perception for both proposed HE and AD method. The quantitative analysis of both proposed HE and AD method had been performed by using different performance metrics such as Signal to Noise Ratio (SNR), Peak Signal to Noise Ratio (PSNR), Mean Square Error (MSE), Figure of Merits (FOM), Structure Similarity Index Measurement (SSIM) and Entropy. Statistical analysis had been performed on the obtained numerical values of different performance metrics. Statistical analysis from Fisher's Least Significance Difference and Duncan test confirmed the best performance of the proposed HE and AD method.

4.2 For proposed contrast enhancement method

Qualitative and quantitative analyses has been performed for performance evaluation of the proposed HE method. The details of qualitative and quantitative analyses have been discussed below.

4.2.1 Qualitative analysis

In proposed contrast enhancing method, the qualitative analysis had been accomplished by using human visual perception. For qualitative analysis of the proposed HE method, real US image of knee joint cartilage and meniscus had been used.

4.2.1.1 Test on Cartilage Image

The original image of knee joint cartilage for qualitative analysis is shown in Fig. 4.1(a). The arrows in Fig. 4.1(a) indicate the upper and lower layers of the cartilage. Meanwhile, the enhancement of the original image by using conventional HE, BBHE, DSIHE, RSIHE, MMBEBHE and proposed MBORBHE are shown in Fig. 4.1(b), 4.1(c), 4.1(d), 4.1(e), 4.1(f) and 4.1(g), respectively. Fig. 4.1(b) shows unnatural brightness enhancement, not only in the cartilage, but also at the upper portion of the cartilage of the knee joint. Though unnatural brightness enhancement was not significant in case of Fig. 4.1(c), some detail of loss artifacts can be observed, in the right and left end side of the reversed 'U' shape cartilage of knee joint. Unnatural brightness enhancement was also noticeable in the case as shown in Fig 4.1(d). At the upper portion of right end side of the reversed 'U' shape cartilage, a big white area was observed, where unnatural brightness enhancement was noticeable, as in Fig. 4.1(c), 4.1(d), 4.1(e) and 4.1(f). On the other hand, natural brightness enhancement could be observed in the case as shown in Fig. 4.1(g). In RSIHE and MMBEBHE as illustrated in Fig. 4.1(e) and 4.1(f), shift in

brightness (darker compared to other enhancement methods) was obvious, in which the contrast decreased around the area of the cartilage.

Measuring the thickness of the cartilage required information of the exact upper and lower edge of the cartilage. In the upper portion, a deep dark line, which was the edge of the upper part of the cartilage, was observable. This deep dark edge was much thinner when observed using the proposed method. This indicates that the imaging on the upper edge of the cartilage is more precise, as can be seen in Fig. 4.1(g). The proposed method was also more precise in case of imaging the lower portion, where it showed thinner and more precise white dotted lines. Some unnatural white artifacts were also observable in case of Fig. 4.1(b), 4.1(c), 4.1(d), 4.1(e) and 4.1(f). However, in case of Fig. 4.1(g), white artefact was not observed very frequently, but a natural enhancement of the shape of cartilage was noticed. Besides that, the reversed 'U' shape of the cartilage was clearly noticeable, and there was a natural enhancement in the upper portion of the cartilage joint. The shape of the cartilage was clearer as compared to the images taken using other methods. In case of Fig. 4.1(b), 4.1(c), 4.1(d), 4.1(e) and 4.1(f), some unnatural tiny white lines could be seen at the border of the cartilage, as well as at the upper portion of the cartilage joint. It was obvious that the white border of the cartilage joint, generated by using MBORBHE, was natural. Therefore, this method had shown to successfully preserve the brightness and details when enhancing the contrast of the image. The resultant images from the conventional HE, BBHE and DSIHE shown in Fig. 4.1(b), 4.1(c) and 4.1(d) also suffered from mean brightness shift, thus resulting in unpleasant contrast enhancement. From the qualitatively analysis as shown in Fig.4.1, it can be concluded that the proposed method can outperform the other methods.

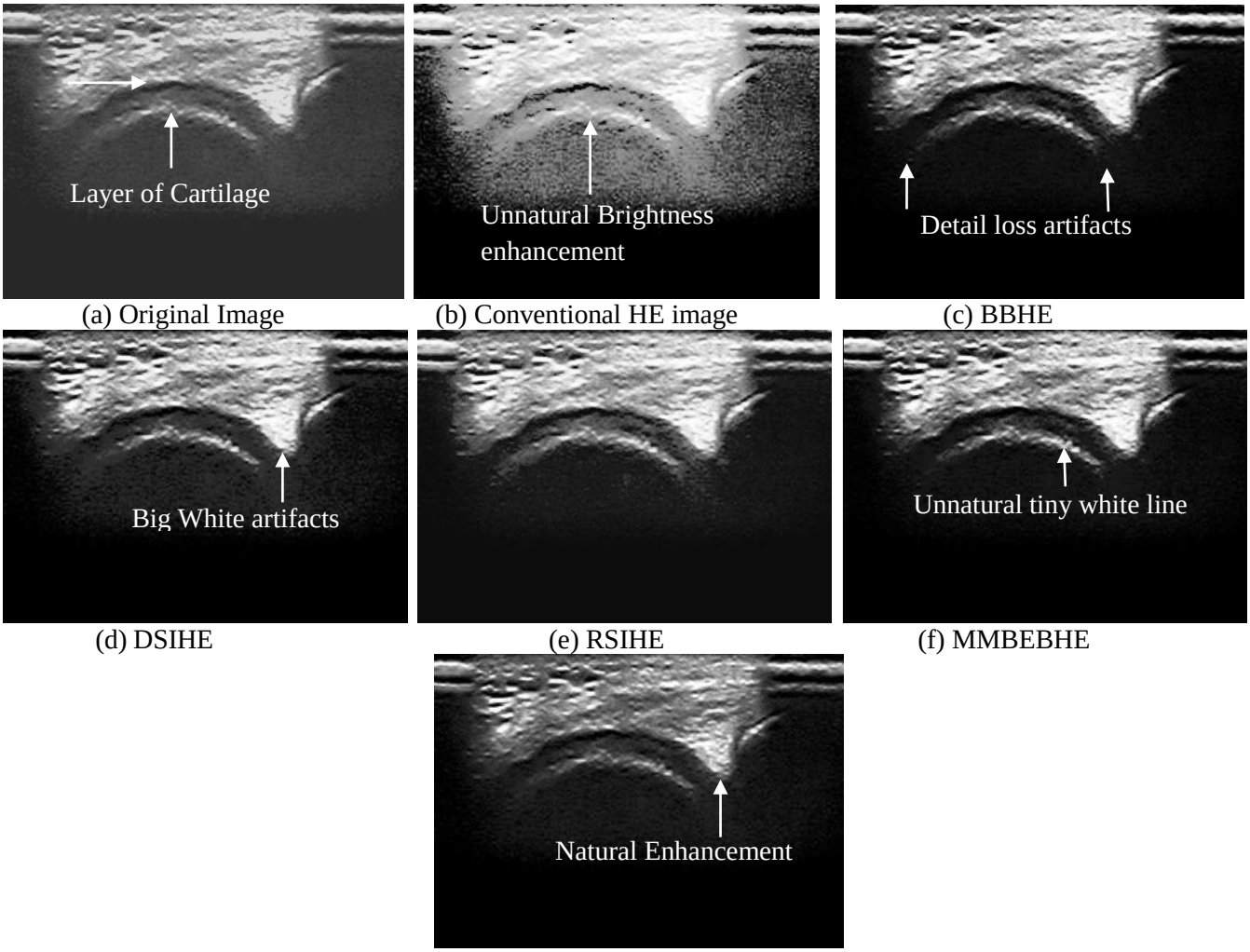

(a) Original Image (b) Conventional HE image (c) BBHE

(d) DSIHE (e) RSIHE (f) MMBEBHE

(g) Proposed method

Figure 4.1: .(a) Original Cartilage Image (b) Conventional HE (c) BBHE (d) DSIHE (e) RSIHE (f) MMBEBHE (g) MBORBHE (proposed)

4.2.1.2 Test on meniscus Image

For the qualitative analysis of the proposed HE method, the original image of knee joint meniscus as shown in Fig. 4.2(a) and the arrows in Fig. 4.2(a) indicate the upper and lower layer of cartilages of knee joints. The enhancement of the original image by using conventional HE, BBHE, DSIHE, RSIHE, MMBEBHE and proposed MBORBHE are shown in Fig. 4.2(b), 4.2(c), 4.2(d), 4.2(e), 4.2(f) and 4.2(g) respectively. The image results from the conventional HE, BBHE and DSIHE (shown in Fig. 4.2(b), 4.2(c) and 4.2(d)) had larger mean brightness, which were much brighter compared to the original image, therefore they resulted in unpleasant contrast

enhancement. In case of Fig. 4.2(b), unnatural brightness enhancement was observed, not only in the meniscus, but also in the upper portion of the tibia and femur of the knee joint. Though unnatural brightness enhancement was not so significant in case of Fig. 4.2(c), some detail loss artifacts were observed between the joint of tibia and lower part of the *'V'* shape cartilage. Unnatural brightness enhancement was also noticeable in case of Fig. 4.2(d). In case of RSIHE and MMBEBHE in Fig. 4.2(e) and 4.2(f), it could be seen that the obvious change in brightness (darker comparing with other enhancement methods) decreased the contrast around the area of the meniscus. These methods also gave less emphasis on detail preservation. In case of Fig. 4.2(e), detail loss artifact in the junction of meniscus and tibia of the knee was observed. In case of Fig. 4.2(f), the detail loss artifacts were also observable in the border of 'V' shaped meniscus. However, in case of Fig. 4.2(g), the detail loss artifacts were not observed very actively. A natural enhancement of the shape of cartilage could be seen. The 'V' shape of the cartilage was clearly noticeable, as shown in Fig. 4.2(g). The shape of the meniscus collateral ligament was also clear compared to the results of other methods. In case of Fig. 4.2(b), 4.2(c), 4.2(d), 4.2(e) and 4.2(f), some unnatural white lines at the border of the cartilage, as well as in the meniscus could be seen. It was also observed that the white border of the cartilage generated by the MBORBHE was natural.

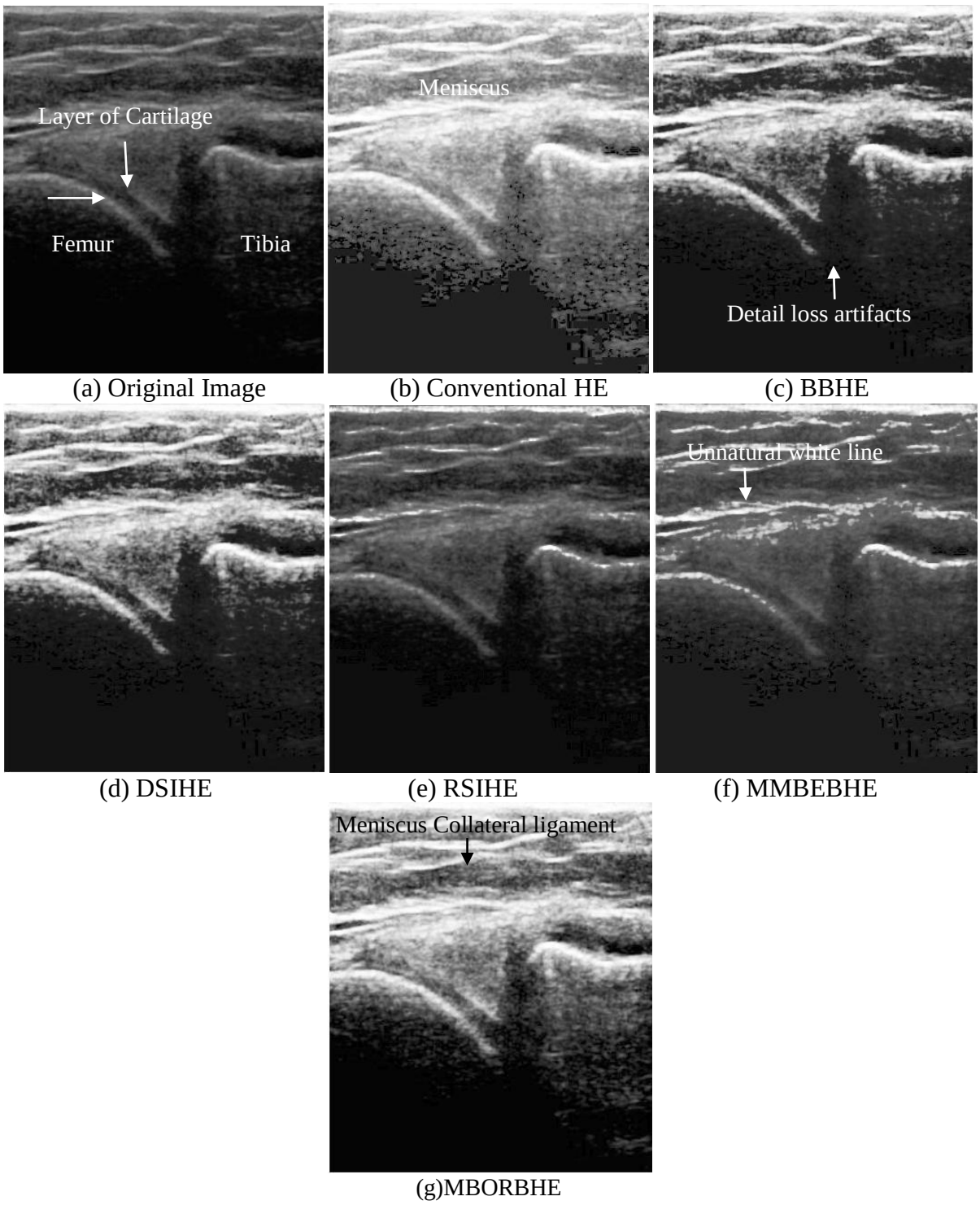

(a) Original Image (b) Conventional HE (c) BBHE

(d) DSIHE (e) RSIHE (f) MMBEBHE

(g)MBORBHE

Figure 4.2: (a) Original Image (b) Conventional HE (c) BBHE (d)DSIHE (e) RSIHE (f)MMBEBHE (g) MBORBHE (proposed). (In case of meniscus image)

Therefore, this proposed method has successfully preserved the brightness and details when enhancing the contrast of the image. From the qualitative analysis as shown in Fig.4.2, it has been proven that the proposed method can outperform the other methods.

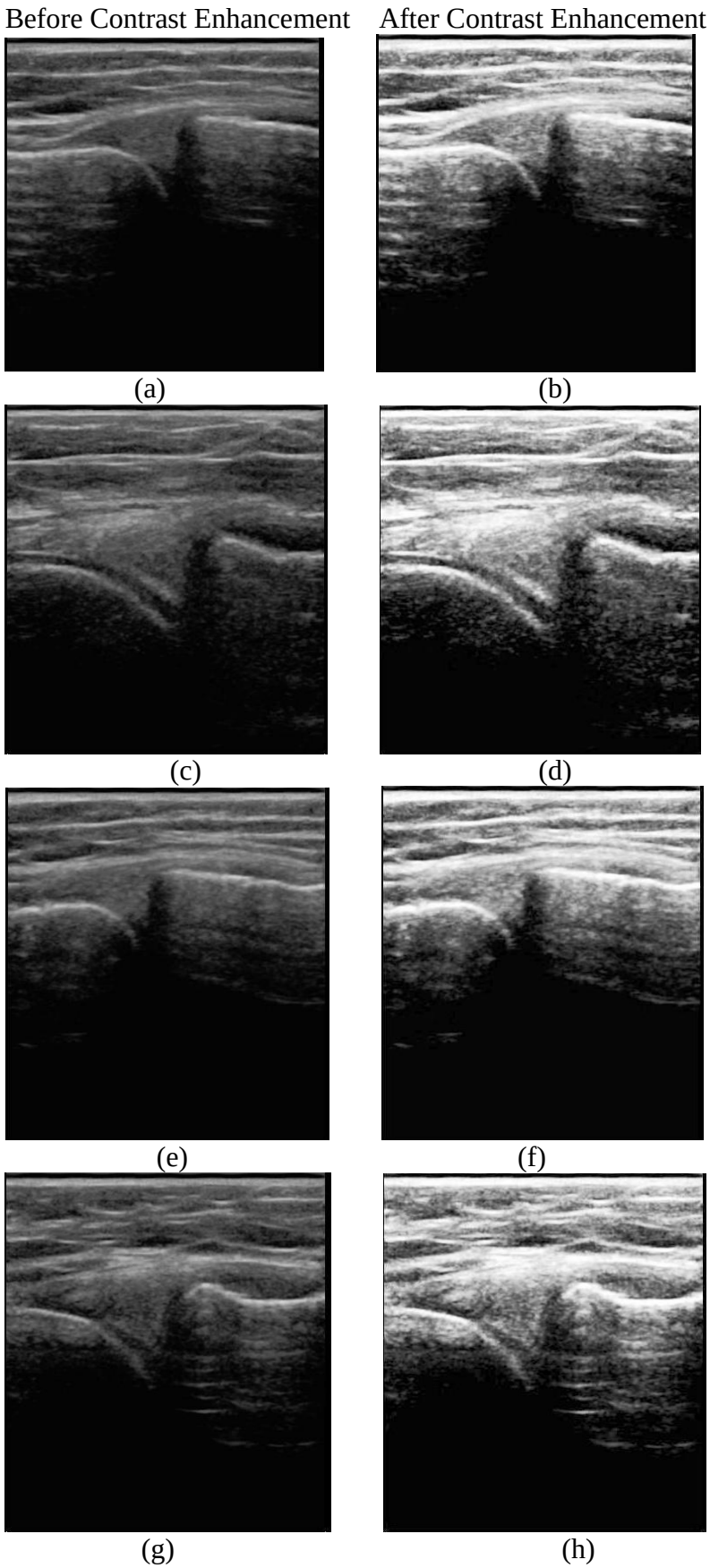

Figure 4.3: US images of knee Meniscus for four subjects before and after contrast enhancement are shown above (a), (b) are input and output image for subject 1. (c), (d) are input and output image for subject 2. (e), (f) are input and output image for subject 3, (g), (h) are input and output image for subject 4

The improvement of the US image of knee meniscus for different subjects after contrast enhancement by the proposed method is shown in Fig.4.3. From the output image as shown in Fig.4.3 (b), it can be said that the darkness of the original image had been removed. In case of Fig.4.3 (d), it was observed that the structure of the cartilage was much identifiable than the original image. By observing Fig.4.3 (f) and (g), it can be concluded that not only the details of the cartilage but the contrast of the knee joint also been significantly improved.

4.2.2 Quantitative analysis

Statistical analysis had been used for quantitative analysis of the numerical values of different performance metrics for contrast enhancement such as SNR, SSIM, and Entropy. The entire test was performed by using SPSS (Version 21). In this analysis, the proposed method (MBORBHE) has been verified and tested able to outperform the other methods.. Table 4.1 shows the mean values of SNR, SSIM and Entropy for different contrast enhancement methods (HE, BBHE, DSIHE, RSIHE, MMBEBHE and MBORBHE) in case of 20 healthy subjects. The mean values of SNR, SSIM and Entropy has been compared for different HE methods. It had been shown that the largest value of SNR was (29.177±1.585) in the proposed method, and the least value was (21.807±0.788) in the conventional HE method. In SSIM and Entropy it could be seen that the height values were in the proposed methods which were (0.833±0.126) and (7.689±0.547), respectively. The least value of SSIM and Entropy were in DSIHE and BBHE, which were (0.260±0.054) and (4.430±0.533) respectively.As seen in Table 4.1 it was observed that MBORBHE and MMBEBHE produced almost similar results for SSIM. The difference of mean SNR between MMBEBHE and MBORBHE were not too large as well. Therefore, further analysis is still required for proving the best performance of the proposed method.

Table 4.1: Mean value of SNR, SSIM and Entropy for different contrast enhancement methods

Methods	Mean SNR (dB)±SD	95% confidence interval of the difference		Mean SSIM±SD	95% confidence interval of the difference		Mean Entropy±SD	95% confidence interval of the difference	
		Lower	Upper		Lower	Upper		Lower	Upper
HE	21.807±0.788	21.457	22.158	0.620±0.017	0.612	0.628	4.552±0.365	4.381	4.724
BBHE	23.987±0.527	23.740	24.234	0.718±0.035	0.702	0.735	4.430±0.533	4.180	4.680
DSIHE	24.999±0.979	24.541	25.458	0.260±0.054	0.234	0.286	4.995±0.615	4.706	5.283
RSIHE	20.458±0.757	20.104	20.813	0.747±0.031	0.732	0.762	4.635±0.374	4.459	4.810
MMBEBHE	26.306±0.714	25.972	26.640	0.813±0.055	0.787	0.839	4.559±0.368	4.387	4.732
MBORBHE	**29.177±1.585**	28.435	29.920	**0.833±0.126**	0.773	0.892	**7.689±0.547**	7.432	7.945

As seen in Table 4.2, it can be said that there was significant difference between the results of different methods for different performance metrics such as SNR, SSIM and Entropy. As the value of sig. was less than 0.05, thus there was significant difference between numerical values of different methods. As a result, these data had been further analyzed by using post hoc test (Fisher's Least Significant Difference and Duncan test) to evaluate the performance of different contrast enhancement methods.

Table 4.2: The one-way ANOVA test by using different contrast enhancement methods in SNR, SSIM and Entropy

		Sum of Squares	df	Mean Square	F	Sig.
SNR	Between Groups	984.546	5	196.909	218.929	0.000*
	Within Groups	102.534	114	0.899		
	Total	1087.080	119			
SSIM	Between Groups	4.508	5	0.902	219.972	0.000*
	Within Groups	0.467	114	0.004		
	Total	4.975	119			
Entropy	Between Groups	159.182	5	31.836	138.991	0.000*
	Within Groups	26.112	114	0.229		
	Total	185.295	119			

*Significant sig. value (sig.<0.05)

Table 4.3 (Fisher's Lest Significant Difference test) shows that there were significant differences among different methods for the value of SNR, as there was no value of sig. larger than 0.05. This result had been confirmed by using Duncan test (Table 4.4), as it was seen in any subset that there was no more than one value.

Table 4.3: Categorization of different methods using Fisher's Least Significant Difference (LSD) for SNR

(I) Method	(J) Method	Mean Difference (I-J)	Std. Error	Sig.	95% Confidence Interval	
					Lower Bound	Upper Bound
HE	BBHE	-2.179*	0.299	0.000	-2.773	-1.585
	DSIHE	-3.192*	0.299	0.000	-3.786	-2.597
	RSIHE	1.349*	0.299	0.000	0.755	1.943
	MMBEBHE	-4.498*	0.299	0.000	-5.092	-3.904
	MBORBHE	-7.369*	0.299	0.000	-7.964	-6.775
BBHE	HE	2.179*	0.299	0.000	1.585	2.773
	DSIHE	-1.012*	0.299	0.001	-1.606	-0.418
	RSIHE	3.528*	0.299	0.000	2.934	4.122
	MMBEBHE	-2.318*	0.299	0.000	-2.913	-1.724
	MBORBHE	-5.190*	0.299	0.000	-5.784	-4.596
DSIHE	HE	3.192*	0.299	0.000	2.597	3.786
	BBHE	1.012*	0.299	0.001	0.418	1.606
	RSIHE	4.541*	0.299	0.000	3.947	5.135
	MMBEBHE	-1.306*	0.299	0.000	-1.900	-0.712
	MBORBHE	-4.177*	0.299	0.000	-4.772	-3.583
RSIHE	HE	-1.349*	0.299	0.000	-1.943	-0.755
	BBHE	-3.528*	0.299	0.000	-4.122	-2.934
	DSIHE	-4.541*	0.299	0.000	-5.135	-3.947
	MMBEBHE	-5.847*	0.299	0.000	-6.441	-5.253
	MBORBHE	-8.719*	0.299	0.000	-9.313	-8.125
MMBEBHE	HE	4.498*	0.299	0.000	3.904	5.092
	BBHE	2.318*	0.299	0.000	1.724	2.913
	DSIHE	1.306*	0.299	0.000	0.712	1.900
	RSIHE	5.847*	0.299	0.000	5.253	6.441
	MBORBHE	-2.871*	0.299	0.000	-3.465	-2.277
MBORBHE	HE	7.369*	0.299	0.000	6.775	7.964
	BBHE	5.190*	0.299	0.000	4.596	5.784
	DSIHE	4.177*	0.299	0.000	3.583	4.772
	RSIHE	8.719*	0.299	0.000	8.125	9.313
	MMBEBHE	2.871*	0.299	0.000	2.277	3.465

*The mean difference is significant at the 0.05 level.

Table 4.4: Categorization of contrast enhancement methods into homogenous subset using the Duncan test for SNR

Method	N	Subset for alpha = 0.05					
		1	2	3	4	5	6
RSIHE	20	20.458					
HE	20		21.807				
BBHE	20			23.987			
DSIHE	20				24.999		
MMBEBHE	20					26.306	
MBORBHE	20						**29.177**
Sig.		1.000	1.000	1.000	1.000	1.000	1.000

Means for groups in homogeneous subsets are displayed.
Uses Harmonic Mean Sample Size = 20.000.

Fisher's Least Significant different test as shown in Table 4.5 indicates that the mean difference between BBHE and RSIHE was -0.029 and was 0.029 between RSIHE and BBHE. The mean difference between MMBEBHE and MBORBHE was -0.019 and was 0.019 between MBORBHE and MMBEBHE. From these data, it can be said that there was no significant mean difference between the values of SSIM in case of BBHE and

RSIHE, as well as MMBEBHE and MBORBHE methods. However, other contrast enhancement methods had significant mean difference among them.

Table 4.5: Categorization of different methods using Fisher's Least Significant Difference (LSD) for SSIM

(I) Method	(J) Method	Mean Difference (I-J)	Std. Error	Sig.	95% Confidence Interval	
					Lower Bound	Upper Bound
HE	BBHE	-0.098*	0.020	0.000	-0.138	-0.058
	DSIHE	0.359*	0.020	0.000	0.319	0.399
	RSIHE	-0.127*	0.020	0.000	-0.167	-0.087
	MMBEBHE	-0.192*	0.020	0.000	-0.232	-0.152
	MBORBHE	-0.212*	0.020	0.000	-0.252	-0.172
BBHE	HE	0.098*	0.020	0.000	0.058	0.138
	DSIHE	0.457*	0.020	0.000	0.417	0.498
	RSIHE	-0.029	0.020	**0.154**	-0.069	0.011
	MMBEBHE	-0.094*	0.020	0.000	-0.134	-0.054
	MBORBHE	-0.114*	0.020	0.000	-0.154	-0.074
DSIHE	HE	-0.359*	0.020	0.000	-0.399	-0.319
	BBHE	-0.457*	0.020	0.000	-0.498	-0.417
	RSIHE	-0.487*	0.020	0.000	-0.527	-0.446
	MMBEBHE	-0.552*	0.020	0.000	-0.592	-0.512
	MBORBHE	-0.572*	0.020	0.000	-0.612	-0.532
RSIHE	HE	0.127*	0.020	0.000	0.087	0.167
	BBHE	0.029	0.020	**0.154**	-0.011	0.069
	DSIHE	0.487*	0.020	0.000	0.446	0.527
	MMBEBHE	-0.065*	0.020	0.002	-0.105	-0.025
	MBORBHE	-0.085*	0.020	0.000	-0.125	-0.045
MMBEBHE	HE	0.192*	0.020	0.000	0.152	0.232
	BBHE	0.094*	0.020	0.000	0.054	0.134
	DSIHE	0.552*	0.020	0.000	0.512	0.592
	RSIHE	0.065*	0.020	0.002	0.025	0.105
	MBORBHE	-0.019	0.020	**0.329**	-0.059	0.020
MBORBHE	HE	0.212*	0.020	0.000	0.172	0.252
	BBHE	0.114*	0.020	0.000	0.074	0.154
	DSIHE	0.572*	0.020	0.000	0.532	0.612
	RSIHE	0.085*	0.020	0.000	0.045	0.125
	MMBEBHE	0.019	0.020	**0.329**	-0.020	0.059

*. The mean difference is significant at the 0.05 level.

As the absolute values of mean difference (between two methods) was above a certain level (level was determined by mean difference of all methods), indicates that, there was significant mean difference between the two methods, if it is below that certain level, there would be no significant mean difference. In other words, if the value of sig. was greater than 0,005, there would be significant difference of mean values. The result of the above analysis is confirmed by using the Duncan test as shown in Table 4.6. where BBHE and RSIHE were categorized in the same subset (sub 3). At the same time, MMBEBHE and MBORBHE were also categorized in the same subset (sub 4).

Table 4.6: Categorization of contrast enhancement methods into homogenous subset using the Duncan test for SSIM

Method	N	Subset for alpha = 0.05			
		1	2	3	4
DSIHE	20	0.260			
HE	20		0.620		
BBHE	20			0.718	
RSIHE	20			0.747	
MMBEBHE	20				0.813
MBORBHE	20				**0.833**
Sig.		1.000	1.000	0.154	0.329

Means for groups in homogeneous subsets are displayed.
Uses Harmonic Mean Sample Size = 20.000.

Fisher Least Significant test as shown in Table 4.7 shows that the mean difference between HE and BBHE was 0.122 (-0.122 between BBHE and HE), -0/082 between HE and RSIHE (0.082 between RSIHE and HE), -0.007 between HE and MMBEBHE (0.007 between MMBEBHE and HE). From these values, it can be said that there was no significant difference for HE and BBHE, HE and RSIHE, HE and MMBEBHE, as the values of sig, for these methods were larger than 0.05. However other contrast enhancement methods had significant difference of the numerical values of entropy.

Table 4.7: Categorization of different methods using Fisher's Least Significance Difference (LSD) for Entropy

(I) Method	(J) Method	Mean Difference (I-J)	Std. Error	Sig.	95% Confidence Interval	
					Lower Bound	Upper Bound
	BBHE	0.122	0.151	**0.420**	-0.177	0.422
	DSIHE	-0.442*	0.151	0.004	-0.742	-0.142
HE	RSIHE	-0.082	0.151	**0.588**	-0.382	0.217
	MMBEBHE	-0.007	0.151	**0.963**	-0.306	0.292
	MBORBHE	-3.136*	0.151	0.000	-3.436	-2.836
	HE	-0.122	0.151	**0.420**	-0.422	0.177
	DSIHE	-0.564*	0.151	0.000	-0.864	-0.265
BBHE	RSIHE	-0.204	0.151	**0.179**	-0.504	0.095
	MMBEBHE	-0.129	0.151	**0.394**	-0.429	0.170
	MBORBHE	-3.258*	0.151	0.000	-3.558	-2.959
	HE	0.442*	0.151	0.004	0.142	0.742
	BBHE	0.564*	0.151	0.000	0.265	0.864
DSIHE	RSIHE	0.360*	0.151	0.019	0.060	0.659
	MMBEBHE	0.435*	0.151	0.005	0.135	0.735
	MBORBHE	-2.693*	0.151	0.000	-2.99	-2.394

	HE	0.082	0.151	**0.588**	-0.217	0.382
	BBHE	0.204	0.151	**0.179**	-0.095	0.504
RSIHE	DSIHE	-0.360*	0.151	0.019	-0.659	-0.060
	MMBEBHE	0.075	0.151	**0.620**	-0.224	0.375
	MBORBHE	-3.054*	0.151	0.000	-3.353	-2.754
	HE	0.007	0.151	**0.963**	-0.292	0.306
	BBHE	0.129	0.151	**0.394**	-0.170	0.429
MMBEBHE	DSIHE	-0.435*	0.151	0.005	-0.735	-0.135
	RSIHE	-0.075	0.151	**0.620**	-0.375	0.224
	MBORBHE	-3.129*	0.151	0.000	-3.429	-2.829
	HE	3.136*	0.151	0.000	2.836	3.436
	BBHE	3.258*	0.151	0.000	2.959	3.558
MBORBHE	DSIHE	2.693*	0.151	0.000	2.394	2.993
	RSIHE	3.054*	0.151	0.000	2.754	3.353
	MMBEBHE	3.129*	0.151	0.000	2.829	3.429

*The mean difference is significant at the 0.05 level.

This result was confirmed by using the Duncan test as shown in Table 4.8, where HE, BBHE, RSIHE, MMBEBHE were categorized in the same subset.

Table 4.8: Categorization of contrast enhancement methods into homogenous subset using Duncan test for Entropy

Method	N	Subset for alpha = 0.05		
		1	2	3
BBHE	20	4.430		
HE	20	4.552		
MMBEBHE	20	4.559		
RSIHE	20	4.635		
DSIHE	20		4.995	
MBORBHE	20			**7.689**
Sig.		.223	1.000	1.000

Means for groups in homogeneous subsets are displayed.
Uses Harmonic Mean Sample Size = 20.000.

According to the result computed by using the values of SNR, SSIM and Entropy, the performance of the contrast enhancement methods were ranked as in Table 4.9. The ranking were done based on the result of Duncan test as shown in Table 4.4, 4.6 and 4.8. As seen in Table 4.4, it was observed that the mean value of SNR for every method are in different subset, therefore, these six methods had been ranked in a descending order from 1 to 6 according to their mean values. Table 4.6 shows that the mean values of

SSIM for MMBEBHO and MBORBHE were in the same subset. It was also observed that mean values of SSIM for BBHE and RSIHE were also in the same subset. Therefore, in case of ranking rank 1st and 3rd occupied two pairs of methods, whereas rank 2nd and 4th remain empty. In Table 4.8, the mean values of Entropy for BBHE, HE, MMBEBHE and RSIHE were in the same subset. Therefore, for rankings they were placed in 3rd and MBORBHE and DSIHE were placed as 1st and 2nd according their values. The empty space as in Table 4.9, were due to readjustment made after conducting post hoc test. It was found that the proposed MBORBHE always outperformed the other methods consistently.. It was ranked first in case of SNR and Entropy. Meanwhile, MMBEBHE was ranked equal with MBORBHE in term of mean SSIM. From this analysis, it had been proved that the proposed method had outperformed the other methods.

Table 4.9: Ranking of different contrast enhancement methods in terms of SNR, SSIM and Entropy. The methods ranking has been computed according to Fisher's Least Significant Difference (LSD) and the Duncan test

Rank	SNR	SSIM	Entropy
1	**MBORBHE**	**MBORBHE**, MMBEBHE	**MBORBHE**
2	MMBEBHE		DSIHE
3	DSIHE	RSIHE, BBHE	RSIHE, MMBEBHE, HE, BBHE
4	BBHE		
5	HE	HE	
6	RSIHE	DSIHE	

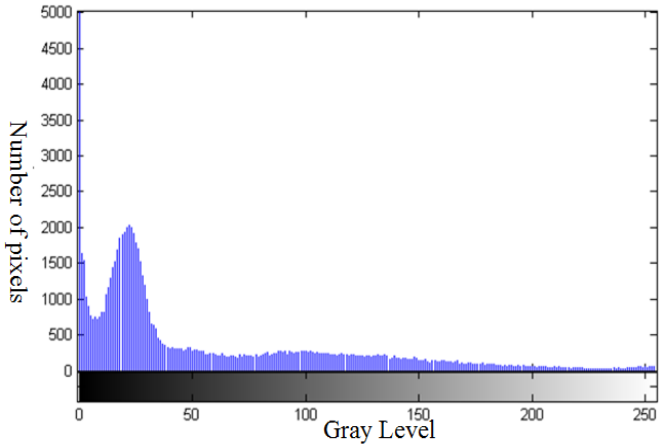

(a) Original image

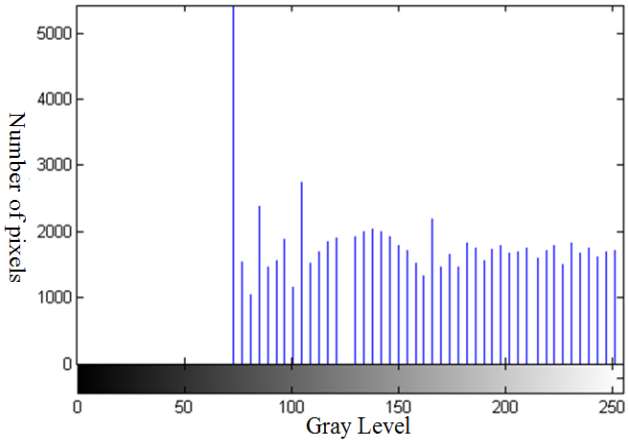

(b) HE based image

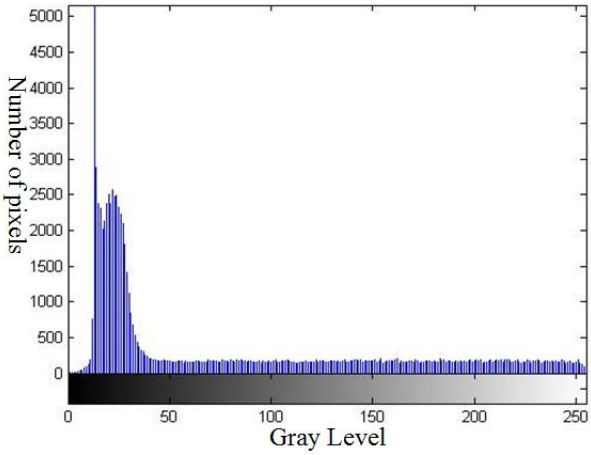

(c) Proposed method

Figure 4.4: (a), (b) and (c) denote the Histogram of US images of knee joint cartilage for original, HE based and proposed method respectively

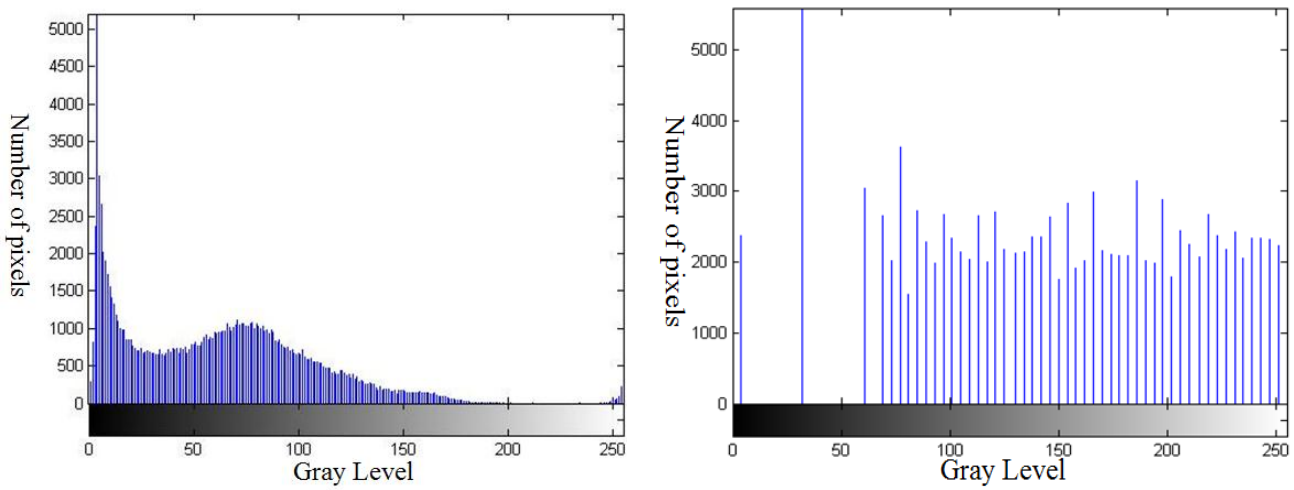

(a) Original image (b) HE based image

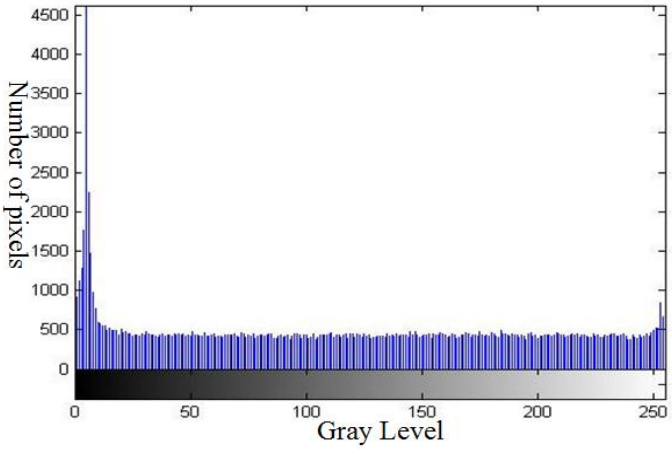

(c) Proposed method

Figure 4.5: (a), (b) and (c) denote the Histogram of US images of knee joint meniscus for original, HE based and proposed method respectively

4.2.2.1 Histogram equalization

The pattern of histograms for the original, HE and MBORBHE method based images for knee joint cartilage and meniscus are shown in Fig.4.4 and 4.5, respectively. As shown in Fig. 4.4(b) and 4.5(b)uncontrolled distribution of histogram was observed. This caused uncontrolled change in contrast, as well as brightness of the HE based image, as shown in Fig.4.1 (b) as well as Fig.4.2 (b).Fig.4.4 (c) and 4.5(c) present the controlled distribution of histogram for the proposed MBORBHE. This resulted in

expected contrast enhancement and brightness preservation of the proposed method, as shown in Fig. 4.1(g) and 4.2(g).

4.2.2.2 Mean shift

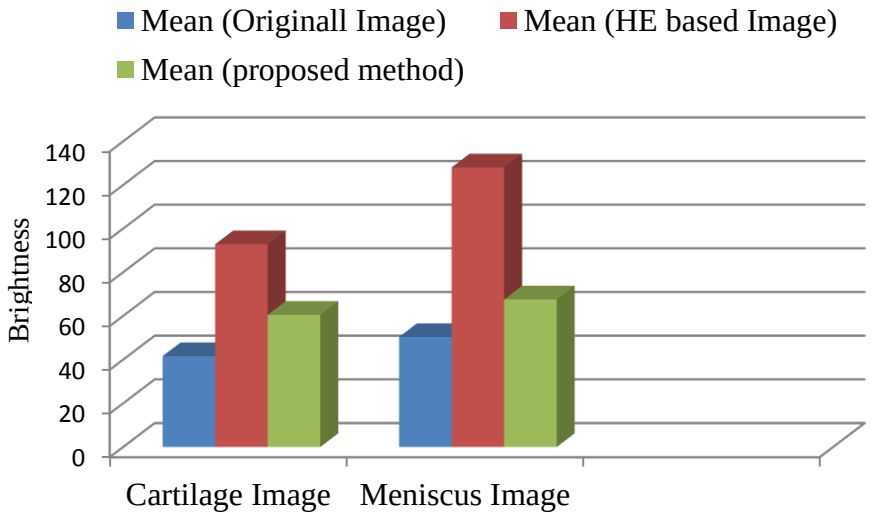

Figure 4.6: Mean of original, HE and Proposed HE method

One of the most encountered problem of HE based enhancement is the mean shift (mean brightness change) of the output images. It happens as intensity value is redistributed at the time of intensity normalization. The above bar chart shows the comparison of mean shift of the proposed method with the original image and HE based image. As seen in Fig.. 4.6 it was clear that HE based method dramatically changed the original mean of the input image, which degraded the brightness of the original image. However, by using the proposed MBORBHE method, it was seen that the mean value was almost equal to the mean value of the original image. This characteristic of the proposed MBORBHE method preserved the brightness of the original image. Therefore, the proposed method is better for brightness preservation compared with other HE methods.

4.2.2.3 Graph by entropy

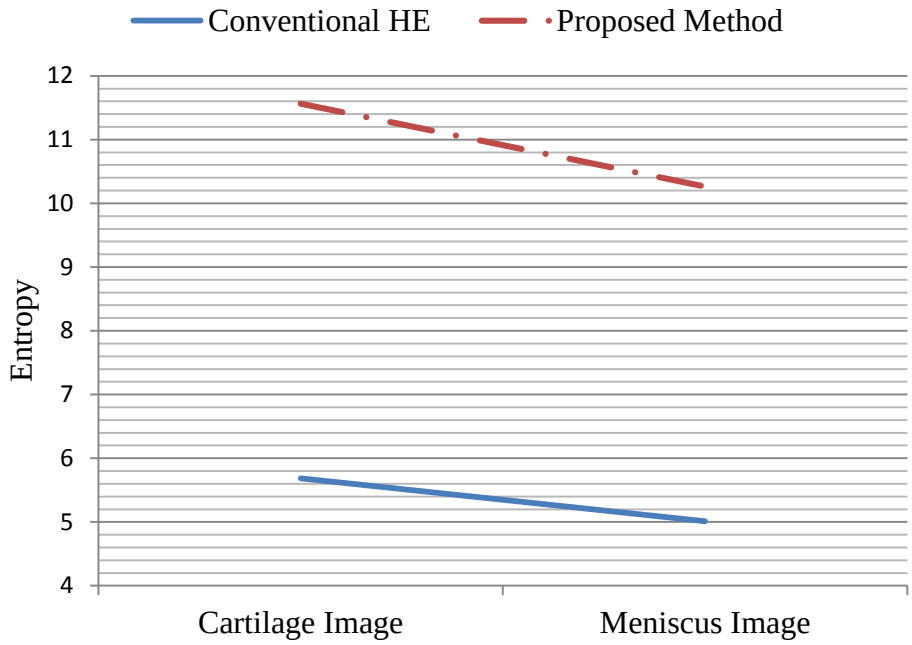

Figure 4.7: Entropy for conventional HE and proposed HE method for two images

Fig. 4.7 shows the graphical presentation of entropy of contrast enhanced images (Cartilage image, Meniscus image) by using conventional HE based method and proposed MBORBHE contrast enhancement method. The solid line (lower one) of the graph represented the values of entropy for conventional HE based methods, while the dotted line (upper one) of the graph indicates the entropy after the contrast enhancement by using the proposed MBORBHE method. From the graphical presentation, it was obvious that the entropy of the contrast enhanced image by using the proposed method was higher than the conventional HE based images. The higher value of entropy meant better contrast enhancement. Therefore, the graphical result proved that the proposed HE method is able for better contrast enhancement compared with other conventional HE methods.

4.3 For proposed AD method

For the performance evaluation of the proposed AD method, qualitative and quantitative analyses had been performed. Qualitative analysis was accomplished by using human visual perception, while quantitative analysis was done by using different performance metrics such as PSNR, SSIM, and FOM.

4.3.1 Qualitative analysis

For the performance evaluation of the proposed AD method, the qualitative analysis of real US image of knee joint cartilage and meniscus had been performed. The proposed method had been compared with different contemporary AD method such as Perona-Malik, NCD SRAD and LPND for qualitative performance evaluation. The qualitative analysis of US images are discussed below.

Firstly, the advantage of using proposed diffusivity function and four gradient thresholds has been confirmed by using the proposed diffusivity function and four gradient threshold separately, in case of conventional AD method. After that, the better performance of the proposed method for speckle noise reduction and edge preservation was evaluated in case of real US image of knee joint cartilage and meniscus.

For the evaluation of edge preservation ability of the proposed g2 function, AD filtering with g2 and g3 diffusivity function had been used, in case of simulated US image as shown in Fig.4.8 Ultrasound model described by Yu et al. (Y. Yu, Acton, S.T., 2002) had been used to simulate the images. Fig. 4.8(a) shows the original image and Fig. 4.8(b) shows the simulated US image. As seen in Fig.4.8(c) and (d), it was also clear that the speckle noise reduction and edge preservation ability of the g2 function were much better than those of g3 function. Here, t=30 and k=0.4 had been used. As seen in

Fig. 4.8, it was clear that the performance of the conductance function g2 was much better than that of g3 for edge preservation and speckle noise reduction.

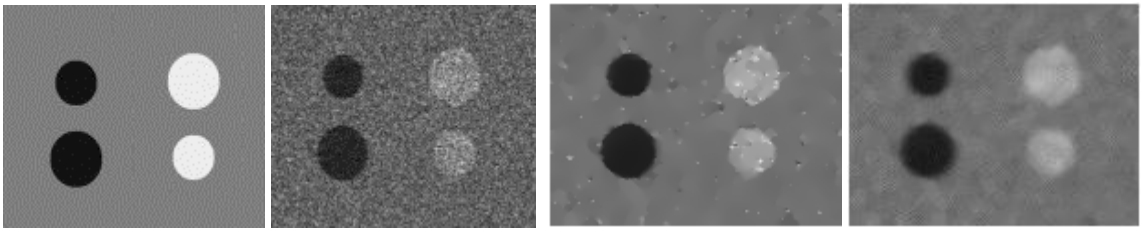

(a) (b) (c) (d)

Figure 4.8: (a) original image. (b) Simulated ultrasound image (c) AD filtering using g2 after 30 iterations (d) AD filtering using g3 after 30 iteration

For finding out the advantage of using four gradient threshold over one and two, portion of the seismic image for AD filtering with one, two and four gradient thresholds had been used**.** Fig. 4.9(a) shows the original image and Fig. 4.9(b) shows AD filtering by using one gradient threshold. Fig. 4.9 (c) and (d) show AD filtering from the use of two and four gradient thresholds, respectively. By comparing the line indicated by the arrows as Fig. 4.9(c) and (d) then it was observed that the starting and the middle of this line were much blurred compared to those as shown in Fig. 4.9(d). This phenomenon was observable in other places as well. Therefore as seen in Fig. 4.9, it can be said that the edge preservation in Fig.4.9 (d) was much better than the edge preservation as shown in Fig.4.9 (b) and Fig.4.9 (c). From Fig. 4.9, it can also be said that selecting one or two gradient threshold value *S* overestimated the threshold value between true edge and noise. This over estimation resulted in quick degradation (over smoothing) of the image edge, as shown in Fig.4.9 (b) and (c). From these it was clear that our proposed method was much better in preserving edge while reducing the speckle noise of the US image, as it had used four gradient thresholds instead of one.

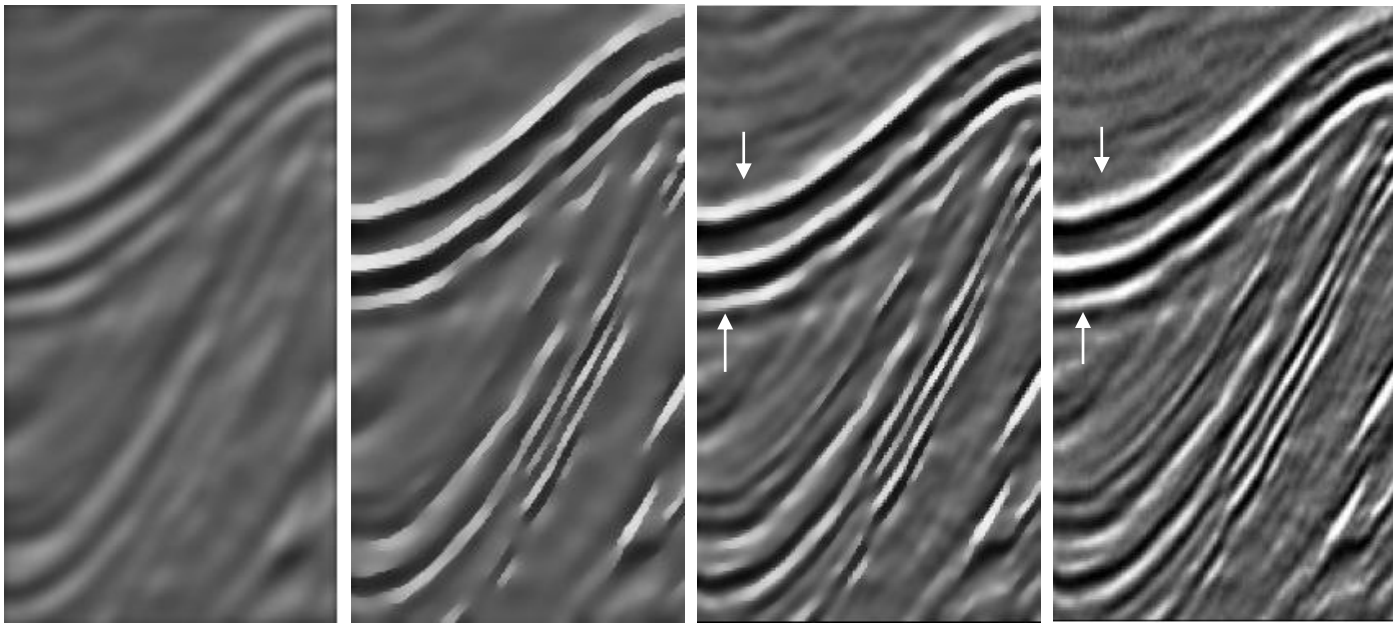

(a) (b) (c) (d)

Figure 4.9: (a) Portion of seismic image. (b) Filtered version with estimated one gradient threshold S after 10 iterations. (c) Filtered version with estimated two gradient threshold after 10 iterations. (d) Filtered version with estimated four gradient threshold

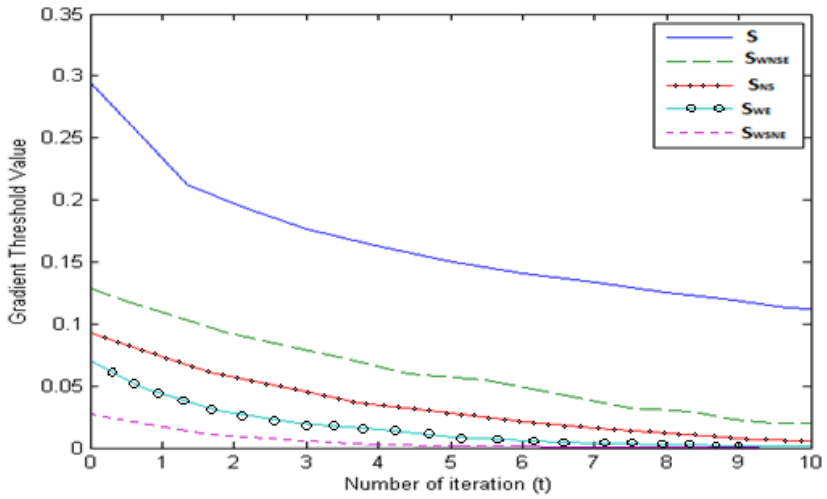

Figure 4.10: The estimation of one gradient threshold parameter *S*, two gradient threshold parameters S_{NS}, S_{EW}, and estimation of four threshold parameters S_{WNSE} and S_{NEWS} of Fig. 4.9 in every iteration with the help of knee algorithm

It is known that the gradient threshold should show decreasing function of time with the number of iterations. As shown in Fig.4.10 it was obvious that gradient threshold parameters showed decreasing function of time. It was also observed that the gradient

threshold estimated for S_{WNSE} in every iteration was much higher than those in S_{NS}, S_{WE}, and S_{WSNE}. The reason for this was that most edges of figure as shown inFig.4.9 were oriented from west-South to North-East direction. Thus, the strength of difference was higher in case of west-North to South-East direction. Larger difference in that direction would certainly obtain higher value of *S* for that direction.

4.3.1.1 Test on Cartilage Image

Fig. 4.11(a) shows the US image of knee joint cartilage. The arrows in Fig.4.11 (a) (Male, 35) indicate the upper layer and lower layer of the cartilage of knee joint. The image as shown in Fig. 4.11(b) was over smoothed, due to overestimation of the gradient threshold, as a result of using only one gradient threshold. The reversed 'U' shape cartilage was fully blurred. Underestimation of gradient threshold was observable, as shown in Fig. 4.11(c) and (d). As a result, the speckle noise was not removed efficiently. These figures were a little bit blurred compare to these in Fig.4.11 (f). As shown in Fig. 4.11(e), the overestimation of gradient threshold which degraded the edge preservation ability of the filter was observed. It also remove the important details of the US image. By observing the output image of the proposed method of Fig. 4.11(f), it can be concluded that edge preservation and noise reduction have been better performed simultaneously.

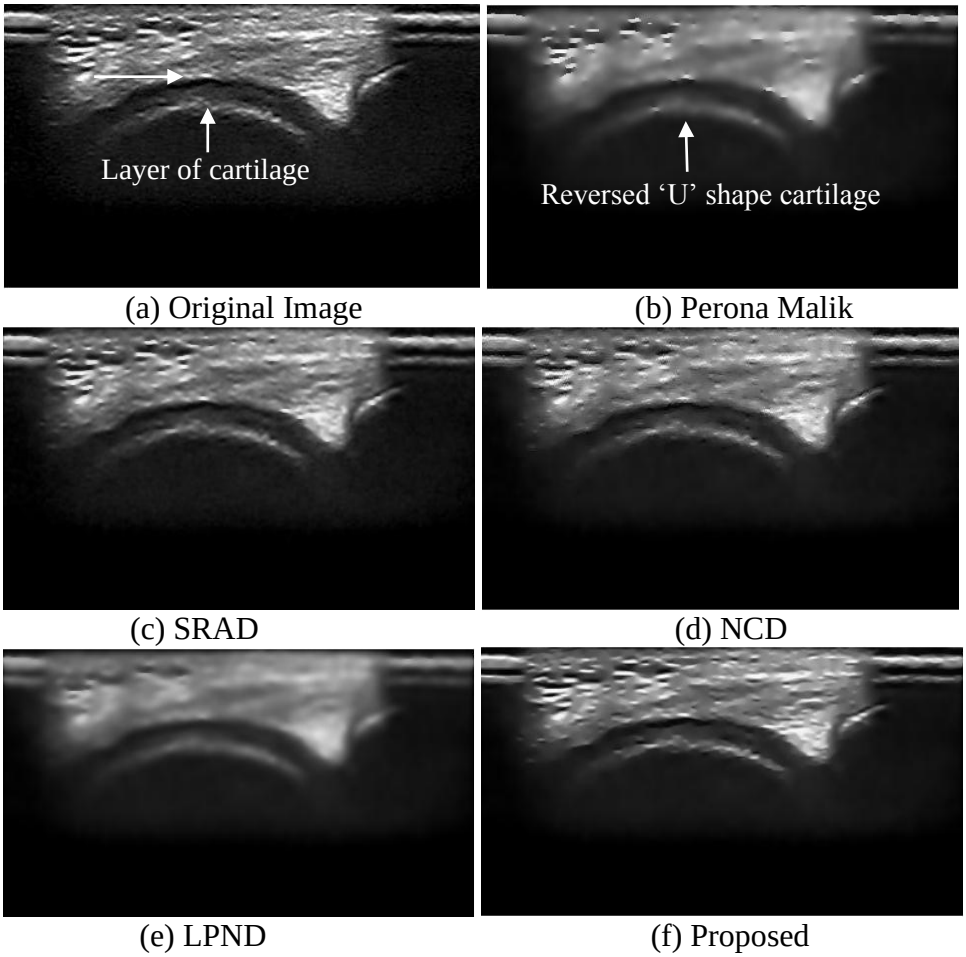

Figure 4.11: US Image of Cartilage for AD (a) Original Image. Resultant image of AD filtered image by using (b) Perona Malik method (c) SRAD method (d) Non-Linear Complex Diffusion method (NCD) (e) LPND (f) Proposed method.

4.3.1.2 Test on Meniscus Image

Fig. 4.12(a) shows the original US image (Male, 27) of knee joint meniscus. The arrows in Fig.4.12 (a) indicate the upper layer and lower layer of the cartilage of knee joint. Fig. 4.12(b), (c), (d) and (e) shows the resultant images of different speckle reduction methods, named as PM, SRAD, NCD and LPND. Fig. 4.12(f) shows the images result for the proposed method. The image as shown in Fig. 4.12(b) is over smooth which degraded the preservation ability of the edge, over estimating the gradient threshold. The ‘V’ shape cartilage is fully blurred. Fig. 4.12(c) shows an underestimated gradient threshold as some noise was left compared with Fig.4.12 (f). As shown in Fig. 4.12(d) it was observed that the edge preservation as well as noise smoothing were both

deteriorating. Some important details had also been removed. The shape of cartilage also became blurred. Fig. 4.12(e) also shows poor edge preservation ability. The degradation of 'V' shape cartilage was fully noticeable. It also removed important details of the US image. Nevertheless, as shown in Fig 4.12(f) it was seen that by using four gradient thresholds and the proposed diffusivity function, it was possible to reduce the noise effectively and preserve the edge of the image efficiently.

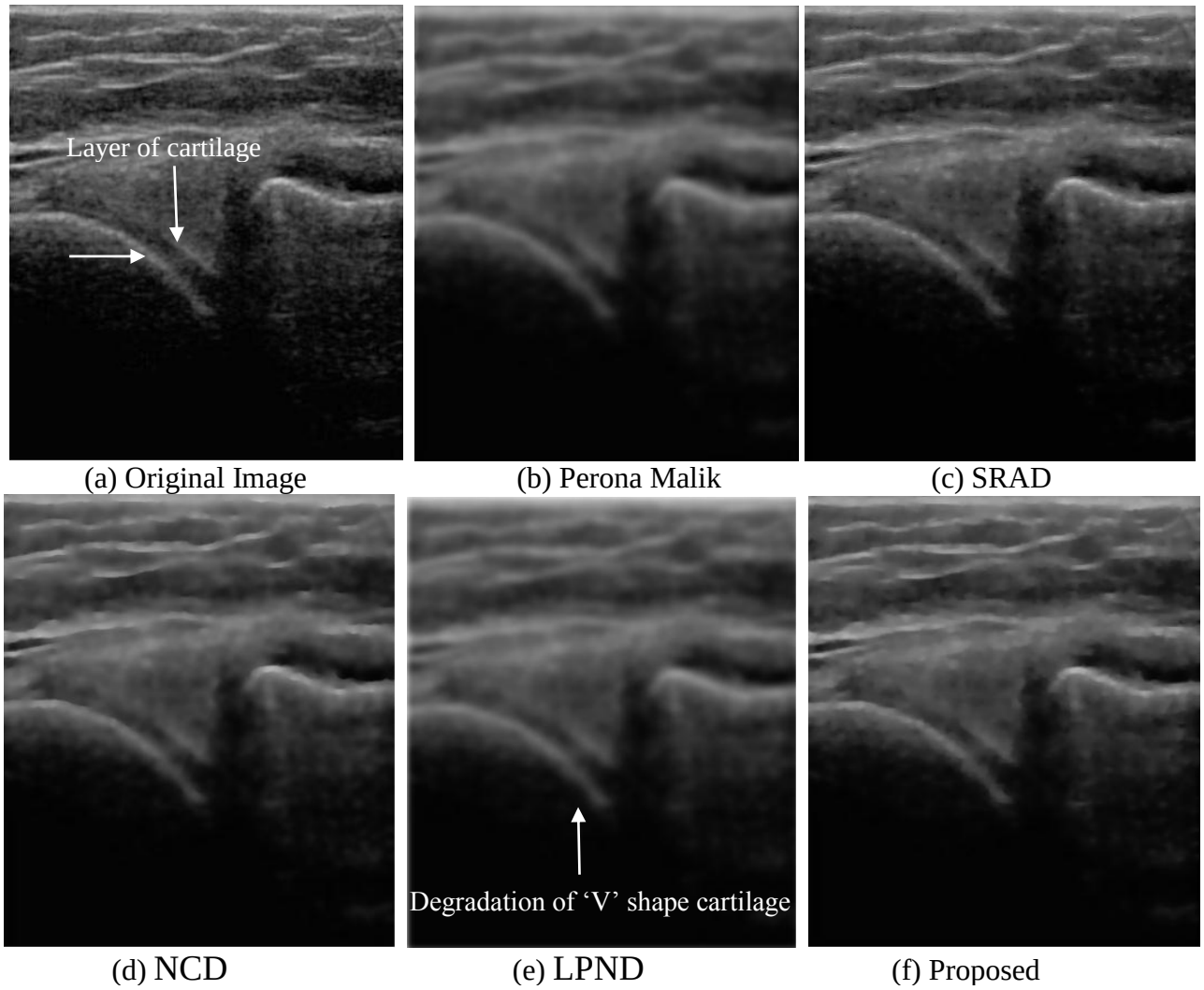

(a) Original Image (b) Perona Malik (c) SRAD

(d) NCD (e) LPND (f) Proposed

Figure 4.12: US image of cartilage for medial side of knee joint for AD (a) Original Image. Resultant image of AD filter by using (b) Perona Malik method (c) SRAD method (d) Non-Linear Complex Diffusion method (NCD) (e) LPND (f) Proposed method.

4.3.2 Quantitative analysis

Different diffusion methods had also been compared for the quantitative analysis, by using different performance metrics (PSNR, SSIM and FOM) for real ultrasound images. Statistical analysis had been performed by using IBM SPSS statistic (version 21). In this analysis, it was shown that the proposed speckle reduction method outperformed others methods. Three quantitative metrics, namely PSNR, SSIM and FOM had been used for the performance analysis of the proposed method.

Table 4.10: Mean value of PSNR, SSIM and FOM with standard deviation for PM, LPND, NCD, SRAD and proposed method

Method	Mean PSNR±SD	95% confidence interval of difference		Mean SSIM±SD	95% confidence interval of difference		Mean FOM±SD	95% confidence interval of difference	
		Lower Bound	Upper Bound		Lower Bound	Upper Bound		Lower Bound	Upper Bound
Perona-Malik	23.088±1.227	22.514	23.663	0.732±0.065	0.702	0.762	0.443±0.056	0.416	0.469
LPND	25.403±0.816	25.021	25.785	0.803±0.038	0.785	0.821	0.480±0.035	0.463	0.496
NCD	25.236±0.793	24.865	25.608	0.850±0.026	0.838	0.863	0.559±0.040	0.540	0.579
SRAD	27.328±0.693	27.003	27.653	0.854±0.018	0.846	0.862	0.671±0.010	0.566	0.577
Proposed	**31.509±1.045**	31.020	31.999	**0.866±0.027**	0.853	0.878	**0.712±0.046**	0.690	0.734

Table 4.10 shows the mean value of PSNR, SSIM and FOM for the filtered US image of 20 healthy subjects for different filtering methods. In case of PSNR and FOM, the height values were 31.509±1.045 and 0.712±0.046. These values were obtained for the proposed AD method. The least values of PSNR and FOM were in case of conventional Perona –Malik (PM) method, which were 23.088±1.227 and 0.443±0.056, respectively, In case of SSIM and FOM, the values for NCD, SRAD and proposed method were almost similar. As the values of different performance metrics for SRAD and proposed method were almost similar, further analysis was also performed to test our hypothesis.

Table 4.11: The one-way ANOVA computed by using different speckle reduction methods in PSNR, FOM and SSIM

		Sum of Squares	df	Mean Square	F	Sig.
PSNR	Between Groups	804.378	4	201.095	229.710	0.000*
	Within Groups	83.166	95	0.875		
	Total	887.544	99			
FOM	Between Groups	0.864	4	0.216	129.222	0.000*
	Within Groups	0.159	95	0.002		
	Total	1.023	99			

SSIM	Between Groups	0.244	4	0.061	40.800	0.000*
	Within Groups	0.142	95	0.001		
	Total	0.386	99			

*Significant sig. value (sig<0.05)

Table 4.11 shows that comparison if there is any significant difference between the values of quantitative metric of different methods or not. As seen in the Table it can be said that there was significant difference among the quantitative values of PSNR, FOM and SSIM for different methods. As the value of sig. was less than 0.05, there was indeed significant difference. As a result, the data was further analyzed by using post hoc test (Fisher's Least Significant and Duncan test) to evaluate the performance of different speckle reduction methods.

Table 4.12: Categorization of different methods using Fisher's Least Significance Difference (LSD) for PSNR

(I) Methods	(J) method	Mean Difference (I-J)	Std. Error	Sig.	95% Confidence Interval	
					Lower Bound	Upper Bound
PM	LPND	-2.314*	0.295	0.000	-2.902	-1.727
	NCD	-2.148*	0.295	0.000	-2.735	-1.560
	SRAD	-4.239*	0.295	0.000	-4.827	-3.652
	PROPOSED	-8.421*	0.295	0.000	-9.008	-7.833
LPND	PM	2.314*	0.295	0.000	1.727	2.902
	NCD	0.166	0.295	**0.574**	-0.420	0.754
	SRAD	-1.924*	0.295	0.000	-2.512	-1.337
	PROPOSED	-6.106*	0.295	0.000	-6.693	-5.518
NCD	PM	2.148*	0.295	0.000	1.560	2.735
	LPND	-0.166	0.295	**0.574**	-0.754	0.420
	SRAD	-2.091*	0.295	0.000	-2.678	-1.504
	PROPOSED	-6.273*	0.295	0.000	-6.860	-5.685
SRAD	PM	4.239*	0.295	0.000	3.652	4.827
	LPND	1.924*	0.295	0.000	1.337	2.512
	NCD	2.091*	0.295	0.000	1.504	2.678
	PROPOSED	-4.181*	0.295	0.000	-4.768	-3.594
PROPOSED	PM	8.421*	0.295	0.000	7.833	9.008
	LPND	6.106*	0.295	0.000	5.518	6.693
	NCD	6.273*	0.295	0.000	5.685	6.860
	SRAD	4.181*	0.295	0.000	3.594	4.768

*The mean difference is significant at the 0.05 level.

Fisher's least significant difference test (Table 4.12) indicates that the mean difference between LPND and NCD was 0.166 and was -0.166 between NCD and LPND. It is insignificant in PSNR. However, other contrast enhancement methods showed significant mean difference. The result was confirmed by using the Duncan test (Table 4.13) which categorized NCD and LPND into the same subset.

Table 4.13: Categorization of speckle reduction methods into homogenous subset using the Duncan test for PSNR

Methods	N	Subset for alpha = 0.05			
		1	2	3	4
PM	20	23.088			
NCD	20		25.236		
LPND	20		25.403		
SRAD	20			27.328	
PROPOSED	20				**31.509**
Sig.		1.000	.574	1.000	1.000

Means for groups in homogeneous subsets are displayed.
Harmonic Mean Sample Size = 20.000.

Fisher least significant difference test as shown in Table 4.14 indicates that the mean difference between NCD and SRAD was -0.011 and was 0.011 between SRAD and NCD. It was insignificant in FOM. Meanwhile other speckle reduction methods showed significant mean difference.

Table 4.14: Categorization of different methods using Fisher's Least Significant Difference (LSD) for FOM

(I) Methods	(J) method	Mean Difference (I-J)	Std. Error	Sig.	95% Confidence Interval	
					Lower Bound	Upper Bound
PM	LPND	-0.037*	0.012	0.005	-0.062	-0.011
	NCD	-0.116*	0.012	0.000	-0.142	-0.091
	SRAD	-0.128*	0.012	0.000	-0.154	-0.103
	PROPOSED	-0.269*	0.012	0.000	-0.295	-0.243
LPND	PM	0.037*	0.012	0.005	0.011	0.062
	NCD	-0.079*	0.012	0.000	-0.105	-0.053
	SRAD	-0.091*	0.012	0.000	-0.117	-0.065
	PROPOSED	-0.232*	0.012	0.000	-0.257	-0.206
NCD	PM	0.116*	0.012	0.000	0.091	0.142
	LPND	0.079*	0.012	0.000	0.053	0.105
	SRAD	-0.011	0.012	**0.358**	-0.037	0.013
	PROPOSED	-0.152*	0.012	0.000	-0.178	-0.126
SRAD	PM	0.128*	0.012	0.000	0.103	0.154
	LPND	0.091*	0.012	0.000	0.065	0.117
	NCD	0.011	0.012	**0.358**	-0.013	0.037
	PROPOSED	-0.140*	0.012	0.000	-0.166	-0.114
PROPOSED	PM	0.269*	0.012	0.000	0.243	0.295
	LPND	0.232*	0.012	0.000	0.206	0.257
	NCD	0.152*	0.012	0.000	0.126	0.178
	SRAD	0.140*	0.012	0.000	0.114	0.166

*The mean difference is significant at the 0.05 level.

This result had also been confirmed by using Duncan test as shown in Table 4.15. It categorized the NCD and SRAD in the same subset.

Table 4.15: Categorization of speckle reduction methods into homogenous subset using the Duncan test for FOM

Methods	N	Subset for alpha = 0.05			
		1	2	3	4
PM	20	0.443			
LPND	20		0.480		
NCD	20			0.559	
SRAD	20			0.571	
PROPOSED	20				**0.712**
Sig.		1.000	1.000	0.358	1.000

Means for groups in homogeneous subsets are displayed.
Uses Harmonic Mean Sample Size = 20.000.

Fisher's least significant difference test as shown in Table 4.16 indicates that the mean difference between NCD and SRAD was -0.003 and was 0.003 between SRAD and NCD. The difference between NCD and PROPOSED was -0.015 and was 0.015 between PROPOSED and NCD. At the same time, the difference between PROPOSED and SRAD is 0.011 and was -0.011 between SRAD and PROPOSED. These were insignificant in SSIM. Other speckle reduction methods showed significant mean difference. The result had been confirmed by using the Duncan test as shown in Table 4.17.

Table 4.16: Categorization of different methods using Fisher's Least Significance Difference (LSD) for SSIM

(I) Methods	(J) method	Mean Difference (I-J)	Std. Error	Sig.	95% Confidence Interval	
					Lower Bound	Upper Bound
PM	LPND	-0.070*	0.012	0.000	-0.095	-0.046
	NCD	-0.118*	0.012	0.000	-0.142	-0.093
	SRAD	-0.122*	0.012	0.000	-0.146	-0.097
	PROPOSED	-0.133*	0.012	0.000	-0.157	-0.109
LPND	PM	0.070*	0.012	0.000	0.046	0.095
	NCD	-0.047*	0.012	0.000	-0.071	-0.023
	SRAD	-0.051*	0.012	0.000	-0.075	-0.026
	PROPOSED	-0.062*	0.012	0.000	-0.086	-0.038
NCD	PM	0.118*	0.012	0.000	0.093	0.142
	LPND	0.047*	0.012	0.000	0.023	0.071
	SRAD	-0.003	0.012	**0.759**	-0.028	0.020
	PROPOSED	-0.015	0.012	**0.210**	-0.039	0.008
SRAD	PM	0.122*	0.012	0.000	0.097	0.146
	LPND	0.051*	0.012	0.000	0.026	0.075
	NCD	0.003	0.012	**0.759**	-0.020	0.028
	PROPOSED	-0.011	0.012	**0.342**	-0.035	0.012
PROPOSED	PM	0.133*	0.012	0.000	0.109	0.157
	LPND	0.062*	0.012	0.000	0.038	0.086
	NCD	0.015	0.012	**0.210**	-0.008	0.039
	SRAD	0.011	0.012	**0.342**	-0.012	0.035

*The mean difference is significant at the 0.05 level.

Table 4.17: Categorization of speckle reduction methods into homogenous subset using Duncan's test for SSIM

Methods	N	Subset for alpha = 0.05		
		1	2	3
PM	20	0.732		
LPND	20		0.803	
NCD	20			0.850
SRAD	20			0.854
PROPOSED	20			**0.866**
Sig.		1.000	1.000	0.238

Means for groups in homogeneous subsets are displayed.
Harmonic Mean Sample Size = 20.000.

The performance of the different speckle reduction methods (PM, LPND, NCD, SRAD and PROPOSED) had been ranked by using the result computed from PSNR, SSIM and FOM. Table 4.18 showed the rank of different methods. Some empty spaces that as in Table 4.18 were the readjustment made after conducting post hoc test. It had been observed that the proposed method outperformed other methods constantly in all the test and was ranked first in PSNR and FOM. However, in SSIM other two methods namely SRAD and NCD also were ranked equal to the proposed method. It was also observed that the conventional Perona-Malik (PM) model always remained at the bottom of the ranking, meaning that it faced a lot of limitations for reducing speckle and edge preserving of the US image.

Table 4.18: Ranking of methods in terms of peak PSNR, SSIM and FOM. The method ranking is computed according to Fisher's Least Significance Difference (LSD) and the Duncan test.

Rank	PSNR	SSIM	FOM
1	**PROPOSED**	**PROPOSED, SRAD, NCD**	**PROPOSED**
2	SRAD		SRAD, NCD
3	NCD, LPND		
4		LPND	LPND
5	PM	PM	PM

All experiments were conducted on a PC with 3.0-GHz Core i5 processor in Matlab 7.9.0 (R2009b). This software had also been used for studying different graphical output. It took 10s, 26s, 9s, 24s and 44s for Perona-Malik, SRAD, CND, LPND and proposed method. For the proposed method it took much longer time as larger computation needed to be is performed.

CHAPTER 5

CONCLUSION AND FUTURE WORK

5.1 Conclusion

This thesis has successfully solved the limitations of US imaging in terms of low contrast and speckle noise. For contrast enhancement, it has used an effective contrast enhancing method named MBORBHE, which enhanced the contrast of the US images, considering detail and brightness preservation. For speckle noise reduction, it has used an improved AD method by developing a new diffusivity function and considering four gradient thresholds instead of one. The proposed contrast enhancing method gives emphasis on the selection of an optimum separating point used for segmenting the histogram of the image. This optimum separating point could be obtained from the three regularization functions. The proposed MBORBHE method was able to preserve better details and brightness during the contrast enhancement of the US image, outperforming other conventional HE methods. In the case of the proposed AD method, which is by using a new diffusivity function and four gradient threshold instead of one, it is able to reduce the speckle noise effectively as well as preserve the edge of the image successfully. For a suitable stopping time for iterations it has used a MAE stopping criterion between two consecutive diffusion iterations that will stop the diffusion automatically. In this thesis, in the proposed HE and AD method, performance has been evaluated qualitatively and quantitatively. This task has been accomplished by comparing different HE and AD methods with the proposed HE and AD method. Real ultrasound images of knee joint meniscus and cartilage have been used for the performance evaluation of the proposed HE and AD method. Qualitative analysis has been performed by using human visual perception. From qualitative observation, it can be concluded that the proposed MBORBHE method was able to preserve brightness and details, when contrast is being enhanced. On the other hand, the other methods only

consider either brightness or detail preservation while ignoring the other one. The proposed AD method which combine three steps mentioned above, also showed better performance that other diffusion methods, not only qualitatively but also quantitatively. The qualitative analysis proves that the proposed AD method outperforms other conventional AD methods in terms of speckle noise reduction and edge preservation. Statistical analysis has been performed for the quantitative analysis for the proposed HE and AD method. The statistical result that has been obtained from Fisher's Least Significance Difference test and Duncan test consistently proves that the proposed HE and AD method outperform other methods.

The proposed HE and AD method can also be used in the case of other medical imaging systems, for the improvement of image quality, such as MRI, X-ray and C.T. The output-improved image of the proposed method could have potentiality for detecting other joint OA as well. Lastly, it can be said that in any kind of medical imaging, for any kind of diagnosis, the proposed method will be helpful.

5.2 Limitation of the proposed method

The main idea of the proposed HE method is to find out the separating point for segmenting the histogram of the input image for which the brightness and detail preservation difference between the contrasts enhanced image and the original image is at its lowest level and the contrast enhancement is at its peak. Sometimes more than one point may be obtained for this, however the output result for the each point of optimum values is not same. So, selecting an accurate point is a limitation of the proposed method. In the proposed AD method, there are only two improved parameters; the diffusivity function, and the gradient threshold. It does not improve the other parameters such as stopping criterion for the proposed AD method. In this study, it used the US

images of 20 healthy subjects. No osteoarthritis US image has used for the contrast enhancement and speckle noise reduction. Clinical evaluation for detection of OA has not also been performed for our proposed method. Therefore, it does not evaluate the osteoarthritis detection parameters, such as reflection coefficient and attenuation by using different filtering methods. The proposed method only improves the US image of knee joint cartilage, which can be helpful for detecting early knee OA.

5.3 Future work

In the proposed HE method, brightness and detail preservation has been considered during the contrast enhancement of the images. For that reason three objective functions have been considered, viz. Preservation of Brightness Score function (PBS), Optimum Contrast Score function (OCS), and Preservation of Detail Score function (PDS). For future work, Preservation of Edge Score function (PES) should be included with the three objective functions to obtain a better output image. In the proposed AD method future work, there will be development of a better stopping criterion that will be suitable for US images and stop the iterations automatically. The future work will also include the use of proposed HE and AD method in US images of knee joint cartilage for OA cases. By using this filtering method, the thickness, sharpness and grey level of cartilage can also be measured, as this filter may reduce the speckle noise and preserve the edge of US cartilage image. The output of the US image will be used for accomplishing the clinical evaluation of the proposed method.

REFERENCES

A. Lopes, R. T., E. Nezry. (1990). Adaptive speckle filters and scene heterogeneity. *Geosci. Remote Sens, 28*, 992-1000.

A.Achim, A. B. (2001). Novel bayesian multiscale method for speckle removal inmedical ultrasound images. *Med.Imaging, 20*(8), 772–783.

A.Achim, A. B. (2001). Novel bayesian multiscale method for speckle removal inmedical ultrasound images. *Med.Imaging, 20*(8), 772-783.

A.J. Teichtahl, A. E. W., M.L. Davies-Tuck, F.M. Cicuttini. (2008). Best Practice & Research Clinical Rheumatology. *Imaging of knee osteoarthritis, 22*, 1061-1074.

A.K.Jain. (1989). Fundamentals of Digital Image Processing. *Prentice-Hallof India*.

A. Achim, Bezerianos, A., & Tsakalides, P. (2001). Novel Bayesian multiscale method for speckle removal in medical ultrasound images. *Medical Imaging, IEEE Transactions on, 20*(8), 772-783.

D. Adam, Beilin-Nissan, S., Friedman, Z., & Behar, V. (2006). The combined effect of spatial compounding and nonlinear filtering on the speckle reduction in ultrasound images. *Ultrasonics, 44*(2), 166-181.

A Shanks Huynh, D. F. A., Monica S. Torres, Margaret K. Baldwin, Robert J. Gillies, David L. Morse. (2011). Development of an Orthotopic Human Pancreatic Cancer Xenograft Model Using Ultrasound Guided Injection of Cells. *PLoS ONE, 6*(5), 1-9.

B.Sahiner. (2007). Malignant and benign breast masses on 3D US volumetric images: effect of computer-aided diagnosis on radiologist accuracy. *Radiology, 242*(3), 716-724.

B.Sahiner. (2008). Malignant and benign breast masses on 3D US volumetric images: effect of computer-aided diagnosis on radiologist accuracy. *Radiology, 242*(3), 316-320.

V. Behar, Adam, D., & Friedman, Z. (2003). A new method of spatial compounding imaging. *Ultrasonics, 41*(5), 377-384.

M. Black, J., Sapiro, G., Marimont, D. H., & Heeger, D. (1998). Robust anisotropic diffusion. *Image Processing, IEEE Transactions on, 7*(3), 421-432.

H. Bliddal, Boesen, M., Christensen, R., Kubassova, O., & Torp-Pedersen, S. (2008). Imaging as a follow-up tool in clinical trials and clinical practice. *Best Practice & Research Clinical Rheumatology, 22*(6), 1109-1126.

JM. Bremner, L. J., Miall WE. (1968). Degenerative joint disease in a Jamaican rural population. *Annals of the Rheumatic Diseases, 27*(4), 326-332.

A. Buades, Coll, B., & Morel, J.-M. (2005). A review of image denoising algorithms, with a new one. *Multiscale Modeling & Simulation, 4*(2), 490-530.

J. A. Buckwalter, & Martin, J. A. (2006). Osteoarthritis. *Advanced Drug Delivery Reviews, 58*(2), 150-167. doi: http://dx.doi.org/10.1016/j.addr.2006.01.006

C. B. Burckhardt,. (1978). Speckle in ultrasound B-mode scans. *Sonics and Ultrasonics, IEEE Transactions on, 25*(1), 1-6.

C.B.Burckhardt. (1987). Speckle in ultrasound B-mode scans. *Sonics Ultrason., 25*(1), 1-6.

CD Control. (2003) Public health and aging: Projected prevalence of self reported arthritis or chronic joint symptoms among persons aged 65 years in United States, 2005-2030.. *MMWR Morb Mortal Wkly Rep,, 52*(21), 489-491.

D.-R. Chen,., Chang, R.-F., Chen, C.-J., Ho, M.-F., Kuo, S.-J., Chen, S.-T., . . . Moon, W. K. (2005). Classification of breast ultrasound images using fractal feature. *Clinical imaging, 29*(4), 235-245.

R. N. Czerwinski,., Jones, D. L., & O'Brien, W. (1999). Detection of lines and boundaries in speckle images-application to medical ultrasound. *Medical Imaging, IEEE Transactions on, 18*(2), 126-136.

D. Adam, E. E., Y.Y. Schechner. (2006). Ultrasound image denoising by spatially varying frequency compounding. *Lecture Notes on Computer Science, 41*(47), 1-10.

D.T. Kuan, A. A. S., T.C. Strand, P. Chavel. (1987). Adaptive restoration of images with speckle. *Acoust. Speech Signal Process. ASSP, 35*, 373-383.

MA. Davis, E. W., Neuhaus JM, Hauck WW. (1988). Sex differences in osteoarthritis of the knee. The role of obesity. *American Journal of Epidemiology, 127*(5), 1019-1030.

L. Douglas. Miller, C. D., Dorothy Sorenson, Ming Liu. (2011). Histological Observation of Islet Hemorrhage Induced by Diagnostic Ultrasound with Contrast Agent in Rat Pancreas. *PLoS ONE, 6*(6), 1-7.

F. Eckstein, C. F., Raynauld J, Waterton JC, Peterfy C. (2006). Magnetic resonance imaging (MRI) of articular cartilage in knee osteoarthritis (OA): morphological assessment. *Osteoarthr Cartil 2006;, 14*((Suppl A)), 46–75.

E. Michael Jung, C. F., Patrick Hoffstetter, Lena Marie Dendl, Frank Klebl, Ayman Agha, Phillipp Wiggermann, Christian Stroszcynski, Andreas Georg Schreyer. (2012). Volume Navigation with Contrast Enhanced Ultrasound and Image Fusion for Percutaneous Interventions: First Results. *PLoS ONE, 7*(3), 1-7.

J. Evans, P. O., Godber, S. X., & Robinson, M. (1994). *Three-dimensional x-ray display techniques.* Paper presented at the IS&T/SPIE 1994 International Symposium on Electronic Imaging: Science and Technology.

F.Catte´ , P. L., J.Morel,T.Coll. (1992). Image selective smoothing and edge detection by nonlinear diffusion. *SIAM J. Numer. Anal., 29*, 182-193.

F.Zhang, Y. M. Y., L.M.Koh,Y.Kim,. (2007a). Nonlinear diffusion in Laplacian pyramid domain for ultrasonic speckle reduction. *IEEETrans.Med.Imag, 26*, 200–211.

F.Zhang, Y. M. Y., L.M.Koh,Y.Kim,. (2007b). Nonlinear diffusion in laplacian pyramid domain for ultrasonic speckle reduction. *Med.Imaging, 26*(2), 207-2011.

Farshad-Amacker, N. A., Lurie, B., Herzog, R. J., & Farshad, M. (2013). Interreader and intermodality reliability of standard anteroposterior radiograph and magnetic resonance imaging in detection and classification of lumbosacral transitional vertebra. *The Spine Journal*.

DT. Felson, N. A., Anderson J, Kazis L, Castelli W, Meenan RF:. (1987). The prevalence of knee osteoarthritis in the elderly. The Framingham Osteoarthritis Study. *Arthritis and Rheumatism, 30*, 914-918.

V. Frost, S., Stiles, J. A., Shanmugan, K. S., & Holtzman, J. (1982). A model for radar images and its application to adaptive digital filtering of multiplicative noise. *Pattern Analysis and Machine Intelligence, IEEE Transactions on*(2), 157-166.

F. kwok, C. C. a. D. N. H. (1983). Comprise of Several Techniques to Obtain Multiple Look SAR Imagery *IEEE Transac. on Geosci and Remote Sensing, , 21*(3), 666-671.

G, ter. Haar. (2007). Therapeutic applications of ultrasound. *Prog Biophys Mol Bio, 93*, 111-129.

G.Gilboa, N. S., Y.Y.Zeevi,. (2004). Image enhancement and denoising by complex diffusion process. *IEEETrans.PatternAnal.Mach.Intell, 26*, 1020–1036.

LR. Gavrilov, T. E., Davies IA. (1996). Application of focused ultrasound for the stimulation of neural structures. *Ultrasound Med Biol, 22*, 179–192.

G. Gerig,., Kubler, O., Kikinis, R., & Jolesz, F. A. (1992). Nonlinear anisotropic filtering of MRI data. *Medical Imaging, IEEE Transactions on, 11*(2), 221-232.

T. Gibson, H. K., Kadir M, Sultana S, Fatima Z, Syed A. Knee pain amongst the poor and affluent in Pakistan. *British Journal of Rheumatology 1996, 35*(2), 146-149.

G. Gilboa, Sochen, N., & Zeevi, Y. Y. (2006). Estimation of optimal PDE-based denoising in the SNR sense. *Image Processing, IEEE Transactions on, 15*(8), 2269-2280.

H.D.Cheng, J. S., W.Ju,Y.Guo,L.Zhang. (2010). Automated breast cancer detection and classification using ultrasound images: a survey,. *Pattern Recognition, 43*(1), 299-317.

H.D.Cheng, J. S., W.Ju,Y.Guo,L.Zhang. (2010). Automated breast cancer detection and classification using ultrasound images: a survey,. *Pattern Recognition,, 43*(1), 299-317.

HA, Valkenburg. (1980). Clinical versus radiological osteoarthritis in the general population. *In: Peyron JG, editor. Epidemiology of osteoarthritis. Paris: Ciba-Geigy,*, 53-58.

D. Hamerman. (1995). Clinical implications of osteoarthritis and aging. *Annals of the Rheumatic Diseases, 54*, 82-85.

J. Hillary Braun a, c., Garry E. Gold. (2012). Diagnosis of osteoarthritis: Imaging. *Bone., 51*, 278-288.

H K., S. N. Choi. (2008). Brightness preservaing weight clustering histogram eualization. *IEEE Trans. Consumer Electronics, 54*, 1329-1337.

D..Hunter, J, Lo, G. H., Gale, D., Grainger, A. J., Guermazi, A., & Conaghan, P. G. (2008). The reliability of a new scoring system for knee osteoarthritis MRI and the validity of bone marrow lesion assessment: BLOKS (Boston–Leeds Osteoarthritis Knee Score). *Annals of the rheumatic diseases, 67*(2), 206-211.

K. Maurer,. Basic data on arthritis: knees, hip and sacro-iliac joints. Adults ages 25-74 years. United States 1971-1975. *U.S. Department of Health, Education and Welfare*.

JE, Kennedy. (2005). High-intensity focused ultrasound in the treatment of solid tumours. *Nat Rev Cancer, 5*, 321-327.

S. Jespersen, Wilhjelm, J., & Sillese, H. (1998). Multi-angle compounding imaging. *Ultrasonic Imaging, 20*(2), 81-102.

C. Kelsy, (2002). Medical Imaging Physics. *4th ed. Health Phys, 86*(6), 912-921.

K.Z.Abd-Elmoniem, A. M. Y., Y.M.Kadah. (2002). Real-time speckle reduction and coherence enhancement in ultrasound imaging via nonlinear anisotropic diffusion. *IEEE Trans. Biomed. Eng, 49*, 997–1014.

M. Karaman,., Kutay, M. A., & Bozdagi, G. (1995). An adaptive speckle suppression filter for medical ultrasonic imaging. *Medical Imaging, IEEE Transactions on, 14*(2), 283-292.

H. Keen, Wakefield, R., & Conaghan, P. (2009). A systematic review of ultrasonography in osteoarthritis. *Annals of the rheumatic diseases, 68*(5), 611-619.

M. Kim, M. C. (2008). Recursively separated and weighted histogram equalization for brightness preservation and contrast enhancement. *iEEE Trans. Consumer Electronics, 54*, 1389–1397.

T. Kim, P. J. (2008). Adaptive contrast enhancement using gain-controllable clipped histogram equalization. *IEEE Trans. Consumer Electronics, 54*, 1803-1810.

Y.-T. Kim:, (1997). Contrast enhancement using brightness preserving bi-histogram equalization. *IEEE Trans. Consumer Electronics, 43*(1), 1-8.

K. Krissian, & Aja-Fernández, S. (2009). Noise-driven anisotropic diffusion filtering of MRI. *Image Processing, IEEE Transactions on, 18*(10), 2265-2274.

K. Krissian, Westin, C.-F., Kikinis, R., & Vosburgh, K. G. (2007). Oriented speckle reducing anisotropic diffusion. *Image Processing, IEEE Transactions on, 16*(5), 1412-1424.

D. Kuan,. T., Sawchuk, A., Strand, T. C., & Chavel, P. (1987). Adaptive restoration of images with speckle. *Acoustics, Speech and Signal Processing, IEEE Transactions on, 35*(3), 373-383.

L, Carmona. The prevalence of 6 rheumatic disease in the Spanish population. *Annals of the Rheumatic Diseases 2000;*.

L. Menashe yz, K. H. z., E. Losina x, M. Kloppenburg k, W. Zhang , L. Li z, D.J. Hunter. (2012). Osteoarthritis and Cartilage." The diagnostic performance of MRI in osteoarthritis: a systematic review and meta-analysis. *Osteoarthritis and Cartilage, 20*, 13-21.

L.C.Gupta, A. G. (1998). X-ray Diagnosis and Imaging,. *thirded.,JayPee Brothers Medical Publishers, NewDelhi, India*.

S. Lau, (1994). Global image enhancement using local information. *Electronics Letters, 30*(2), 122-123.

J.-S. Lee, (1980). Digital image enhancement and noise filtering by use of local statistics. *Pattern Analysis and Machine Intelligence, IEEE Transactions on*(2), 165-168.

J. Lee, S. (1986). Speckle suppression and analysis for synthetic aperture radar. *Optim.Eng., 25*(5), 636-643.

Li, F.-K., Croft, C., & Held, D. N. (1983). Comparison of several techniques to obtain multiple-look SAR imagery. *Geoscience and Remote Sensing, IEEE Transactions on*(3), 370-375.

Li, X., & Chen, T. (1994). Nonlinear diffusion with multiple edginess thresholds. *Pattern Recognition, 27*(8), 1029-1037.

T. Loupas,., McDicken, W., & Allan, P. (1989). An adaptive weighted median filter for speckle suppression in medical ultrasonic images. *Circuits and Systems, IEEE Transactions on, 36*(1), 129-135.

Ł. Paczesny, M., and Jacek Kruczyn´ ski, MD, PhD†. (2011). Semin Ultrasound CT MRI. *Ultrasound of the Knee, 32*, 114-124.

Medical Benefits Reviews Task Group Diagnostic Imaging Review Team Department of Health and Ageing February 2012 Review, Australia.

D. Mittal, Kumar, V., Saxena, S. C., Khandelwal, N., & Kalra, N. (2010). Enhancement of the ultrasound images by modified anisotropic diffusion method. *Medical & biological engineering & computing, 48*(12), 1281-1291.

P. Mrázek, & Navara, M. (2003). Selection of optimal stopping time for nonlinear diffusion filtering. *International Journal of Computer Vision, 52*(2-3), 189-203.

Rao. Navalgund, J. W. S. (2002). Ultrasound imaging," in Encyclopedia of Imaging Science&Technology,. *J. Hornak, Ed.*, 1412-1435.

NSP, Ibrahim. H. K. (2009). Image sharpening using sub-regions histogram equalization. *IEEE Trans. Consumer Electronics, 55*, 891-895.

O.Michailovich, A. T. (2006). Despeckling of medical ultrasound images. *Ultrason.Ferroelectr.Freq.Control, 53*(1), 64-78.

S. Oliveria, A., Felson, D. T., Reed, J. I., Cirillo, P. A., & Walker, A. M. (1995). Incidence of symptomatic hand, hip, and knee osteoarthritis among patients in a health maintenance organization. *Arthritis & Rheumatism, 38*(8), 1134-1141.

S. Osher, & Rudin, L. I. (1990). Feature-oriented image enhancement using shock filters. *SIAM Journal on Numerical Analysis, 27*(4), 919-940.

S. Ovireddy,., & Muthusamy, E. (2014). Speckle Suppressing Anisotropic Diffusion Filter for Medical Ultrasound Images. *Ultrasonic imaging, 36*(2), 112-132.

P. Perona, J. M. (1990). Scale space and edge detection using anisotropic diffusion. *IEEE Trans. Pattern Anal. Mach. Intell., 12*, 629-639.

P.M.Shankar. (2006). Speckle reduction in ultrasonic images through a maximum likelihood based adaptive filter,. *Phys.Med.Biol, 51*, 5591-5602.

P.Perona, J. M. (1990). Scale space and edge detection using anisotropic diffusion,. *IEEE Trans. Pattern Anal. Mach. Intell, 12*, 629–639.

M. Petrou,., & Petrou, C. (2010). *Image processing: the fundamentals*: John Wiley & Sons.

V. Rallabandi, P. S. (2008). Enhancement of ultrasound images using stochastic resonance-based wavelet transform. *Computerized Medical Imaging and Graphics, 32*, 316-320. doi: 10.1016/j.compmedimag.2008.02.001

B. Scott. Raymond, L. H. T., Jonathan D. Dewey, Nathan J. McDannold, Kullervo Hynynen, Brian J. Bacskai. (2008). Ultrasound Enhanced Delivery of Molecular Imaging and Therapeutic Agents in Alzheimer's Disease Mouse Models. *PLoS ONE, 3*(5), 1-7.

Y. Seungjoon, J. H. O., Yungfun P:. (2003). Contrast enhancement using histogram equalization with bin underflow and bin overflow. *In Proceedings of the 2003 International Conference on Image Processing, ICIP 2003, Barcelona, Catalonia, Spain.*, 881-884.

T. Sim KS,. C., Tan YY:. (2007). Recursive sub-image histogram equalization applied to gray scale images. *Pattern Recognit Letters, 28*, 1209-1221.

C. Soong-Der, R. A. (2003a). Contrast enhancement using recursive mean-separate histogram equalization for scalable brightness preservation. *iEEE Trans. Consumer Electronics, 49*, 1301-1309.

C. Soong-Der, R. A. (2003b). Minimum mean brightness error bi-histogram equalization in contrast enhancement. *iEEE Trans. Consumer Electronics, 49*, 1310-1319.

P. Stetson, Graham, F., & Macovski, A. (1997). Lesion contrast enhancement in medical ultrasound imaging. *IEEE Transactions on Medical Imaging, 16*(4), 416-425.

Q. Sun, , Hossack, J. A., Tang, J., & Acton, S. T. (2004). Speckle reducing anisotropic diffusion for 3D ultrasound images. *Computerized Medical Imaging and Graphics, 28*(8), 461-470.

T. Marshburn, E. L., A. Sargsyan, et al.,. (2004). Goal-directed ultrasound in the detection of long-bone fractures. *J. Trauma, 57*, 329-332.

M. Tamaki, K. Y. (1994) Osteoarthritis of the knee joint: a field study. Nippon Seikeigeka Gakkai Zasshi. *Journal of the Japanese Orthopaedic Association, 68*(9), 737-750.

Yu. Tinghe, J. L. (2011). Adverse Events of Extracorporeal Ultrasound-Guided High Intensity Focused Ultrasound Therapy. *PLoS ONE, 6*(12), 1-9.

G. Trahey,., Smith, S., & Van Ramm, O. (1986). Speckle pattern correlation with lateral aperture translation: Experimental results and implications for spatial compounding. *Ferroelectrics and Frequency Control,, 33*(3), 257-264.

C. Tsiotsios,., & Petrou, M. (2013). On the choice of the parameters for anisotropic diffusion in image processing. *Pattern recognition, 46*(5), 1369-1381.

Tur, M., Chin, K.-C., & Goodman, J. W. (1982). When is speckle noise multiplicative? *Applied optics, 21*(7), 1157-1159.

V. Noble, E. L., T. Marshburn. (2003). Long bone ultrasound, making the diagnosis in remote locations. *J. Trauma, 54*, 800-806.

VT, Tzonchev. Prevalence of osteoarthrisits in Bulgaria. In: Bennett PH, Wood PHN, editors. Population studies in the rheumatic diseases. *Excerpta Medica, 1968*, 413-415.

Q. Wang, W. R. (2007). Fast image/video contrast enhancemnt based on weighted thresholded histogram equalization. *IEEE Trans. Consumer Electronics, 53*, 757-764.

Z. Wang, , Bovik, A. C., Sheikh, H. R., & Simoncelli, E. P. (2004). Image quality assessment: from error visibility to structural similarity. *Image Processing, IEEE Transactions on, 13*(4), 600-612.

J. William Tyler, Y. T., Michael Finsterwald, Monica L. Tauchmann, Emily J. Olson,Cassondra Majestic. (2008). Remote Excitation of Neuronal Circuits Using Low-Intensity, Low-Frequency Ultrasound. *PLoS ONE, 3*(10), 1-11.

M. Wilson, (2009). Preparing a patient for an 'X-ray': A student nurse's pespective of radiographic imaging. *Journal of Orthopaedic Nursing, 13*, 115-118.

X. Hao, S. G., X. Gao,. (1999). A novel multiscale nonlinear thresholding method for ultrasound speckle suppressing. *Med. Imag, 18*, 787-794.

Yu, J., Tan, J., & Wang, Y. (2010). Ultrasound speckle reduction by a SUSAN-controlled anisotropic diffusion method. *Pattern Recognition, 43*(9), 3083-3092.

Yu, J., Wang, Y., & Shen, Y. (2008). Noise reduction and edge detection via kernel anisotropic diffusion. *Pattern Recognition Letters, 29*(10), 1496-1503.

Yu W, Q. C., Baeomin Z:. (1999). Image enhancement based on equal area dualistic sub-image histogram equalization method. *iEEE Trans. Consumer Electronics, 49*(1), 68-75.

Yu, Y., Acton, S.T. (2002). Speckle reducing anisotropic diffusion. *IEEE Trans. Image Processings, 11*(11), 1260-1270.

F. Zhang, Yoo, Y.M., Koh, L.M., Kim, Y. (2007). Nonlinear diffusion in Laplacian pyramid domain for ultrasonic speckle reduction. *IEEE Trans. Med. Imag, 26*(2), 200-2011.

Z. Chao, C. Q., Xiubao Sui. (2012). Range limited bi-histogram equalization for image contrast enhancement. *Optik- International Journal for Light and Electron Optics 2012*.

SUPPLEMENTARY

LIST OF PUBLICATIONS AND PAPERS PRESENTED

1. M.B. Hossain, K.W. Lai, B. Pingguan-Murphy, Y.C. Hum, M.I. Mohd Salim, and Y.M. Liew, Contrast enhancement of ultrasound imaging of the knee joint cartilage for early detection of knee osteoarthritis, Biomedical Signal Processing and Control. **13**, (2014) p. 157-167.
2. M.B. Hossain, K.W. Lai, B. Pingguan-Murphy, Y.C. Hum, M.I. Mohd Salim, and Y.M. Liew, An Improved Anisotropic Diffusion Method for Speckle-Noise Reduction with Edge Preservation in Ultrasound Image of knee Articular Cartilage, 'World Scientific Journal' (Major Revision)

APPENDIX

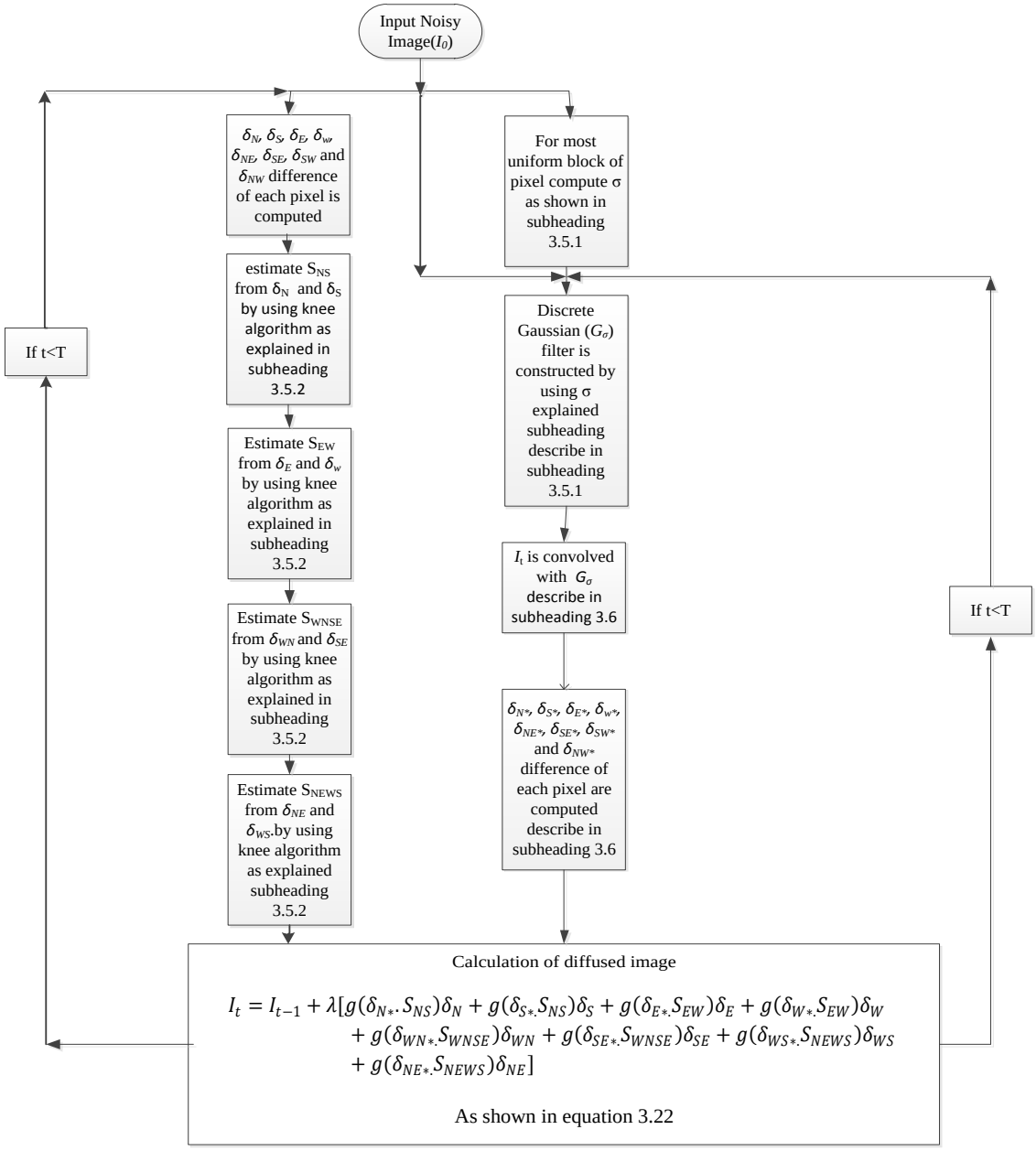

Fig: Algorithm for speckle noise reduction method

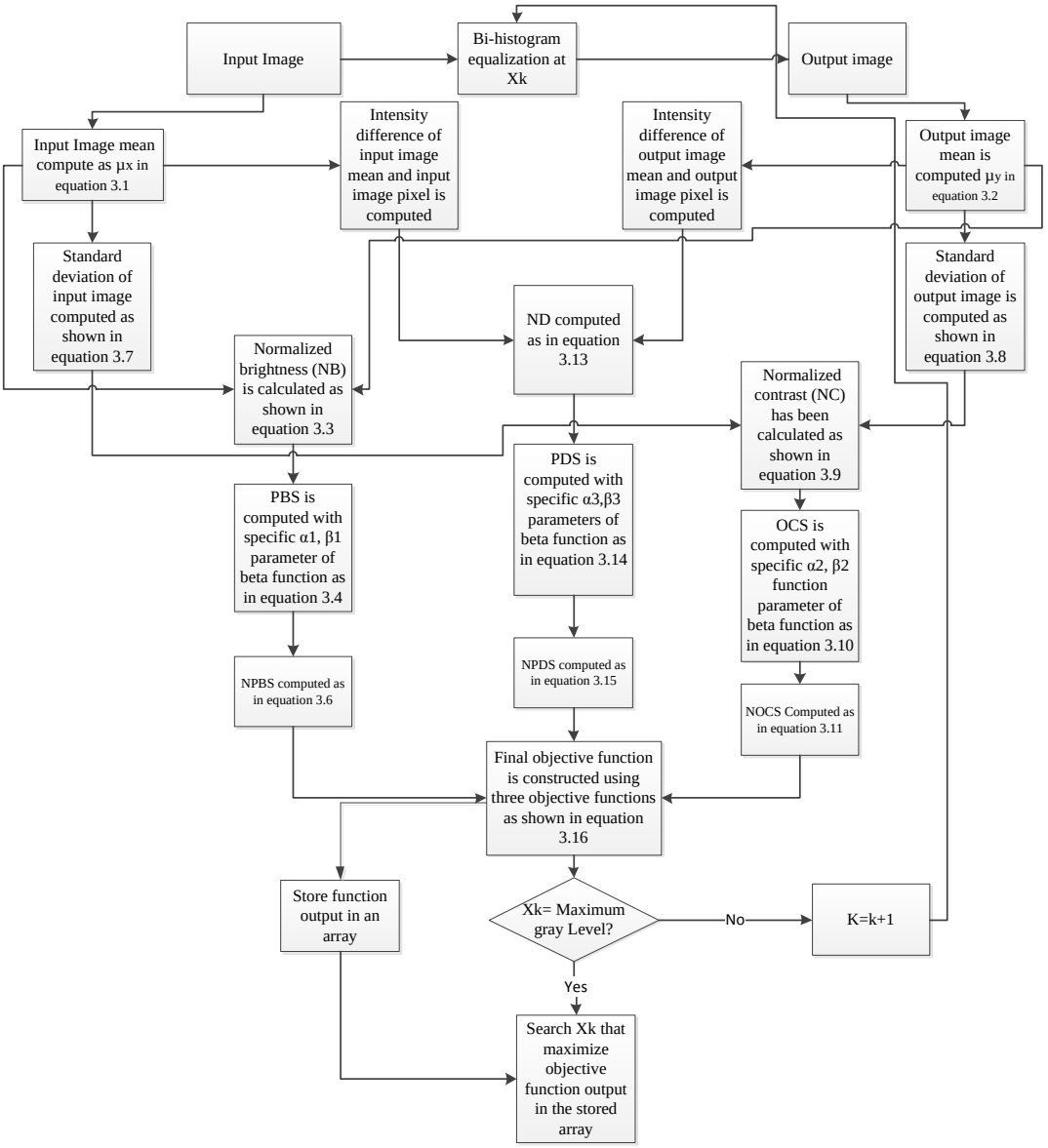

Fig: Algorithm for contrast enhancement method